

Measurement of two-photon absorption  
laser-induced Lyman- $\alpha$  fluorescence:  
A diagnostic for atomic number densities of hydrogen  
isotopes in magnetically confined fusion plasmas

von  
Diplom-Physiker  
**Christian Seiser**  
aus Lörrach

Dem Fachbereich 4 (Physik)  
der Technischen Universität Berlin  
zur Verleihung des akademischen Grades  
**Doktor der Naturwissenschaften**  
vorgelegte Dissertation

Berlin 1998  
D 83

Arbeit eingereicht am: 14. Mai 1998

Tag der mündlichen Prüfung: 5. Juni 1998

Promotions-Ausschuß:

Vorsitzender: Prof. Dr. Jürgen Sahm

Berichter: Prof. Dr. Burkhard Wende (PTB)

Prof. Dr. Horst Weber

*to my parents  
with deep gratitude*

“Physics would be dull and life most unfulfilling if all physical phenomena around us were linear. Fortunately, we are living in a nonlinear world.”

*Y. R. Shen, The Principles of Nonlinear Optics*

## Abstract

Measurement of Doppler-free *two-photon absorption laser-induced Lyman- $\alpha$  fluorescence* ( $L_\alpha$ -TALIF) allows for isotope-selective determination of small atomic number densities (H, D, T) in magnetically confined plasmas. Its future application at *fusion plasmas* requires quantitative studies of this novel technique. A first feasibility study was performed recently in a close cooperation between the Physikalisch-Technische Bundesanstalt (Berlin) and the Max-Planck Institut für Plasma Physik (Berlin). The aim of this experimental study was to prove the potential of  $L_\alpha$ -TALIF measurements as a *density diagnostic for hydrogen isotopes* at the *plasma generator PSI-1*. This device is operated by the Institut für Plasma Physik and comes close in its plasma parameters to values similar to those of fusion plasma machines. The conducted analysis included the determination of the detection sensitivity of  $L_\alpha$ -TALIF measurements achievable at PSI-1.

This work reports on the predictions, which are made for  $L_\alpha$ -TALIF measurements at fusion plasmas. It introduces into the basic principles of  $L_\alpha$ -TALIF theory and the advantages, which are provided by inducing  $L_\alpha$ -TALIF absorption *Doppler-freely*. A newly comprehensive approach to the yield of fluorescence photons at the Lyman- $\alpha$  wavelength ( $\lambda = 122$  nm) is presented.

The main experimental equipment, e.g. the *pulsed UV-laser spectrometer* ( $\lambda = 243$  nm) and  *$L_\alpha$ -detection system*, which had been developed for this study is explained. However, the work's central part is covered by the presentation of various results obtained from extensive *quantitative*  $L_\alpha$ -TALIF measurements at PSI-1. For example, deuterium densities as small as  $10^{10}$  cm<sup>-3</sup> were determined reliable in a measurement volume as small as 0.1 cm<sup>3</sup> within a plasma beam of 12 cm in diameter. For such measurements, a background radiation of the PSI-1 plasma had to be overcome, which lies in the same order of magnitude like the number commonly stated for tokamak fusion plasmas.

Based on the experience gained by this work an assessment of the future potential of  $L_\alpha$ -TALIF measurements as an isotope selective density diagnostic for fusion plasmas is given. Densities as small as  $10^8$  cm<sup>-3</sup> shall be measurable with high spatial resolution and single shot accuracy as required for fusion diagnostics.

Presented talks in conjunction with this work:

13<sup>th</sup> November 1997 *Zwei-Photonen induzierte Lyman- $\alpha$  Fluoreszenz am PSI-1:*

*Eignungsnachweis als Tokamak-Diagnostik.*

Institut für Plasma-Physik, KFA Jülich, Germany.

26<sup>th</sup> November 1997 *Experimentelle Ergebnisse der zweiphotonen induzierten*

*Lyman- $\alpha$  Fluoreszenz am PSI-1.*

Seminar zur Stark-Verbreiterung von Prof. G. Röpke;

Universität Rostock, Germany.

9<sup>th</sup> March 1998

*Lyman- $\alpha$  Ausbeute bei Zwei-Photonen-LIF für die Tokamak-Diagnostik.*

DPG-Frühjahrstagung. Bayreuth, Germany: P 7.1.

# Contents

<b>1 Introduction</b> .....	<b>1</b>
<b>2 Physical Basics of Two-photon Absorption Laser-induced Lyman-<math>\alpha</math> Fluorescence</b> .....	<b>7</b>
2.1 Two-photon absorption laser-induced Lyman- $\alpha$ fluorescence .....	8
2.1.1 Principle of Doppler-free application .....	8
2.1.2 Kinetic temperatures by use of a residual Doppler width .....	10
2.2 Theoretical predictions for $L_\alpha$ -TALIF in magnetically confined plasmas .	11
2.2.1 Magnetically confined fusion plasmas .....	11
2.2.2 The PSI-1 plasma .....	14
2.3 Absolute atomic number densities .....	16
2.4 The Lyman- $\alpha$ yield .....	18
<b>3 Experimental Setup</b> .....	<b>26</b>
3.1 The plasma generator PSI-1 .....	27
3.1.1 Technical description .....	27
3.1.2 VUV emission of PSI-1 plasmas .....	29
3.2 Single-mode UV-laser-spectrometer .....	31
3.2.1 Tunable laser radiation at $\lambda = 243$ nm .....	31
3.2.2 Passive frequency locking with an optogalvanic reference cell .....	37
3.3 Lyman- $\alpha$ detector system .....	38
3.3.1 The photomultiplier tube .....	39
3.3.2 The oxygen $L_\alpha$ -filter .....	43
3.3.3 Calibration of the $L_\alpha$ -detector system .....	44

---

<b>4 Experimental Results</b> .....	<b>45</b>
4.1 Preparatory examinations .....	46
4.1.1 Spectral bandwidth of the laser .....	46
4.1.2 Spectral bandwidth of the $L_\alpha$ -absorption profile .....	47
4.1.3 $L_\alpha$ -yield for real laser irradiance distributions .....	49
4.1.4 Error discussion for the $L_\alpha$ -yield .....	52
4.1.5 Analysis of fluorescence reabsorption at PSI-1 .....	53
4.2 Principle of measurements .....	54
4.2.1 Data recording and $L_\alpha$ -TALIF measurements .....	54
4.2.2 Statistical analysis of the $L_\alpha$ -TALIF signals .....	55
4.3 Atomic densities and $L_\alpha$ -background .....	57
4.3.1 $L_\alpha$ -background emission at PSI-1 .....	57
4.3.2 Measurement of atomic number densities .....	59
4.3.3 Error discussion for atomic number densities .....	61
4.3.4 $L_\alpha$ -TALIF detection limit at PSI-1 .....	62
4.4 Kinetic plasma temperatures at PSI-1 .....	62
<b>5 Conclusion</b> .....	<b>64</b>
<b>6 List of Symbols</b> .....	<b>67</b>
<b>7 Literature</b> .....	<b>71</b>
<b>Acknowledgements</b> .....	<b>79</b>
<b>Curriculum Vitae</b> .....	<b>80</b>



# 1

## Introduction

Humankind strives continually to improve its standard of living. In many parts of the world, this is still strongly linked with a growing consumption of energy. In order to provide for this energy in spite of the evident limitation of fossil fuels, new sources of energy and methods of energy production are investigated. *Controlled nuclear fusion* is a promising candidate, which might contribute a significant supply of energy.

Nuclear fusion offers various advantages over nuclear fission, and its fuel components are rather easily available in large amounts [1]. This has encouraged scientists all over the world to improve our understanding of how to drive terrestrial nuclear fusion in a controlled, profitable way. The demanding aim is to use nuclear fusion peacefully in power plants in a not too distant future.

Early steps towards an understanding of fusion date back to the first half of this century [2...5]. Today, scientific and engineering progress has reached a point where it is possible to build an *International Thermonuclear Experimental Reactor* (ITER) [6...8]. ITER is designed as a tokamak fusion device which would allow to study the self-sustained burn of ignited plasmas for the first time. Additionally, ITER is to demonstrate the successful handling of most of the relevant scientific and technological aspects needed when fusion delivers more energy than it consumes.

This latter goal might be reached in the middle of next century with a first demonstration fusion reactor DEMO [9], which shall follow to ITER.

The successful operation of large tokamaks such as ITER requires many sophisticated diagnostic tools which provide detailed information about the plasma state. The ITER Expert Group on Diagnostics has set up a table of about 50 physical quantities which have to be measured with good spatial and temporal resolution in order to operate and control ITER [10, 11]. In this list, the ratio of the *number densities* of deuterium and tritium – the heavy hydrogen isotopes used as fuel components for fusion energy production – is shown several times: In the plasma core, knowledge of  $N_T/N_D$  is necessary for fuel control, and in the plasma edge and the divertor region,  $N_T/N_D$  and also  $N_H/N_D$  are required for fuelling optimization and plasma dilution control.

The hot *plasma core* is almost completely ionized and the densities refer to the ions. The cooler *edge and divertor regions* of the plasma are dominated by atoms, so that the densities are *atomic number densities* in these regions. However, the rate of charge-exchange processes is very high in magnetically confined fusion plasmas. This allows to obtain the ion density ratios from the corresponding atomic density ratios [12] if they can be measured in the plasma core. Therefore, the discussion will be confined to atomic density measurements in the following.

Important physical quantities of fusion plasmas in our context are particle densities  $N$  and kinetic temperatures  $T$ . In the central regions of fusion plasmas, atom densities are only  $10^8 \text{ cm}^{-3}$  or less, and kinetic ion and atom temperatures exceed 3 keV. (As usual in fusion physics, temperatures are given as the corresponding thermal energies  $k_B T$ .) In the plasma edge and also in the divertor region, atomic densities are significantly higher, due to the lower temperatures in the eV range.

These conditions prevent the application of certain types of density measurement techniques. In particular, the high kinetic temperatures result in strong *Doppler*<sup>#</sup> *broadening* of all atomic one-photon spectral lines. Even at a temperature of only 1 eV, the Doppler-broadened spectral lines of deuterium and tritium overlap to a large extent, despite the isotopic shift (see Fig. 2.1 below). Therefore, one-photon excitation of fluorescence, for example, as employed by Mertens and Silz at TEXTOR 94 [13], cannot be used to distinguish between deuterium and tritium already at moderate temperatures. Obviously, a *Doppler-free* measurement technique is necessary to determine the deuterium to tritium density ratio.

---

# Christian Doppler (1803-1853), Austrian physicist.

Doppler-free measurements can be realized with *two-photon laser spectroscopy*, which also offers good spatial and temporal resolution in addition to isotope selectivity [14].

If an atomic transition is excited by absorption of two photons with opposite momenta, each of which provides half the transition energy, the Doppler shifts of the photon frequencies as seen by the atom cancel (except for small relativistic second and higher order contributions) regardless of the atomic velocity. Such a two-photon excitation scheme is already utilized for polarization spectroscopy [15] and four-waves mixing [16]. These two methods have the advantage that the signal to be measured is a highly directional signal beam (probe laser beam or collimated signal beam generated by frequency mixing of three incoming laser beams). However, both methods require rather high densities to produce measurable effects. Particle densities may be high enough for these methods in the divertor region, but constructional constraints do not allow their application in that part of a fusion reactor.

A measurement technique which is better suited for fusion plasmas is *two-photon absorption laser-induced fluorescence* (abbreviation: TALIF). Its main advantages are:

- high spatial and temporal resolution
- Doppler-free, isotope-sensitive method
- contributions to the signal from all atoms, cold and hot ones,
- direct access to density ratios without any modelling
- easily modified to measure kinetic temperatures via residual Doppler widths.

The main problems of the TALIF method are the production of intense laser radiation at the proper wavelength and the detection of the induced fluorescence radiation against the background of thermal plasma radiation.

The most direct way to get the desired information on atomic densities is induced absorption from the *ground-state level* (principal quantum number  $n = 1$ ): Most of the atoms in a high-temperature dilute plasma are found in the ground state (there is no thermodynamical equilibrium with Boltzmann distribution of energy level populations under these circumstances). As target level, the *first excited level* ( $n = 2$ ) is most suitable because its excitation can be done with radiation of wavelength 243 nm, while higher excited target levels would require shorter wavelengths.

The  $2S \rightarrow 1S$  transition being known as the *Lyman<sup>#</sup>- $\alpha$  resonance line*, this particular TALIF scheme is abbreviated as  $L_\alpha$ -TALIF here. Based on theoretical investigations [28] which were subsequently refined [32], the use of  $L_\alpha$ -TALIF for the determination of neutral particle densities in magnetically confined fusion plasmas was first proposed by Voslamber in 1990.

According to the status reports of the Engineering Design Activity (EDA) phase for ITER, the  $L_\alpha$ -TALIF technique is of special interest for the measurement of the *number density ratio* of the fuel components deuterium and tritium in the *edge* of fusion plasmas [17] where the densities are sufficiently high. A well-founded understanding of the neutral and charged particles densities, currents and temperatures at the plasma edge is essential for optimized fusion reactor design and operation, the more so as the core plasma parameters are strongly correlated with the edge plasma conditions. Nevertheless, an extension of the range of applicability of the  $L_\alpha$ -TALIF technique *towards the centre* of the plasma would be highly desirable, but is difficult. To a certain extent, an increase of laser pulse energy can compensate for the decrease of atomic densities. Based on current expertise, it should be possible to reach atomic number densities  $N \leq 10^8 \text{ cm}^{-3}$  with pulse energies of 100 mJ per beam. However, the usefulness of increased laser pulse energies is eventually limited by *ionization* due to absorption of a third photon (for a detailed discussion, see Chapter 2.4). According to a proposal by Voslamber and Mandl [18], another possibility to improve the effectiveness of the TALIF measurement method may be offered by the higher hydrogen densities in close vicinity of *neutral particle beams* which are injected into the plasma for heating and diagnostic purposes [19, 20].

In principle, the suitability of  $L_\alpha$ -TALIF for density ratio measurements in a magnetically confined *fusion plasma* might be tested directly at one of the existing fusion research devices such as ASDEX Upgrade (Garching, Germany), TEXTOR 94 (Jülich, Germany), or JET (Cullham, Great Britain), where the plasma parameters are similar to those planned for ITER. However, the coordination of such test measurements with the regular long-term research programme at these major sites would be a particularly complex undertaking. Therefore, it seemed to be more reasonable to demonstrate the *feasibility of  $L_\alpha$ -TALIF* at a small machine first, which can be operated and accessed more easily. The plasmas generated by such smaller machines are certainly not fusion plasmas, but come close in their parameters to plasma conditions found in certain regions of true fusion plasmas, e. g. the plasma edge or the divertor.

---

# Theodore Lyman (1874-1954), US American physicist.

---

The *plasma generator PSI-1* at the Berlin division of the Max-Planck-Institut für Plasmaphysik (IPP; Garching, Germany) is such a smaller plasma device. It is a linear discharge for plasma-wall interaction studies and research and development in the field of plasma diagnostics. In 1992, the Physikalisch-Technische Bundesanstalt (PTB; Berlin, Germany) and the IPP established a cooperation with the intention to carry out a feasibility study of  $L_{\alpha}$ -TALIF atomic density measurements at the PSI-1 device. In order to characterize the novel measurement technique as comprehensively as possible, absolute density measurements in hydrogen-deuterium gas mixtures were to be done at various PSI-1 discharge currents. This required the determination of the sensitivity of the  $L_{\alpha}$ -fluorescence detection system.

The main issues to be solved were:

- *Laser spectrometer*

- Stability control
- Measurement of the properties of the laser radiation at 243 nm in terms of frequency, pulse energy, irradiance distribution and beam overlap in the TALIF measurement volume
- Solution of the nonlinear rate equations for the Lyman- $\alpha$  yield, the mean number of fluorescence photons emitted per atom under specified laser excitation and plasma conditions

- *Detection system*

- Adaption to the unknown background irradiances over the whole operating range of PSI-1.
- Calibration of the detector system sensitivity at hydrogen's Lyman- $\alpha$  wavelength of 121.6 nm.

The laser spectrometer and the final detection system were developed by PTB. The laser spectrometer was considered to be the most difficult part in the project. PTB succeeded in developing an *all-solid-state laser system* based on injection-seeded Nd:YAG lasers, an optical parametric oscillator equipped with Titanium-Sapphire amplifiers, and a final sum-frequency mixing unit. The system was ready for use early in 1994. The detection system was originally considered less difficult. However, first approaches were not successful. Modifications made by the PTB lead to an operational detection system, and first *qualitative* measurements of  $L_{\alpha}$ -TALIF signals were done at PSI-1 in September 1994.

Those measurements at a device, whose characteristic in respect to Lyman- $\alpha$  emission was practically unknown, elucidated the special requirements to be fulfilled by the detection system. In 1994, it became evident that an entirely new design of the detection system was necessary in order to conduct the feasibility study successfully. With a *VUV spectrometer set up* at the PTB all relevant optical components of the detection system were tested and characterized. The spectrometer served also for the development of an oxygen gas filter and the calibration procedure of the detection system. The new, versatile detection system was ready for operation and first *quantitative*  $L_\alpha$ -TALIF measurements were taken at the PSI-1 in June 1996.

Preparations for the *first quantitative* measurements were the starting point for the PhD thesis presented here. Work for it begun in April 1995 with the aim to extract *absolute atomic number densities* from Doppler-free  $L_\alpha$ -TALIF signals measured in hydrogen and deuterium gas mixtures at PSI-1. In addition, *kinetic temperatures* were planned to be determined by introducing a suitable crossing angle between the two laser beams. This causes a residual Doppler width of the two-photon absorption line profile, which is temperature dependent.

The *structure of the thesis* is as follows: Chapter 2 gives an overview of the theory. After a brief introduction of the  $L_\alpha$ -TALIF technique itself (Ch. 2.1), the application of this diagnostic technique at the edge of fusion plasmas is discussed (Ch. 2.2). Chapters 2.3 and 2.4 derive the formulae linking the fluorescence signal to the atomic number density and the computation of the  $L_\alpha$ -yield. Chapter 3 describes the plasma generator PSI-1 and the experimental setup, focusing on the two main components: the laser spectrometer (Ch. 3.2) and the detection system (Ch. 3.3). Chapter 4 presents the main experimental results subdivided into preparatory examinations, principle of measurements, plasma background emission, atomic number densities as well as the kinetic temperature measured at standard PSI-1 plasmas. Finally, chapter 5 contains a summary of the results and a conclusion.

# 2

## Physical basics of two-photon absorption laser-induced Lyman- $\alpha$ fluorescence

An early experiment, who reported the use of laser-induced fluorescence (LIF) for *plasma diagnostic* was done by Stern and Johnson in 1975 [21]. As a remote, active but non-interfering measurement technique it has been superior to passive spectroscopy [22] in respect to spatial resolution and ability to probe for example the distribution of a special species within the plasma.

However, this kind of *one*-photon absorption LIF suffers from the need to discriminate between laser radiation and fluorescence, because their wavelengths may sometimes lie close to each other. This is only one of several disadvantages, which can simply be overcome by use of *two*-photon absorption LIF. Of course, its most important benefit is to allow *Doppler-free* measurements, as will be explained in Chapter 2.1.

Already in 1931 Maria Goeppert-Mayer developed generally the theory for *two-photon absorption* in her PhD thesis [23]. Typically for that extraordinarily creative time, scientists had to await the advent of *lasers* until they could proof many theoretically predicted phenomena. In 1961 Kaiser and Garrett succeeded in delivering the experimental proof for two-photon absorption [24]. Two-photon absorption laser-induced fluorescence with *hydrogen* was done for the first time by Hänsch and coworkers in 1975 [25]. Although still not yet a widespread technique,

*two-photon absorption laser-induced fluorescence* (TALIF) is described comprehensively in review articles [26] and textbooks [14]. For convenience of the reader, Chapter 2.1.1 summarizes the important features of *Doppler-free TALIF* briefly. Allowing for a small residual Doppler width, also kinetic temperatures can be measured with TALIF, as shall be explained in Chapter 2.1.2.

If one intends to apply laser-induced fluorescence successfully in a special environment, it is important to have an idea about the environment's influence on the atoms or molecules. This holds especially for magnetically confined fusion plasmas, whose strong electric and magnetic fields have a considerable influence on the eigenstates of the atoms. Because this aspect is elementary for the assessment of TALIF as a fusion-plasma diagnostic, Chapter 2.2 will give a short review of the main *theoretical predictions* of Voslamber and Seidel. Chapter 2.3 develops the formalism needed for the calculation of *absolute atomic number densities*. Finally, this chapter of theory is closed with Chapter 2.4. There, the *Lyman- $\alpha$  yield* is introduced - a quantity, which is essential for the *absolute* measurement of atomic number densities.

## 2.1 Two-photon absorption laser-induced Lyman- $\alpha$ fluorescence

### 2.1.1 Principle of Doppler-free application

The thermal velocity distribution of the atoms leads to a Doppler broadening of the spectral lines. The higher the temperature in a gas is, i.e. the more kinetic energy its particles have, the bigger becomes the Doppler broadening of absorption and emission lines of atomic transitions. In all cases where such lines, e.g. of different isotopes of an element, lie within the Doppler broadening of neighbouring lines, a selective measurement is hampered.

In Figure 2.1, calculated Gauß<sup>#</sup> profiles represent the Doppler-broadened Lyman- $\alpha$  resonance lines of hydrogen (H) and its isotopes deuterium (D) and tritium (T) at a kinetic energy of 1 eV, i.e. a temperature of 11600 K. For one can see, already a kinetic temperature of only 1 eV would make it difficult to measure the line shapes of deuterium and tritium separately in situations, where both are present.

---

# Carl Friedrich Gauß (1777-1855), German mathematician, astronomer and physicist.



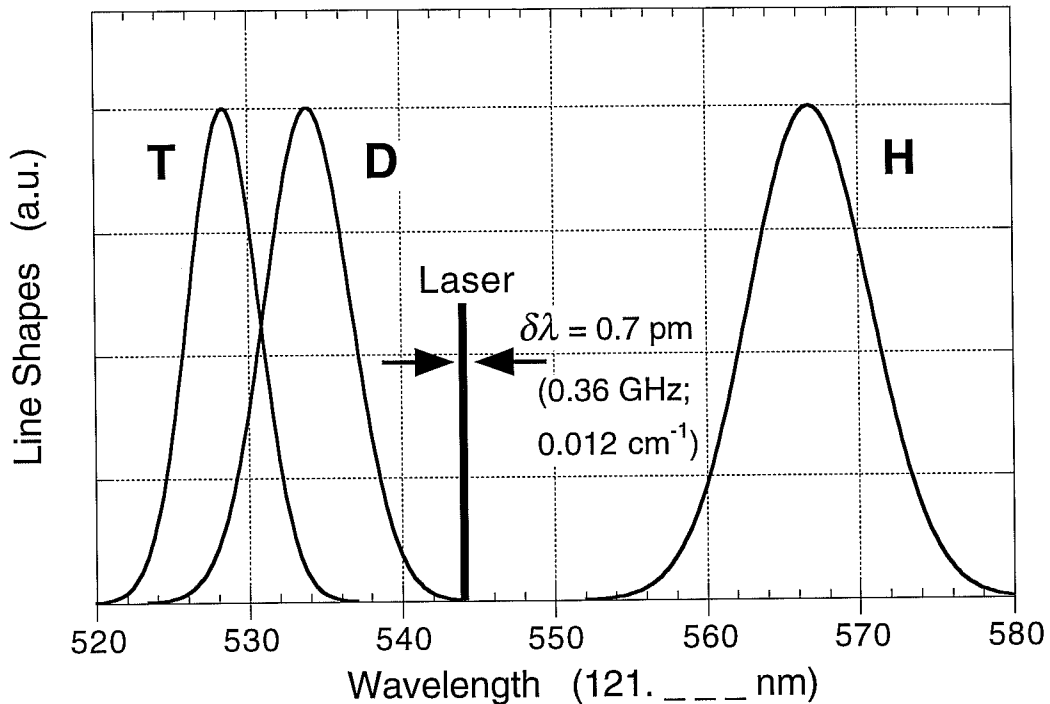


**Figure 2.1** Calculated Doppler broadening of the line shapes of hydrogen, deuterium and tritium for a kinetic temperature of  $T = 1$  eV. Other broadening effects have been neglected. The spectral bandwidth of the laser system, which was used for the TALIF measurements, is indicated for comparison, as well.

However, *two-photon absorption laser induced fluorescence* (TALIF) allows for Doppler-free measurements, i.e. is an *isotope selective* diagnostic for hydrogen, deuterium and tritium even under true fusion plasma conditions. A general introduction into TALIF is given for example in a comprehensive review article of Bloembergen and Levenson [26].

The key issue is to overcome the Doppler broadening by use of *two* laser beams A and B, whose photons have equal energy. If each beam is delivering a photon for the two-photon absorption process, *energy conservation* demands that the frequency of the used laser radiation to be equal to half of the resonance frequency of the transition, which is to excite.

Sending the laser beams collinearly but in opposite directions through the gas under examination, there will be *no momentum transfer* to the atoms of the gas, if one photon is absorbed from the one laser beam and the other necessary photon is absorbed from the other beam, respectively. Consequently, the important non-relativistic linear Doppler broadening, which is the relevant Doppler broadening contribution at the plasma generator PSI-1, is eliminated. However, due to a finite spread in laser beam divergency and frequency bandwidth, in reality the linear

Doppler effect can only be reduced to a negligible size, but not exactly to zero.

Under the sole aspect of energy conservation both photons for the absorption process could be delivered from just one of the laser beams *alone*. However, in such a case the excitation is not Doppler-free. Indeed, as we will see in another context (Ch. 3.2.2), this is what happens if the laser beams are linearly polarized. But using two counterpropagating laser beams of equal *circular polarization*, a two-photon absorption process can only occur, if one photon is absorbed from *each* beam.

Different to one-photon absorption, with two-photon absorption only such transitions can be induced, whose change  $\Delta l$  in the orbital quantum number  $l$  is

$$\Delta l = 0, \pm 2 . \quad (2.1)$$

Due to the relatively high occupation densities in atomic ground states, it is convenient to start the laser induced excitation out of the ground state 1S. Considering Eq. (2.1), the next atomic level to reach with two-photon absorption is the 2S level. This transition in hydrogen isotopes is called *Lyman- $\alpha$*  ( $L_\alpha$ ) transition and so we name the here used TALIF technique in shorthand notation:  $L_\alpha$ -TALIF.

Hydrogen and deuterium were the species we used in *all* our experiments. Of course, tritium is more important regarding fusion-plasma fuel control than is hydrogen. However, tritium is radioactive and therefore much more difficult to handle. For there is no significant difference between tritium and deuterium in our context, we didn't had to bother with it in this work.

### 2.1.2 Kinetic temperatures by use of a residual Doppler width

The *kinetic temperature*  $T$  is the temperature, which can be assigned to a gas or plasma with particles having the most probable kinetic energy  $E_k$ :

$$E_k = \frac{1}{2} m v^2 = k_B T , \quad (2.2)$$

where  $v$  is the most probable velocity of the particles,  $m$  is the mass of a particle and  $k_B$  the Boltzmann constant. Knowledge of  $T$  is generally not only helpful for a good understanding of plasma behaviour, but in our context necessary for analysing the TALIF measurement results correctly.

Using the known relation connecting the temperature  $T$  of a gas to the Doppler broadening  $\Gamma$  of atomic transition line  $\nu_\alpha$ :

$$T = \frac{m c^2}{8 k_B \ln(2)} \left( \frac{\Gamma}{\nu_\alpha} \right)^2 \quad (2.3)$$

it is possible to calculate  $T$  from the corresponding *full*  $L_\alpha$ -Doppler width  $\Gamma$ .

But how do we know  $\Gamma$ ? Well, by modifying the experimental setup slightly from Doppler-free excitation with exactly counterpropagating laser beams into a setup, where a small crossing angle  $\gamma$  in the order of  $10^{-3}$  radians is introduced between the wave vectors  $\vec{k}_A$  and  $\vec{k}_B$  of the two laser beams A and B. Consequently, the absorption lines become slightly Doppler-broadened. Their spectral width is now called a *residual Doppler width*  $\Delta v_{rD}$ , for it is still not the full Doppler width as in the case with both colinear laser beams propagating in the same direction.

The crossing angle  $\gamma$  is defined as  $180^\circ$  in case of parallel laser beams - yielding full Doppler broadening  $\Gamma$  - and  $0^\circ$  in case of perfectly anti-parallel beams (eliminated linear Doppler broadening). For any arrangement in between, the residual Doppler width  $\Delta v_{rD}$  is given by:

$$\Delta v_{rD} = \Gamma \cdot \sqrt{\frac{1}{2} + \frac{1}{2} \cdot \cos(180^\circ - \gamma)} \quad (2.4)$$

If the laser frequency is now *tuned* above the two-photon absorption resonance, the profile of the Lyman- $\alpha$  fluorescence can be measured in dependence of laser frequency detuning. The FWHM of this profile is the residual Doppler width  $\Delta v_{rD}$ . Equations (2.3) and (2.4) yield the kinetic temperature of the species whose Lyman- $\alpha$  transition was excited.

## 2.2 Theoretical predictions for $L_\alpha$ -TALIF in magnetically confined plasmas

### 2.2.1 Magnetically confined fusion plasmas

Starting in 1988 Voslamber proposed the determination of magnetic field direction in tokamaks from laser-induced Lyman- $\alpha$  fluorescence by use of *one-photon* absorption [27]. Two years later he went on with his studies towards a *two-photon* absorption laser-induced Lyman- $\alpha$  fluorescence scheme under tokamak conditions [28]. This time, Voslamber described furthermore the possibility to use this technique for the *determination of atomic number densities*.

For there had already been accumulated much knowledge and experimental experience about two-photon polarization spectroscopy in the high-temperature laboratory of the PTB at that time [29], it was possible to discern the potential of this

technique for measurement of isotope density ratios in plasmas [30].

Theoretical calculations of Doppler-free *two-photon absorption profiles*  $L(\nu)$  for a  $1S \rightarrow 2S$  laser-induced excitation of deuterium and tritium under *tokamak conditions* were included in that proposal, too. They have been done by Voslamber and Seidel and include on the one hand the fine-structure, hyper-fine structure and the Zeeman splitting of the atoms as well as the Lamb shift. On the other hand, several broadening mechanisms, which act on the natural line width of the absorbing atoms, were considered, too. They are:

- relativistic Doppler broadening,
- motional and collisional Stark broadening.

Figures 2.2...2.4 show the *central components* of two-photon absorption profiles of hydrogen, deuterium and tritium under typical fusion-plasma conditions, i.e. densities ( $N_i = 5 \cdot 10^{13} \text{ cm}^{-3}$ ) and magnetic field strengths ( $B = 5 \text{ T}$ ). The independent variable is the detuning  $\Delta\nu$  of the laser frequency  $\nu$  from half of the unshifted Lyman- $\alpha$  resonance  $\nu_\alpha$ . The parameter for the group of shown curves is the kinetic temperature of the atoms, ranging between  $10^6$  and  $10^8 \text{ K}$  (0.9 - 9 keV).

Compared to the Doppler-broadened line shapes shown in Figure 2.1, the line shapes in Figures 2.2...2.4 are considerably slimmer. Independent from species and temperatures this widths are of the order of GHz, what is matching well to the bandwidth (0.36 GHz) of the laser-spectrometer. The slight temperature dependent shift is sufficiently small and allows for density determination with sufficient accuracy at a fixed laser frequency.

However, above a kinetic temperature  $T = 3 \cdot 10^7 \text{ K}$ , i.e. a kinetic particle energy of roughly 3 keV, the two-photon absorption and therefore the radiant intensity of the induced fluorescence signal, becomes too small for convenient signal-to-noise ratio [28, 32]. Of course, this limit is not meant as an absolute one. But at such temperatures, one has probably to invest heavily in fighting against plasma background radiation.

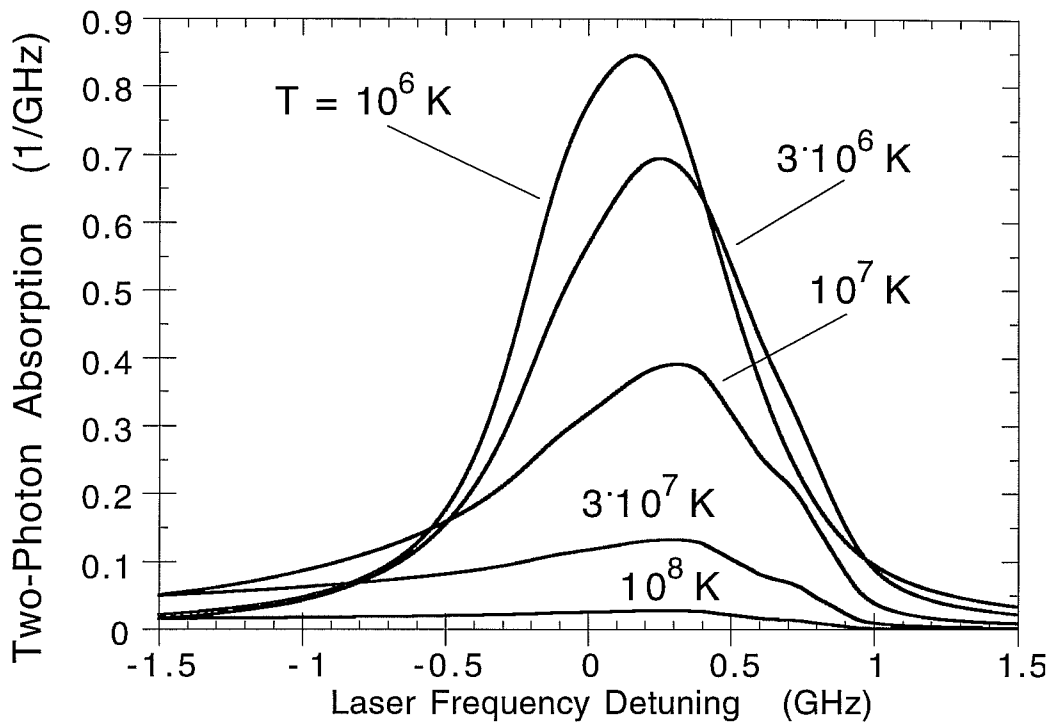


Figure 2.2 Calculated line shape  $L$  of two-photon absorption in hydrogen for various kinetic temperatures  $T$ . The free variable is the detuning of laser frequency from half the Lyman- $\alpha$  resonance [31]. The frequency integral of  $L$  is normalized to unity.

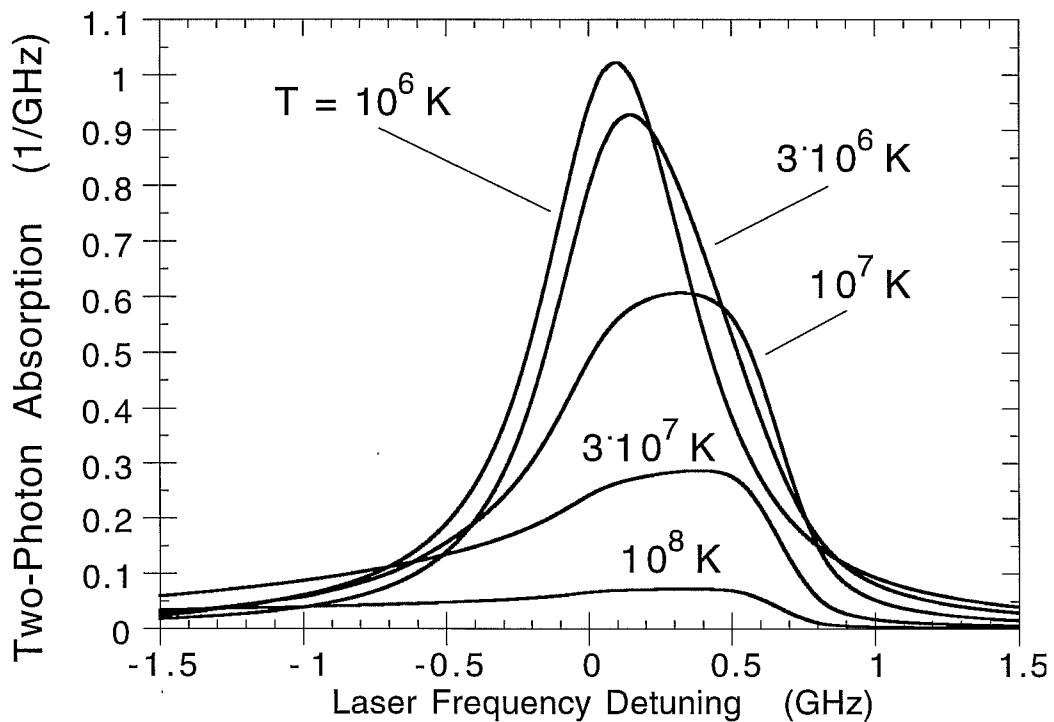
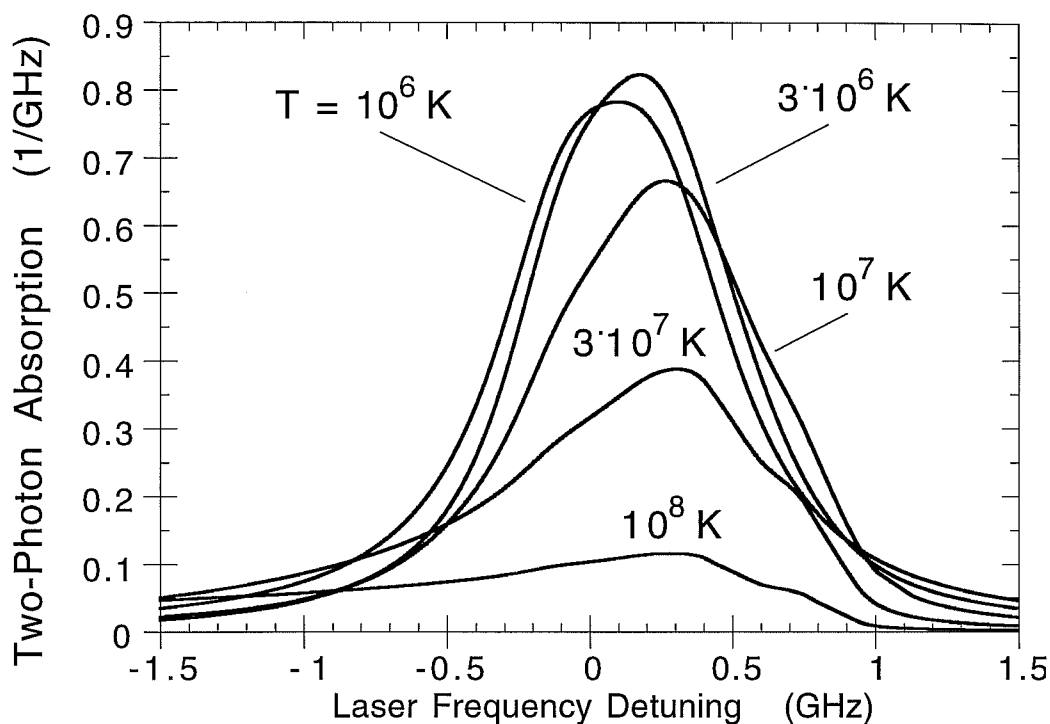


Figure 2.3 Calculated line shape  $L$  of two-photon absorption in deuterium for various kinetic temperatures  $T$ . The free variable is the detuning of laser frequency from half the Lyman- $\alpha$  resonance [31]. The frequency integral of  $L$  is normalized to unity.



**Figure 2.4** Calculated line shape  $L$  of two-photon absorption in tritium for various kinetic temperatures  $T$ . The free variable is the detuning of laser frequency from half the Lyman- $\alpha$  resonance [31]. The frequency integral of  $L$  is normalized to unity.

### 2.2.2 The PSI-1 plasma

Conditions at the *plasma generator PSI-1* of the Max-Planck-Institut are different from fusion plasmas in several respects. Namely temperature and magnetic field strength are much smaller compared to big plasma machines (e.g. ASDEX Upgrade, TEXTOR 94, JET).

This means that the line shapes  $L$  for two-photon absorption in the PSI-1 are different as well. Figure 2.5 and 2.6 show the equivalent PSI-1 curves for hydrogen and deuterium, respectively. Both were calculated for a kinetic particle energy of 3 eV and ion densities  $N_I$  of  $10^{12} \text{ cm}^{-3}$  and  $10^{13} \text{ cm}^{-3}$ .

The broadening of every single component of the Stark-Zeeman triplet is much smaller compared to the previously shown line shapes for tokamak conditions. The same is true for the splitting itself, especially in deuterium. Interesting to note is the strong influence of the Stark broadening on the shape of the absorption lines, which is mainly related to the ion density  $N_I$ . With smaller densities, the line profile in deuterium is slim and compact. Therefore, under PSI-1 conditions the excitation of deuterium is a lot more efficient compared to the one of hydrogen.

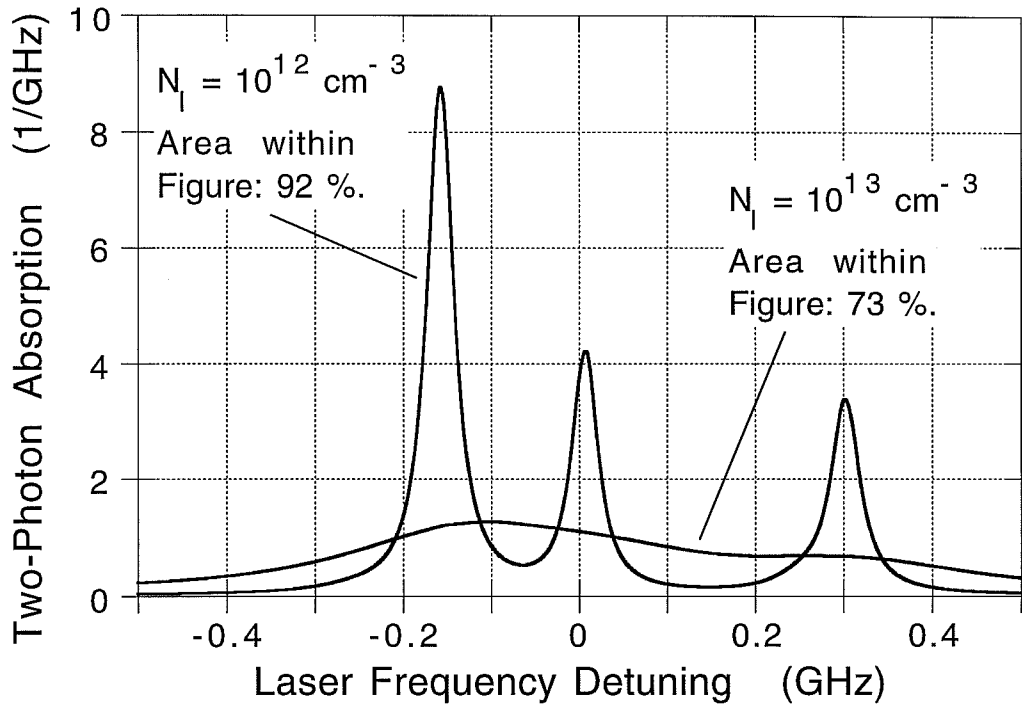


**Figure 2.5** Calculated line shapes  $L$  of two-photon absorption in hydrogen for PSI-1 conditions. The free variable is the detuning  $\Delta\nu$  of the laser's frequency from half of the Lyman- $\alpha$  frequency [31].

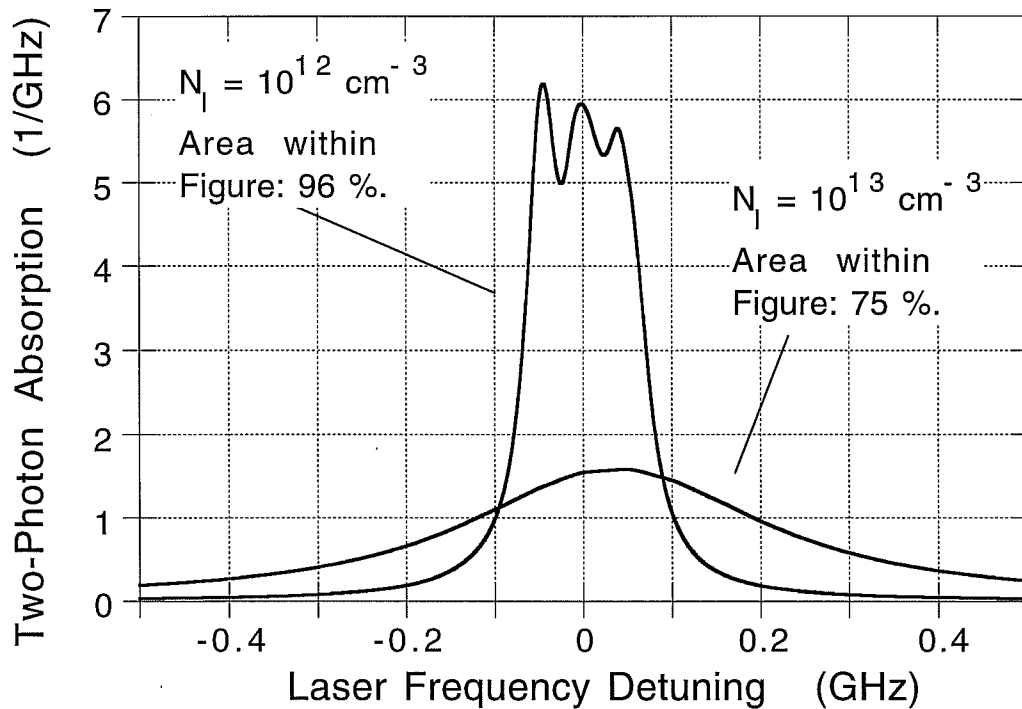


**Figure 2.6** Calculated line shapes  $L$  of two-photon absorption in deuterium for PSI-1 conditions. The free variable is the detuning  $\Delta\nu$  of the laser's frequency from half of the Lyman- $\alpha$  frequency [31].

Consequently, we did perform most of the measurements at the PSI-1 with deuterium. Even in hydrogen-deuterium plasmas we concentrated on the density for deuterium.

Further theoretical predictions of Seidel claimed that there should be no significant shift of the wavelength with respect to the unperturbed Lyman- $\alpha$  transition if  $L_\alpha$ -TALIF measurements are done at the PSI-1. Furthermore, it was said that the fluorescence signal is to occur within an interval of 10ns after the laser pulse, whose FWHM was 2.5 ns. Both predictions were verified by experiments, which are explained in the following chapters.

This verification points out that Voslamber and Seidel's theory considering the application of  $L_\alpha$ -TALIF at fusion-plasmas, delivers also correct results for PSI-1 conditions. Hence this verification supports the conviction that predictions for fusion plasmas are correct as well.

## 2.3 Absolute atomic number densities

Now we are going to consider what quantities have to be measured in order to get absolute values of the *atomic number density* by use of Doppler-free  $L_\alpha$ -TALIF.

As a consequence of pulsed two-photon excitation the time integrated laser induced radiant intensity  $\langle I_{LIF} \rangle$  of the  $L_\alpha$ -TALIF signal and the atomic number density  $N$  are linked as follows:

$$\langle I_{LIF} \rangle := \int_{\Delta t} I_{LIF} dt = \int_V N \cdot Y dV' \cdot Q_\gamma / 4\pi , \quad (2.7)$$

where  $V$  is the measurement volume in the plasma,  $Y$  is the time integrated Lyman- $\alpha$  fluorescence yield,  $Q_\gamma$  stands for the energy per photon at the Lyman- $\alpha$  wavelength 121.6 nm and  $\Delta t$  is the length of the TALIF signal in time.

The determination of absolute values of the density  $N$  requires the measurement of absolute of  $\langle I_{LIF} \rangle$ , i.e. a *calibrated detection system*.

Calibration of our  $L_\alpha$ -fluorescence detection system was easily done by use of a special Lyman- $\alpha$  lamp L (Ch. 3.3). During calibration, a  $L_\alpha$ -lamp of known radiant intensity  $I_L$  sheds a constant irradiance  $E$  onto the detection system. This yielded a dc current  $C_L$  at the output of the photomultiplier tube in the detection system:



$$C_L \sim E = I_L \cdot \Omega_L . \quad (2.8)$$

$\Omega_L$  is the easily measurable solid angle between the lamp L and the and the collecting lens in the image system of the detector (Figure 3.6). So the calibration delivered the constant of proportionality between an irradiance  $E$  falling onto the detection system and the resulting dc current  $C$ .

Now, when the stationary plasma background radiation was observed with the detection system, the direct current  $C_P$  of the PMT was proportional to the plasma radiant intensity  $I_P$  and the used solid angle  $\Omega_P$  equivalently to Eq. (2.8).

In both relations the constant of proportionality is the same, thus it is:

$$C_L / C_P = I_L \cdot \Omega_L / (I_P \cdot \Omega_P) . \quad (2.9)$$

Therefore, the measurement of the dc currents  $C_L$  and  $C_P$  yielded the radiant intensity  $I_P$  of the observed plasma.

The absolute value of the radiance  $L_P$  of the plasma background radiation is:

$$\begin{aligned} L_P &= I_P / A \\ &= (C_P / C_L) \cdot (\Omega_L / \Omega_P) \cdot I_L / A , \end{aligned} \quad (2.10)$$

where  $A$  is the two-dimensional projection of the observed plasma measurement volume in the plasma onto the PMT entry slit.

We have seen, that the radiance  $L_P$  of the plasma can be found by *passive* observation. Now we proceed to *active* spectroscopy. Performing TALIF on a plasma with pulsed laser radiation yields time dependent current pulses  $C(t)$  at the PMT due to the laser-induced fluorescence signal. However, these current pulses are superimposed to the dc current  $C_P$ , produced by the above mentioned, quasi stationary plasma background radiation  $L_P$ .

The time integrated signal  $S_{LIF}$  of a single current pulse  $C(t)$  is proportional to the time integrated radiant intensity  $\langle I_{LIF} \rangle$  of the laser-induced fluorescence and the solid angle  $\Omega_{LIF}$ , under which the detection system collects the fluorescence:

$$S_{LIF} \sim \langle I_{LIF} \rangle \cdot \Omega_{LIF} . \quad (2.11)$$

Although the radiant intensity  $I_P$  of the plasma background radiation is not pulsed, an equivalent equation can be stated for  $I_P$  and  $\Omega_P$  with respect to the same time integration interval  $\Delta t$ . Again the constant of proportionality in both relations is the same. This time it considers the transmittance of the detection system. Therefore:

$$S_{LIF} / S_P = \langle I_{LIF} \rangle \cdot \Omega_{LIF} / (I_P \cdot \Omega_P) . \quad (2.12)$$

Equation (2.9) delivers  $I_P$ , which is inserted into rearranged Eq. (2.12):

$$\langle I_{\text{LIF}} \rangle = (S_{\text{LIF}} / S_P) \cdot (C_P / C_L) \cdot (\Omega_P / \Omega_{\text{LIF}}) \cdot (\Omega_L / \Omega_P) \cdot I_L . \quad (2.13)$$

Together with Eq. (2.10) it follows for the radiant intensity  $I_{\text{LIF}}$ :

$$\langle I_{\text{LIF}} \rangle = (S_{\text{LIF}} / S_P) \cdot (\Omega_P / \Omega_{\text{LIF}}) \cdot L_P . \quad (2.14)$$

By combining equations (2.7) and (2.14) and using the equation for the photon radiance of the plasma background  $L'_P = L_P / Q_Y$ , finally one gets:

$$N = 4\pi \cdot (S_{\text{LIF}} / S_P) \cdot (\Omega_P / \Omega_{\text{LIF}}) \cdot L'_P \cdot \Delta t / (V \cdot Y) . \quad (2.15)$$

This is the very equation showing directly all the input quantities needed to get absolute atomic number densities. The Lyman- $\alpha$  yield  $Y$  is the only calculated quantity in this equation. The comprehensive approach for calculating  $Y$  under consideration of all experimental relevant parameters is explained in the next chapter.

## 2.4 The Lyman- $\alpha$ yield

The Lyman- $\alpha$  yield  $Y$  is defined as the *probability* for the emission of a two-photon induced Lyman- $\alpha$  photon per atom in the ground state. It depends on the spatial and temporal distribution of the laser irradiance in the measurement volume and other experimental parameters. For completeness, the irradiance's frequency dependence was considered, too.

Figure 2.7 shows a simplified energy level diagram for hydrogen together with all transitions taken into account in this work. Apart from minor changes in the given wavelengths this diagram is valid for deuterium and tritium, too.

As already explained with the calculated absorption profiles in Figure 2.6, density measurements focused on deuterium because it has a more compact and less splitted absorption profile compared to hydrogen. This advantage holds good in the whole ion density range of the PSI-1. Measurements of the two-photon absorption profile in deuterium at PSI-1 always showed a broadened profile much larger than the Zeeman splitting, what can be seen in Fig. 2.6. Determination of its spectral width shall be explained in Chapter 4.1. *Fine-structure* for the 2P level can be neglected here.

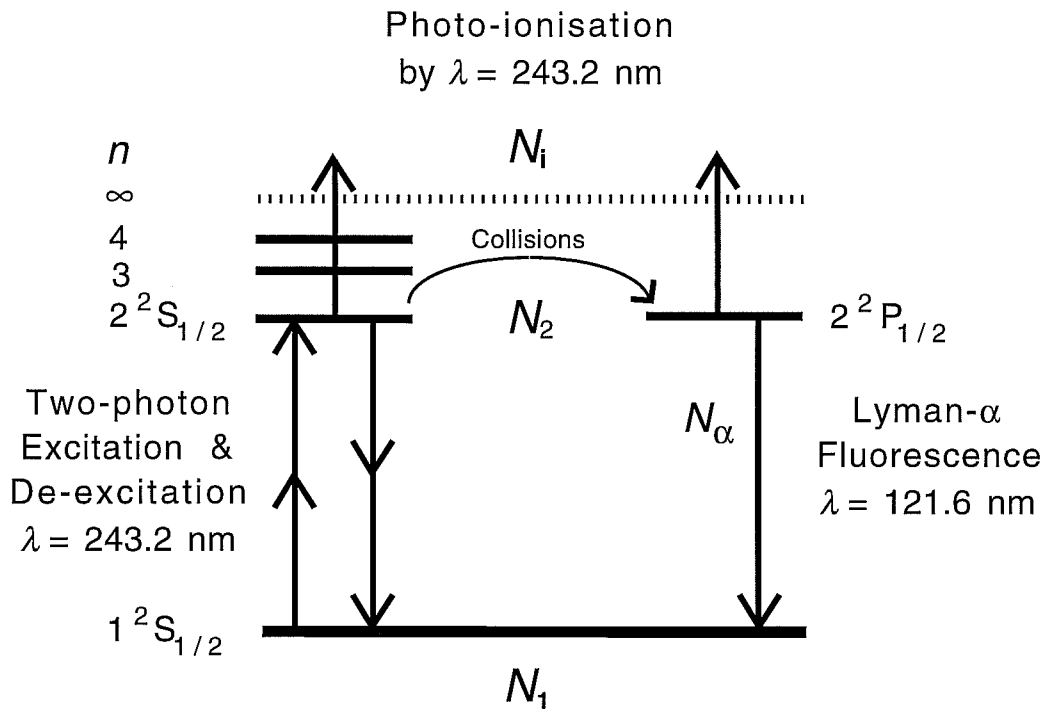


**Figure 2.7** Excitation, de-excitation and ionisation processes in the atoms of the plasma while laser radiation is present.

By laser-induced two-photon absorption the atoms perform a  $1S \rightarrow 2S$  transition. This process now decreases the amount  $N_1$  of atoms in the ground state, and increases the number  $N_2$  of atoms in the excited state  $n = 2$ . Afterwards they are *collisionally transferred* into the  $2P$  level, from which spontaneous one-photon emission occurs. Under tokamak plasma conditions the collision transfer is less important because the level excited by two-photon absorption is a strong mixture of the eigenstates for the  $2S$  and  $2P$  levels.  $N_\alpha$  is the number of atoms who decay in this kind by emitting a fluorescence photon at the  $L_\alpha$ -wavelength (121.6 nm). The quantity  $N_2$  comprises all the  $n = 2$  excited atoms, not caring whether they are in the  $S$  or  $P$  orbital. This is possible, for all the atoms excited to  $n = 2$  must either change from  $2S \rightarrow 2P$  and immediately decay, or undergo ionization by absorbing a third photon each.  $N_i$  is the number of ionized atoms. They are lost for the process under examination because recombination is negligible within the duration of a 2.5 nano-seconds lasting laser pulse.

Next, we take a closer look at the *temporal* and *spatial distribution* of the laser irradiance. Laser radiation, which induced the described processes, was pulsed laser radiation. For the plasma beam at PSI-1 had a considerable velocity orthogonally to the axis of the laser beams, with each laser pulse at a repetition rate of 10 Hz a new

volume of atoms was excited by each laser pulse. Because the basic plasma parameters at PSI-1 could be kept constant on time periods, which are much longer than the inverse of the repetition rate, the plasma can be regarded as stationary from laser pulse to laser pulse.

However, looking at the quantities  $N_x$  ( $x = 1, 2, i, \alpha$ ) on the time scale of a single laser pulse, i.e. on the *sub-nanosecond* scale, they are time dependent:  $N_x = N_x(t)$ . To consider this time dependence within the calculation of the  $N_x$  values, the irradiance  $E$  is set to be varying accordingly to the temporal pulse profile of the laser, i.e.  $E = E(t)$ . It was not kept constant as in the work of Goeckner and Goree [33] - and it was treated even space dependent as we will see later.

The shape  $E(t)$  of the irradiance  $E$  was taken from the measured temporal shape of the laser pulses. Figure 2.8 shows such a temporal pulse profile.  $E(t)$  was not reproduced mathematically in an identical way, but has been approximated. Examinations with variations in the mathematical representation of the pulse structure showed a negligible error contribution by this simplification.

The approximation was derived from a Gauss-function by cutting it into two symmetrical parts. The full width at half maximum (FWHM) of this function  $Z(t)$  is chosen to be equal to the measured value.

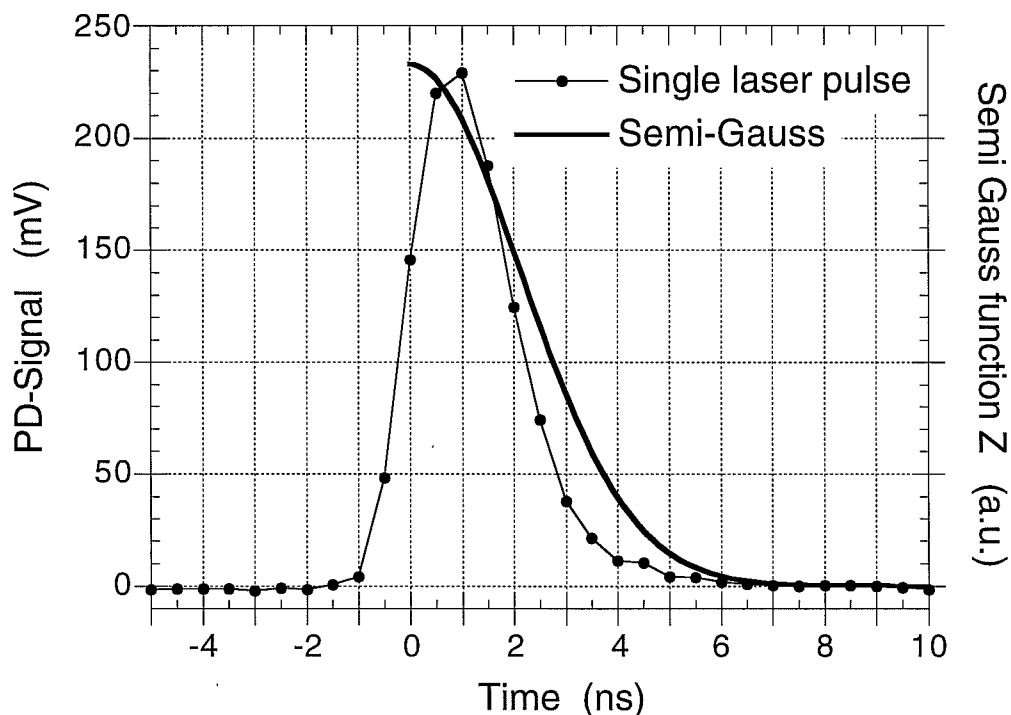


**Figure 2.8** A measured typical laser pulse profile is shown. For the calculations it is approximated with good accuracy by a semi Gauss-shaped function  $Z(t)$ .  $Z$  is normalized to unity.

Now, a short *preview* is given on the procedure of calculating the yield  $Y$  for actual experimental conditions [34]. The whole calculation is a three-step process. Firstly,  $Y$  is calculated in dependence of the quoted semi-Gauss temporal profile and the frequency domain, in the irradiance range of interest:

$$Y = Y(E[t, \nu]) . \quad (2.16)$$

In a second step the actual spatial irradiance distributions of the laser beams have to be incorporated into the computation, delivering the corresponding yield distribution. Finally, in the third step, the *average value* from this yield distribution is calculated.

Now, before establishing the coupled rate equations, a look at the single processes is taken. The *excitation rate*  $R_{12}$  for the two-photon induced excitation from the  $n = 1$  level is given by:

$$R_{12} = \sigma_{12} \cdot L(\nu_A + \nu_B) \cdot (E_A / (h \cdot \nu_A)) \cdot (E_B / (h \cdot \nu_B)) \cdot G, \quad (2.17)$$

where  $\nu_A, \nu_B$  are the frequencies of the two laser beams A and B.  $L$  is the line shape function of the absorbing ground state atoms,  $\sigma_{12}$  is the two-photon absorption cross section of the hydrogen isotope's 1S $\rightarrow$ 2S transition:

$$\sigma_{12}^{(2)} = 1.43 \cdot 10^{-43} \text{ m}^4 \quad [35, 36], \quad (2.18)$$

and  $G$  is a factor describing the statistical interdependence of the two beams [37]. In case of two coherent, single-longitudinal mode beams  $G$  equals 1 [39].

In this work the two beams were made by splitting a single laser beam into two parts. Therefore, it was essentially:  $\nu_A = \nu_B =: \nu$ .

Thus, the *ionisation rate*  $R_{2c}$  is readily written in form of:

$$R_{2c} = \sigma_{2c} \cdot (E_A + E_B) / (h \cdot \nu) . \quad (2.19)$$

$\sigma_{2c}$  denotes the cross section for ionisation out of the first excited state in hydrogen isotopes and has the value:

$$\sigma_{2c} = 4.70 \cdot 10^{-22} \text{ m}^2 \quad [28] . \quad (2.20)$$

As mentioned before the irradiance  $E$  is treated spectrally and temporally resolved:

$$E_x(\nu, t) = E_x \cdot Z(t) \cdot V(\nu) \quad (x = A, B) \quad (2.21)$$

$E_x(\nu, t)$  can be factorized into a triple product:  $E_x$  is a constant irradiance defined as the mean value in time and frequency; the semi Gauss function  $Z(t)$  shown in Figure 2.8 and  $V(\nu)$ , which is a Gauss function describing the spectral shape of the single-mode laser radiation. Both functions  $Z$  and  $V$  are normalized to unity and

are taken to be the same for the two counterpropagating laser beams A and B. Both beams may only differ in their mean irradiance  $E_x$  due to differences in pulse energy of beam A and B for they propagate along different optical paths into the measurement volume.

Equation (2.21) inserted into Eq. (2.17) and integrated over all frequencies yields:

$$\begin{aligned} R_{12}(t) &= \iint V(\nu_A) \cdot V(\nu_B) \cdot L(\nu_A + \nu_B) d\nu_A d\nu_B \cdot Z^2(t) E_A E_B \sigma_{12} / (h\nu)^2 \\ &= (4 \ln 2 / \pi)^{1/2} \cdot (2 \cdot \delta\nu_V^2 + \delta\nu_L^2)^{-1/2} \cdot Z^2(t) E_A E_B \sigma_{12} / (h\nu)^2 \quad (2.22) \end{aligned}$$

by use of a simple transformation in the variables  $q := \nu_A + \nu_B$ . This transformation allows to solve the convolution integral easily for all the profiles are Gauss profiles.  $\delta\nu_V$  and  $\delta\nu_L$  denote the FWHM values of the spectral function  $V$  and the absorption line shape function  $L$ . Measurement yielded  $(0.45 \pm 0.04)$  GHz and  $(0.36 \pm 0.02)$  GHz for  $\delta\nu_V$  and  $\delta\nu_L$ , respectively (Ch. 4.1.1).

Now, that the excitation rate  $R_{12}(t)$  is only time dependent, it is ready for a temporal integration. Within the laser-induced processes elucidated by Figure 2.7,  $R_{12}(t)$  occurs not only at the excitation but also at the stimulated emission  $2S \rightarrow 1S$ , i.e.  $R_{12} = R_{21}$ . However,  $R_{12}$  and  $R_{21}$  are acting on different population densities  $N_1$  and  $N_2$ , respectively.

The corresponding *coupled rate equations* describing the temporal evolution of the processes shown in Figure 2.7 are the following:

$$dN_1/dt = -N_1 c_{12} \cdot E(t)^2 + N_2 c_{12} \cdot E(t)^2 + N_2 \cdot \tau_{21}^{-1} \quad (2.23)$$

$$dN_2/dt = N_1 c_{12} \cdot E(t)^2 - N_2 c_{12} \cdot E(t)^2 - N_2 \cdot \tau_{21}^{-1} - N_2 c_i \cdot 2 \cdot E(t), \quad (2.24)$$

where  $E(t) := (E_A + E_B) \cdot Z(t) / 2$  is set.  $c_{12}$  and  $c_i$  are constants including the cross section for two-photon excitation and the ionization cross section, respectively:

$$\begin{aligned} c_{12} &:= 9.8 \cdot 10^{-5} (\text{MW}/\text{cm}^2)^{-2} \text{ns}^{-1} \\ c_i &:= 5.8 \cdot 10^{-3} (\text{MW}/\text{cm}^2)^{-1} \text{ns}^{-1}. \end{aligned}$$

The first part in the differential equations accounts for the nonlinear two-photon absorption excitation. It carries a negative sign in Eq. (2.23) for it depletes the ground state and hence a positive sign in Eq. (2.24) for it fills the  $2S$  state. The next term stands for stimulated emission.  $\tau_{21}$  is the *decay constant*, which includes not only the decay time for the Lyman- $\alpha$  fluorescence ( $\tau = 1.6$  ns [38]) but also the time needed for the  $2S \rightarrow 2P$  collisional transfer. This transfer time, which is representing the collisions with charged particles, is depending on the *ion* number density in the plasma, not on the measured atomic, i.e. neutral particle density.

Temporal resolved measurements of the Lyman- $\alpha$  fluorescence relative to the inducing laser pulses allowed for a measurement of  $\tau_{21} = (8 \pm 1)$  ns (Chapter 4.2). The complete term  $N_2 \cdot \tau_{21}^{-1}$  gives the number of photons at Lyman- $\alpha$  per time unit. Time integrated, it is the *decisive quantity* to be measured by our detection system. Finally, the last term in Eq. (2.24) accounts for the ionisation losses out of the  $n = 2$  level.

*Recombination* of atoms and *reabsorption* of Lyman- $\alpha$  fluorescence radiation are not included in the differential equations: Recombination on the 2.5 ns time scale is negligible and reabsorption of Lyman- $\alpha$  radiation was not measurable (Ch. 4.1.5) and therefore negligible in first order as well.

For  $N_1$  is the atomic number density which we are seeking for, Eqs. (2.23) and (2.24) have to be divided by  $N_1$  in order to account for a *relative* evolution of the population densities. The Lyman- $\alpha$  *yield*  $Y$  is now defined as the temporally integrated change of the relative population density  $N_2^r := N_2(t) / N_1(t=0)$  due to Lyman- $\alpha$  fluorescence:

$$Y := \int N_2(t) \cdot \tau_{21}^{-1} dt / N_1(t=0) . \quad (2.25)$$

Equations (2.23) and (2.24) display the strong dependence of the induced transitions on the laser irradiance  $E(t)$  and consequently the mean value  $E_x$  in Eq. (2.21). Figures 2.9 and 2.10 show the temporal evolution of the relative population densities  $N_1^r$  and  $N_2^r$  for two different values of  $E_x$ , relevant in the density measurements.

The ground state got depleted by the laser pulses and recovers after 20 ns to 76 % of its initial value, whereas with  $E = 200$  MW/cm<sup>2</sup> this value becomes 31% - more as half as low. The peak population in the excited state now reaches 20%, when an irradiance of 100 MW/cm<sup>2</sup> just yields about 12%. However, twice as much irradiance on this level isn't beneficial as one can see in the yield values  $Y$ .

An irradiance of  $E = 100$  MW/cm<sup>2</sup> generates a fluorescence yield of  $Y = 9.5\%$ , when twice as much irradiance generates just a value of  $Y = 8.4\%$ . This can be understood by looking at the percentage  $N_1^r$  of excited atoms, which get lost due to ionisation. Doubling of  $E$  results in an ionisation that is three times as high.

Therefore, the higher rate of excited atoms with 200 MW/cm<sup>2</sup> cannot be transferred efficiently into  $L_\alpha$ -photons anymore. The reason for this is the much higher ionisation loss with  $E = 200$  MW/cm<sup>2</sup>.

The optimum irradiance  $E_{opt}$  can be found by searching the maximum of the yield function  $Y = Y(E)$ . A graphical presentation of this function is given in Figure 2.11.

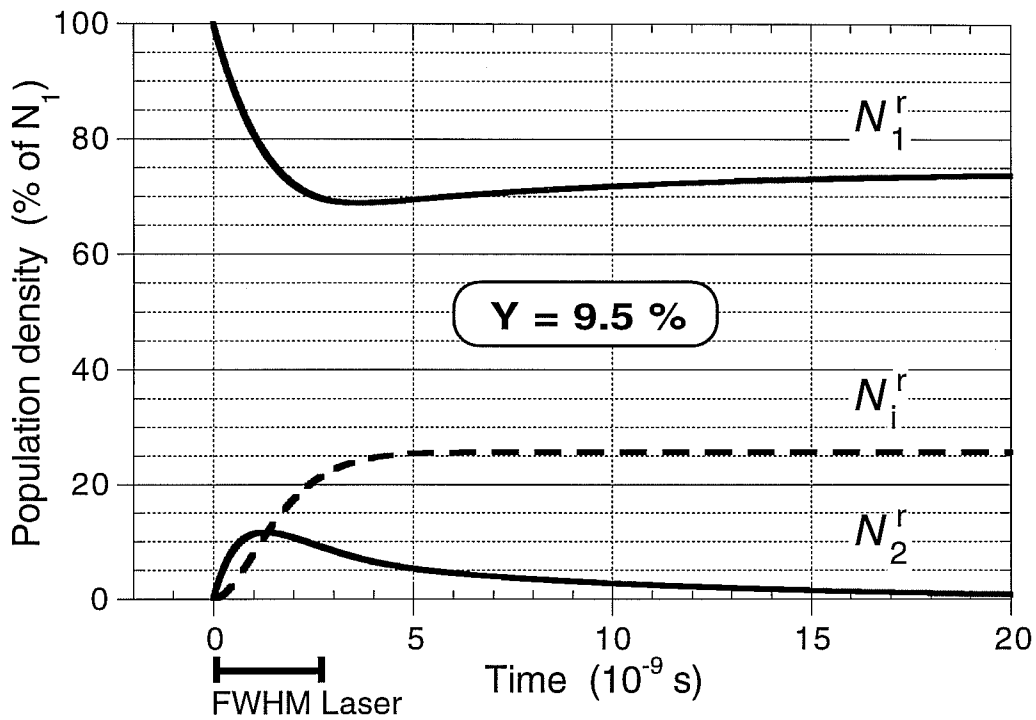


Figure 2.9 Temporal evolution of relative population densities for an irradiance of 100 MW/cm<sup>2</sup>. The laser pulse length of 2.5 ns is indicated, too.

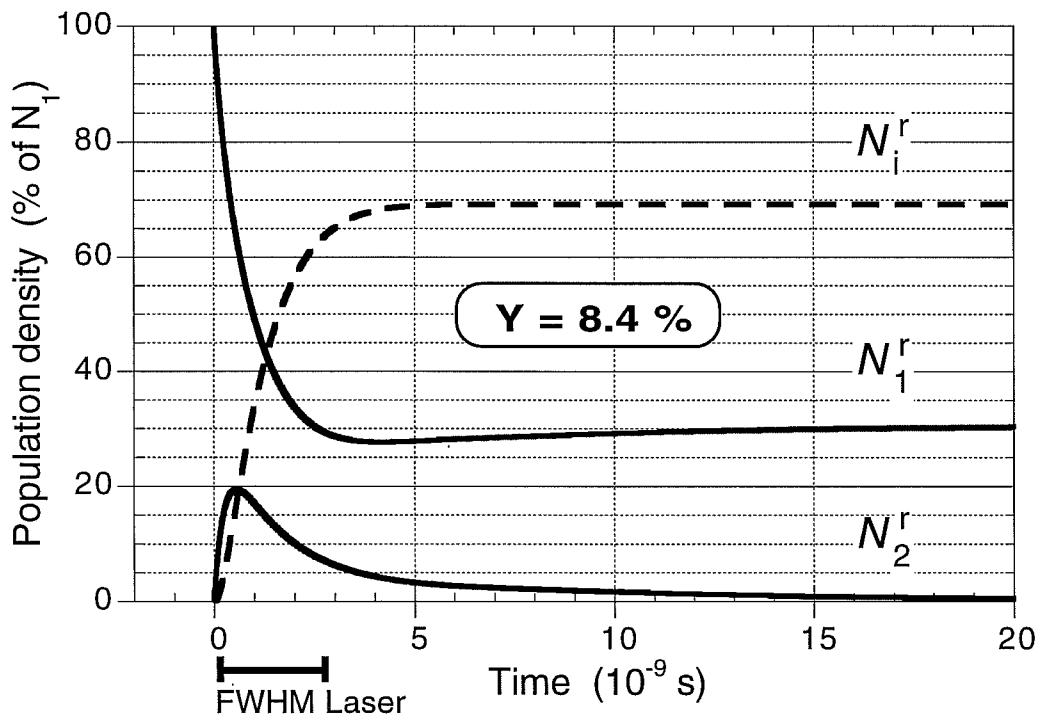


Figure 2.10 Temporal evolution of relative population densities for an irradiance of 200 MW/cm<sup>2</sup>. The laser pulse length of 2.5 ns is indicated, too.



Photo-ionisation has no significant influence below irradiances of approximately  $20 \text{ MW/cm}^2$  and  $Y$  varies proportional to the square of  $E$ . However, with the onset of photo-ionisation for increasing irradiances, the Lyman- $\alpha$  yield gets rapidly dominated by photo-ionisation. This is expressed by the pronounced maximum of the function  $Y(E)$  in Fig. 2.11.

Looking for the *optimum irradiance*  $E_{\text{opt}}$ , clearly it is the very one belonging to the biggest value of  $Y$ . Unfortunately, in reality the spatial distribution of a laser's irradiance is not a homogeneous one. Nevertheless, it allows to optimize the spatially averaged  $L_\alpha$ -yield  $Y^*$  (Ch. 4.1.3).

Adjusting the magnitude of the laser irradiance, Figure 2.9 recommends to chose the *irradiance interval* in a way, that it lies around  $E_{\text{opt}}$  but preferably at the right-handed slope. By this, little fluctuations in the laser pulse energy or in the beam overlap within the measurement volume can be minimised in its effects on  $Y$ .

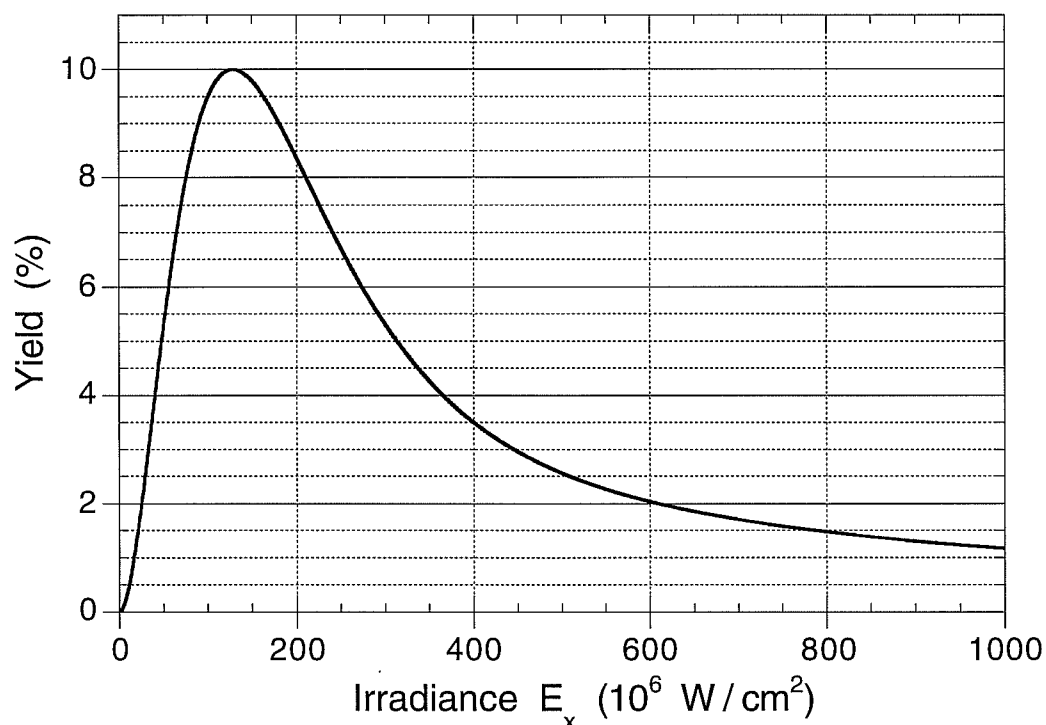


Figure 2.11 Lyman- $\alpha$  fluorescence yield  $Y$  varying with irradiance  $E_x$  per beam.

# 3

## Experimental Setup

The experimental setup consists of three main components:

- the laser spectrometer,
- the detection system and
- the plasma generator PSI-1.

The *laser spectrometer* is the source of pulsed, tunable laser radiation around UV wavelengths of 243 nm, which are needed for inducing the  $1S \rightarrow 2S$  transition in hydrogen isotopes by two-photon absorption. The term “laser spectrometer” designates the complete source, i.e. not only the *lasers* but does comprise the *optogalvanic wavelength reference*, too. Chapter 3.2 deals with the spectrometer.

Once having been excited, the atoms can relax spontaneously by emitting Lyman- $\alpha$  fluorescence, i.e. at a wavelength of 121.6 nm. This fluorescence radiation, which had a duration of approximately 10 ns, has to be measured in order to get the desired atomic number densities according to Eq. (2.15). To measure LIF we used a *VUV-detection system*, which is equipped with several filter systems to reduce background radiation of the hydrogen-deuterium plasmas. This UV-detection system and its most important features shall be described in Chapter 3.3.

The Berlin division of the Max-Planck-Institut für Plasma Physik (IPP) operates the *plasma generator PSI-1*. An aspect for its operation is to serve for the development of plasma diagnostics. We did use the PSI-1 for demonstrating the potential of two-photon absorption laser-induced Lyman- $\alpha$  fluorescence ( $L_\alpha$ -TALIF).

## 3.1 The Plasma Generator PSI-1

### 3.1.1 Technical description

The plasma generator PSI-1 produces a *stationary, magnetically guided plasma beam*, generated by a stabilized high-current arc discharge, which can burn continuously for several hours. It was established to study low-temperature plasmas like they occur for example in the divertor region of tokamaks. Furthermore, it is specially suited for the development of new tokamak related plasma diagnostic. Figure 3.1 shows a cross section of the generator. The length of the generator is about 3 m, the diameter of the vacuum vessel is 0.6 m and the one of the plasma beam ranges between 5...12 cm.

On the right-hand side of the drawing one can see the cathode ( $\text{LaB}_6$ ) and the hollow anode made of copper. Between both electrodes a steady state plasma is generated with discharge currents in between 50...1000 A. The discharge power normally ranges below 200 kW. Deuterium, hydrogen and argon are the used gases. They can be used in mixed ratios as well. Linearly expanding through the differential pumping stages and beam shaping diaphragms (graphite), the plasma beam expands into the *observation chamber*. All the way the beam is guided by the magnetic field, which is produced by four magnetic coils. Finally, the plasma beam hits a neutralizer plate.

Parameter	$\text{H}_2, \text{D}_2$ Plasma
Base Pressure (mbar)	$3 \cdot 10^{-8}$
Working Pressure (mbar)	$10^{-2} \dots 10^{-4}$
Magnetic Field (T)	0.05 ... 0.1
Particle Density @ $T = 1000 \text{ K}$ ( $\text{cm}^{-3}$ )	$10^{14} \dots 10^{12}$
Electron Density ( $\text{cm}^{-3}$ )	$< 2 \cdot 10^{12}$
Electron Temperature (eV)	$\leq 15$

**Table 3.1** Typical parameters at observation chamber of PSI-1 [40].

Table 3.1 gives typical values for the main parameters at the observation chamber.

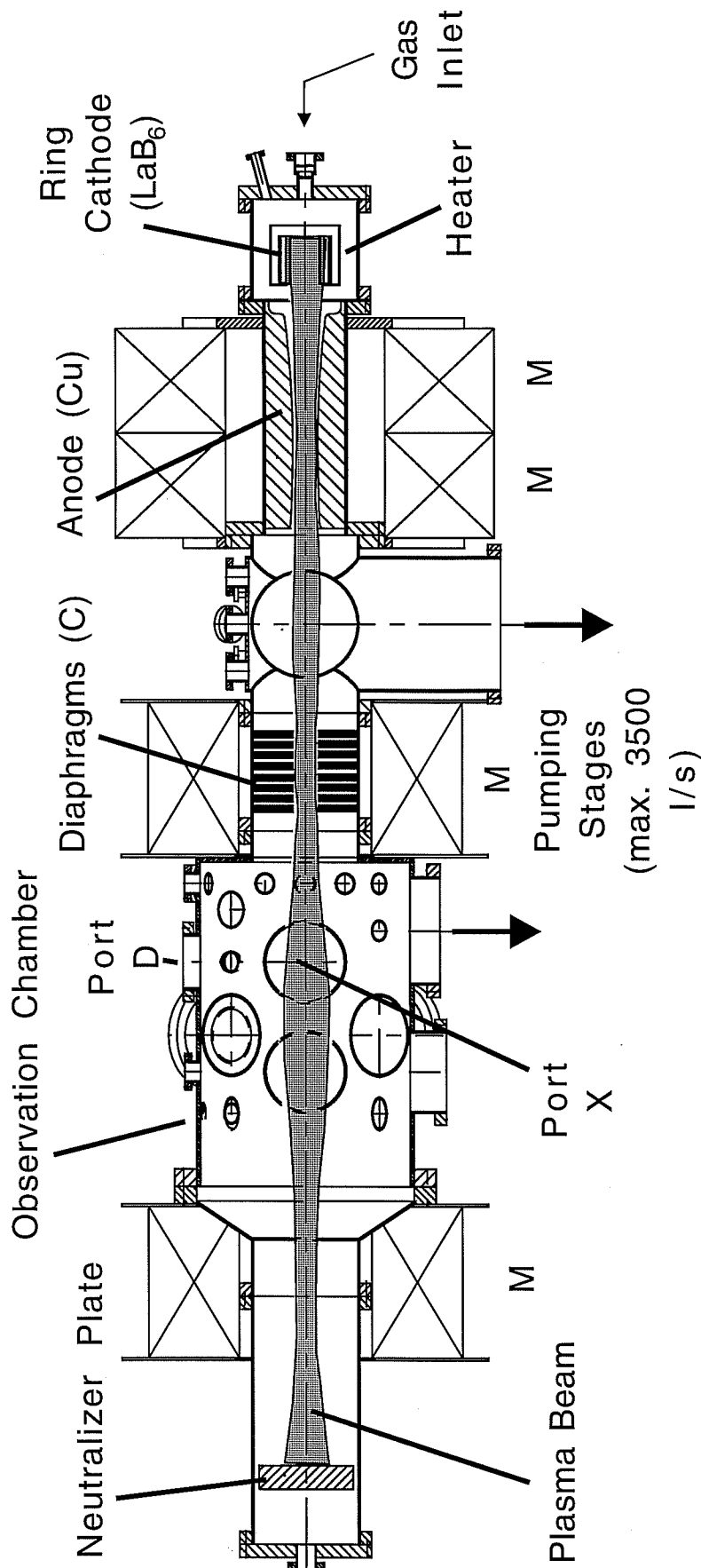


Figure 3.1 Horizontal side view cross section of the plasma generator PSI-1 [41]. The stationary plasma is produced by an anode-cathode discharge, before it expands magnetically guided towards the neutralizer plate. The magnet coils are denoted with the letter M. D marks the port at which the detection system was mounted on top of PSI-1. The laser beams enter PSI-1 at port X propagating orthogonally through the plasma beam.

The observation chamber is the very part of the generator where our  $L_\alpha$ -TALIF measurements took place. At this section (port D) we placed the VUV Lyman- $\alpha$  detection system, looking downwards into the plasma beam.

It is important to notice, that despite the plasma beam velocity, i.e. the velocity of the ions ( $\approx 1$  km/s) which collide with the neutral atoms, nor the mean kinetic energy of the atoms itself was large enough to let the excited atoms leave the observed measurement volume ( $0.1 \text{ cm}^3$ ) within the fluorescence time of about 8 ns. By the way, this assessment is an example for the need of measuring the atom's kinetic energy.

First tests of the VUV-detection system at PSI-1 for the optimization of the signal-to-background ratio  $S_{\text{LIF}} / S_{\text{BG}}$  (Eq. (2.15)) led to a rapid decrease of the PMT's sensitivity. The reason was a very strong VUV background emission of PSI-1. Consequently, the at that time unquantified VUV emission characteristic of PSI-1 had to be measured by passive spectroscopy for a better understanding of the environment for  $L_\alpha$ -TALIF measurements at PSI-1.

### 3.1.2 VUV emission of PSI-1 plasmas

For measuring the VUV emission characteristic of PSI-1, an Actron Research VUV-Spectrometer (ARC Model UHV M-502) with moderate resolution ( $\Delta\lambda = 1 \text{ nm}$ ) was attached to the PSI-1 at a distance of about 1.5 m away from the plasma beam. It was used with the same photomultiplier tube (PMT) and  $\text{MgF}_2$  collecting lens as they were used in the  $L_\alpha$ -detection system for the  $L_\alpha$ -TALIF measurements.

Data were recorded by reading the PMT signal current with an electrometer (Keithley EM 617), which had pico amps sensitivity. The dark current signal of the spectrometer-PMT system was measured by just closing a shutter in front of the spectrometer.

Figure 3.2 shows the spectral variation of the PMT signal due to the VUV background emission of PSI-1 in a deuterium standard plasma at a discharge current of 300 A.

The deuterium Lyman- $\alpha$  peak at 122 nm reaches 200 nA. However, it is truncated in this view graph just to resolve the dynamics of the background emission beside Lyman- $\alpha$ . As one can see, the broadband contribution is significant:

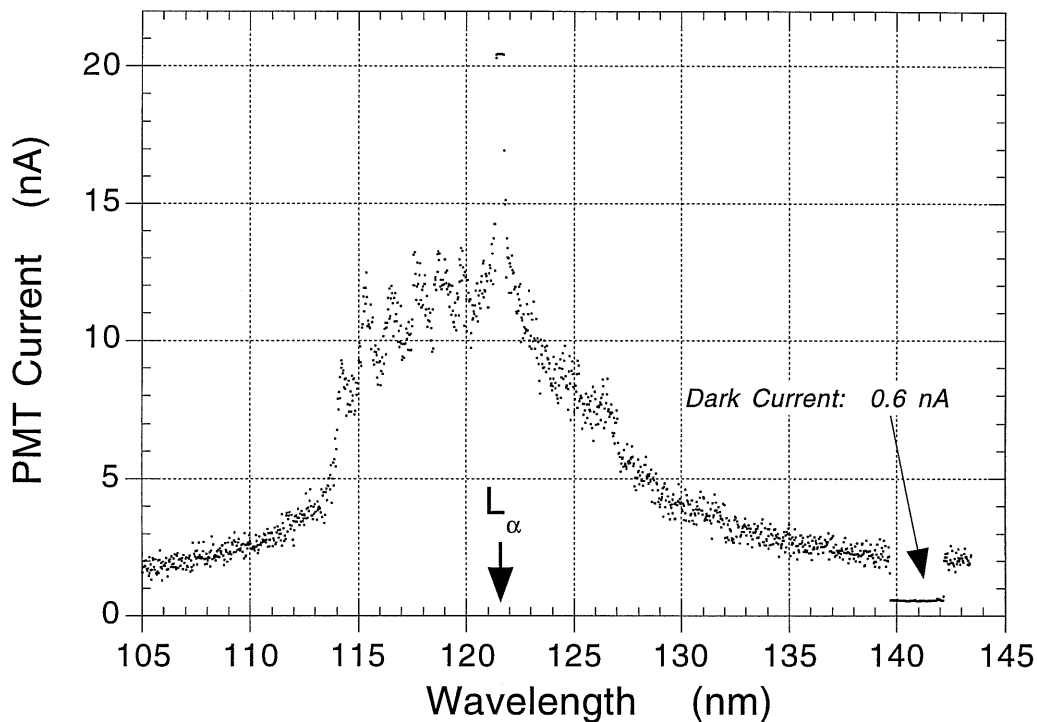


**Figure 3.2** Photomultiplier current signal for the PSI-1 background VUV-emission in the relevant range around Lyman- $\alpha$ . The peak at Lyman- $\alpha$  reaches 200 nA but is truncated in this show graph just to show the detailed structure of the background on both sides of the main peak. The dark current of the spectrometer-PMT system is shown, as well.

The spectral integral without the Lyman- $\alpha$  peak is 6.6 times bigger than the one including only the Lyman- $\alpha$  peak. This broadband emission is explained by the fluorescence of those deuterium molecules, which get excited by collisions with ions of the plasma beam. In that respect, the VUV-background emission of PSI-1 resembles the one of a Lyman- $\alpha$  hydrogen lamp (Fig. 3.7).

Figure 3.2 shows that PSI-1 plasmas are very clean ones, for there are no emission lines of impurity elements like carbon, oxygen or nitrogen.

The sharp decline of the signal current at 114 nm and 127 nm display the PMT's sensitivity and shall be explained with the discussion of the detection system in Chapter 3.3.1.

## 3.2 Single-Mode UV-Laser-Spectrometer

Two-photon absorption is generally characterized by a very small cross section. High irradiances are therefore needed to stimulate two-photon processes sufficiently strong. It is not only essential for a measurement technique to deliver strong signals, but in many applications time resolved information as well. Both requirements can be fulfilled, if *pulsed laser radiation* is used for TALIF measurements. Moreover, if information on atomic number densities shall be gained with every laser pulse, the laser spectrometer must operate with *high stability* in its main parameters like pulse energy, spectral and temporal FWHM etc.

As we have already seen (Ch. 2.1), owing to its simple but very powerful principle, TALIF is an *isotope-selective* diagnostic technique. However, tearing the right benefits out of its potential requires *tunable* laser radiation in the UV spectral range, as one can see by looking at the graphical representation of Lyman- $\alpha$  wavelengths [98a] of all three hydrogen isotopes in Figure 2.1. The generation of this UV laser radiation is described in Chapter 3.2.1. High stability in the performance of the laser-spectrometer also means *good frequency lock* to the desired transition frequency. The optogalvanic principle delivers a practical tool to find and fix the laser frequency to the  $L_{\alpha}$ -transition in hydrogen or deuterium. Chapter 3.2.2 introduces briefly into this technique.

### 3.2.1 Tunable laser radiation at $\lambda = 243$ nm

Aiming to use  $L_{\alpha}$ -TALIF as a diagnostic tool at big plasma machines (e.g. at tokamaks) is deeply linked with the need to use experimental equipment as robust and maintenance friendly as ever possible. *Solid-state lasers* are known for their ease of use and maintenance [42].

A laser system, coming close to these requirements in high shot-to-shot reproducibility was developed by the PTB [43...46]. It is an *all solid-state* laser system, consisting of nothing but commercially available components. However, they were combined with an underlying strategy in a way that yielded much more UV-pulse

energy than commercial available systems itself can provide today. The workhorse can be a single pulsed Nd:YAG laser operating injection seeded in order to get *single-longitudinal mode* operation. The resulting small bandwidth and constant wavelength of the laser radiation are important for an efficient two-photon excitation. However, to get ample laser pulse energy as easy as possible we used two Nd:YAG lasers.

Both Nd:YAG lasers were equipped with frequency-conversion extensions: In specially designed crystals the laser irradiance induces nonlinear processes, which may allow for sum-frequency mixing or difference-frequency mixing. In our case, the fundamental wavelength ( $\lambda = 1064$  nm) of YAG laser no. 1 is converted into 532 nm through second-harmonic generation (SHG). The fundamental radiation of YAG laser no. 2 is converted into 355 nm through third-harmonic generation (THG). Table 3.2 shows their features.

	Nd:YAG Laser No. 1	Nd:YAG Laser No. 2
Model	GCR-250 with Enhanced Spatial Mode Option	Powerlite 9010
Manufacturer	Spectra-Physics, CA, USA	Continuum, CA, USA
Used Output Wavelength (nm)	532	355
Pulse Operation Mode	injection-seeded, Q-switched, single-longitudinal mode (SLM)	
Temporal FWHM (ns)	8	7
Repetition Rate (Hz)	10	
Pulse Energy (mJ)	560	320

**Table 3.2** Characteristics of used Nd:YAG lasers

The SH of Nd:YAG no. 1 pumped a tunable *optical parametric oscillator* (OPO) [47], whose output at a wavelength of 772 nm was amplified in Titanium-Sapphire (Ti:Sa) crystals afterwards. The Ti:Sa crystals were also pumped with the radiation at 532 nm.

Now, in order to get tunable UV-laser radiation around 243 nm for the  $1S \rightarrow 2S$  transition in hydrogen isotopes by two-photon absorption, the TH output of YAG laser no. 2 at 355 nm was sum-frequency mixed with the amplified infrared output of the OPO.



The OPO system we used, based on the work of Bosenberg and Guyer [48]. In the early 90's they succeeded in constructing a single-longitudinal mode OPO with KTP crystals. They integrated their OPO and the following Titanium-Sapphire amplifiers in a versatile PC controlled package. The Ti:Sa amplifiers not only contributed increased power but also better beam quality and irradiance stability. The characteristic features of the OPO-Ti:Sa-system after we improved it for our needs are given in Table 3.3. The follower to the model we modified is nowadays called Mirage 800 and distributed by Continuum.

Modell	HRL-100Z-3A
Manufacturer	STI Optronics, WA, USA
Pump Source for OPO and Amplifier	injection-seeded, high beam quality laser radiation at 532 nm: $450 \text{ mJ} < Q < 625 \text{ mJ}$
OPO Tuning Range (nm)	710 ... 910 (incl. 1 mirror change)
Amplifier	Titanium:Sapphire
Output Pulse Energy	up to 100 mJ @ 772 nm
Temporal FWHM (ns)	2.5
Beam Quality (*D.L.)	< 3
Bandwidth (MHz)	< 500 MHz (SLM)
Output Polarization	> 95% linear
Continuous SLM Scanning Range (cm <sup>-1</sup> )	> 100
Max. Scan Rate (cm <sup>-1</sup> /min)	1

**Table 3.3** Characteristics of the OPO-Ti:Sa-system after we have improved it.

Figure 3.3 shows the combination of all three laser systems into a tabletop arrangement. The final step in the generation of radiation at 243 nm is the sum-frequency mixing of 772 nm and 355 nm in a crystal made of  $\beta$ -Barium Borate (BBO). BBO is a material specially designed for the application in nonlinear optics and provides excellent characteristics for frequency conversion of laser radiation into the UV.

The result is linearly polarized, small-bandwidth  $\Delta\nu = (0.36 \pm 0.04)$  GHz laser radiation at 243 nm with pulse energies up to 50 mJ in  $\Delta t = (2.5 \pm 0.2)$  ns at a pulse repetition rate of 10 Hz. The *efficiency* for the energy and peak-power conversion from the Nd:YAG fundamental (1064 nm) to the radiation at 243 nm was 2% and 7%, respectively.

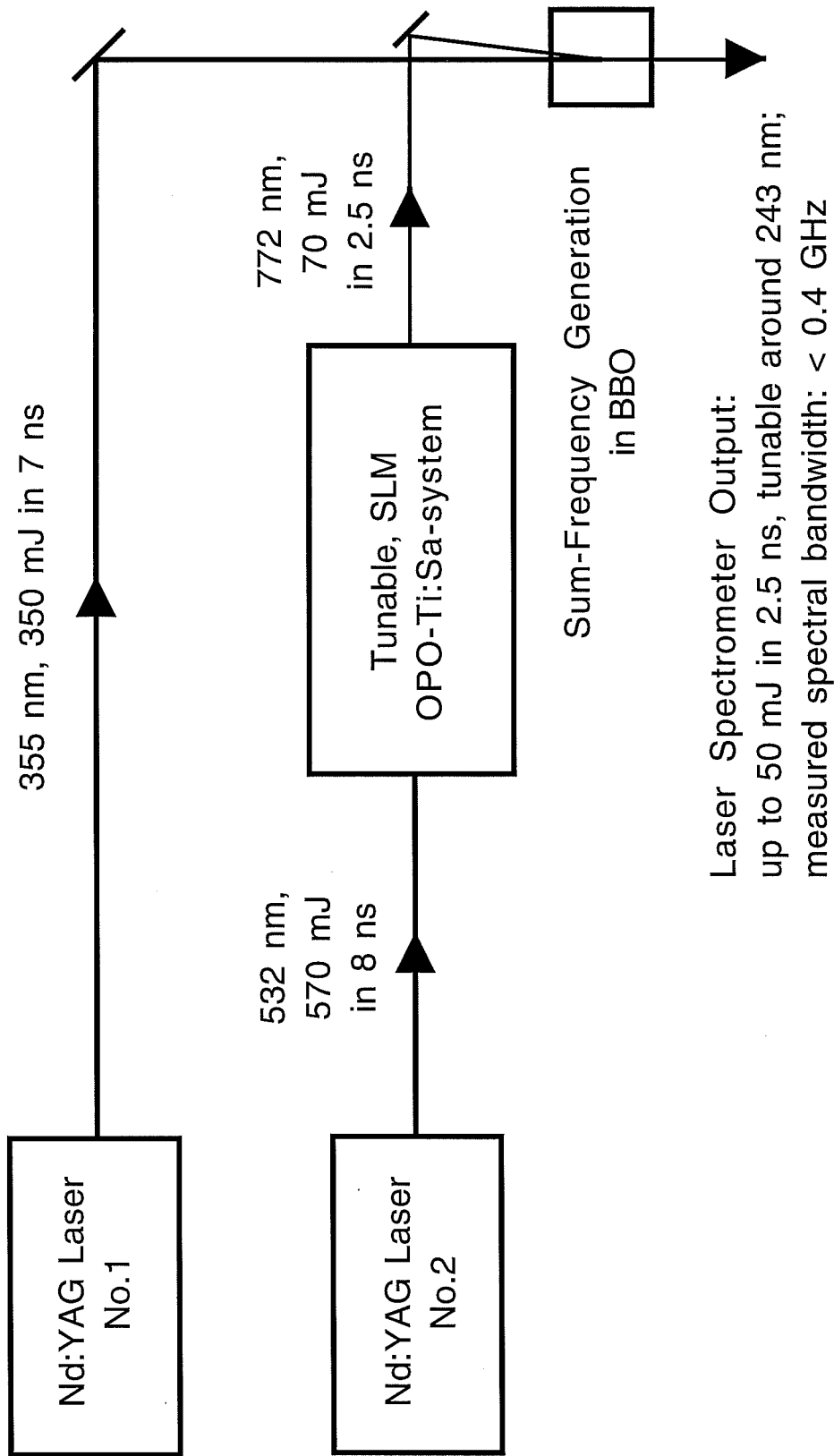


Figure 3.3 Arrangement of the different laser systems within the laser spectrometer.

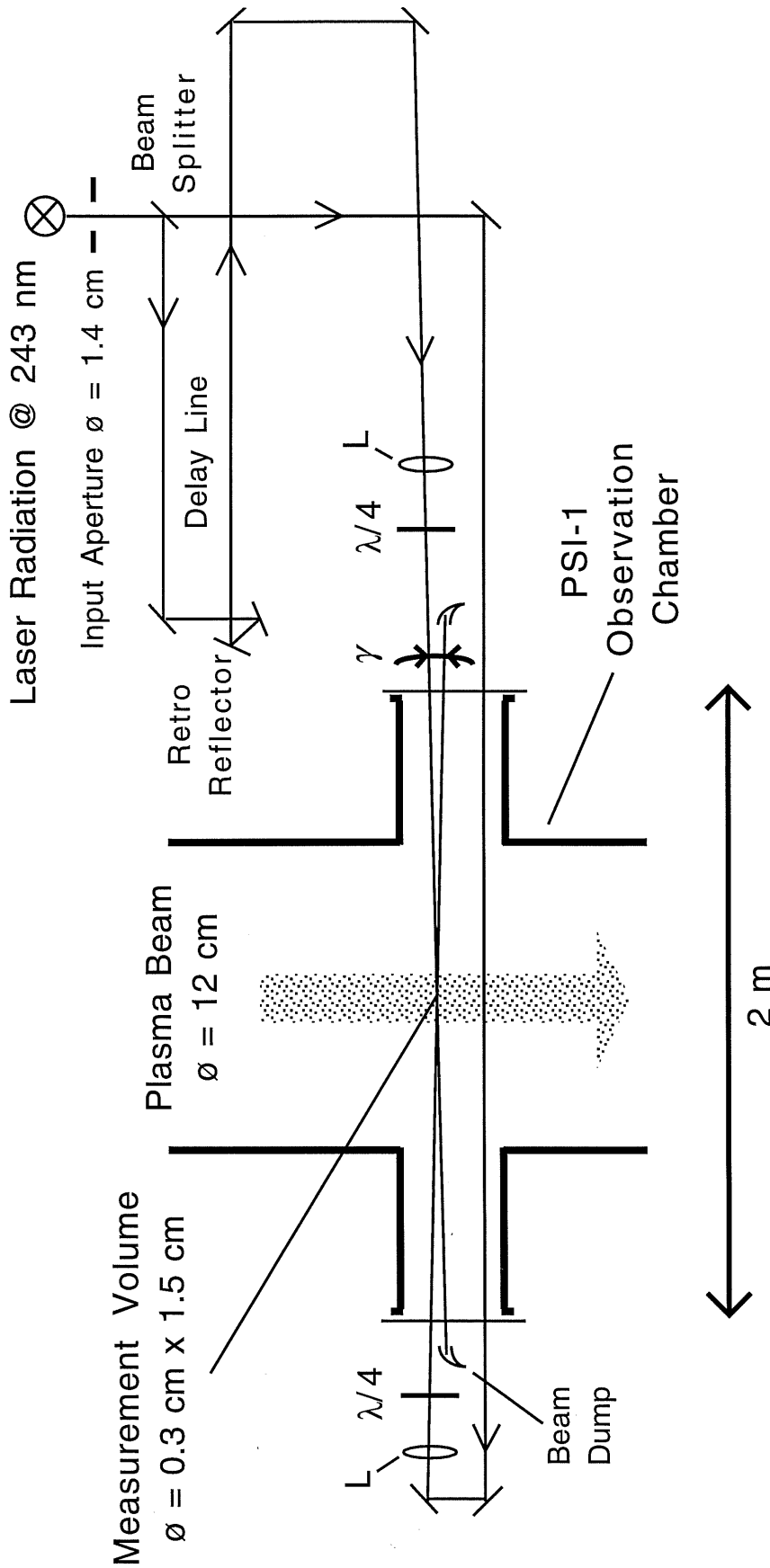
High shot-to-shot stability is valid for the pointing stability ( $10^{-5}$ ) and the irradiance distribution, too. The laser system was located in a laboratory next to the PSI-1. Travelling a distance of approximately 20 m the laser radiation at 243 nm reached the final laser beam preparatory equipment besides the plasma generator.

Figure 3.4 explains this preparation and the optical beam paths for the laser radiation at PSI-1. The laser beam arriving from the laser spectrometer passed through an aperture ( $\varnothing = 1.4$  cm) and was *split into two beams* of equal energy using a beam splitter. One beam was then sent through the PSI-1 observation chamber to the other side of the machine through port X in Fig. 3.1. At the other side of PSI-1 it was redirected into PSI-1 passing through a *collecting lens* ( $f = 1.4$  m). It was located 1.1 m away from the measurement volume producing a beam diameter of 0.3 cm there. The other beam was treated equally after he was sent through a delay line via a retro-reflector in order to let this beam arrive at the measurement volume at the same time as the other beam (which had first to travel to the other side of PSI-1). Both lenses were precisely positioned by step motors moving vertically and horizontally.

*Quarter wave plate* transformed linear into circular polarization. Windows for the laser radiation at 243 nm to enter the vacuum chamber were made out of UV grade synthetic fused silica (UVGSFS) and carried a broadband anti-reflection coating. They were carefully installed at the observation chamber of the PSI-1 to avoid any stress induced birefringency that would have disturbed the circular polarization of the two beams.

The correct path for the laser beams directly through the area under observation by the  $L_{\alpha}$ -detection system, was determined in the following way: Laser radiation at 243 nm was scattered from a small target to the detection system. The target could be brought to the observed area at a time, when the PSI-1 had been opened for maintenance purposes. Laser radiation only lead to a PMT signal, when it had maximum pulse energy and was scattered directly into the  $L_{\alpha}$ -detection-system. Normal stray light of laser radiation at PSI-1 could not be measured with  $L_{\alpha}$ -detection-system, as shall be explained later.

Moving the target and the laser beam axis allowed to maximize the PMT signal, delivering the correct position of the measurement volume. At the beginning of each  $L_{\alpha}$ -TALIF measurement the laser beam axis could be *optimized within a few minutes* by moving the two collimating lenses and maximizing thereby the  $L_{\alpha}$ -TALIF signal at the PMT.



**FIGURE 3.4** Top view on the laser beam arrangement at PSI-1 as used for measurements of kinetic temperatures, i.e. with a small crossing angle  $\gamma$ . Laser radiation arrived from an adjacent laboratory and was split into two beams at the beam splitter. One beam was then sent through the PSI-1 observation chamber while the other was delayed equivalently by use of a retro reflector. Quarter wave plates transformed the linear into circular polarization and a motor driven lens ( $L$ ) for each beam focused them into the observation chamber.

### 3.2.2 Passive frequency locking with an optogalvanic reference cell

In order to find the exact laser wavelength for  $L_{\alpha}$ -TALIF in hydrogen and deuterium the *optogalvanic effect* was used: interaction of resonant radiation with atoms, e.g. in a gas discharge can induce variation in the electrical properties of the discharge. A comprehensive review article dealing with this technique was given by Barbieri and Beverini [49].

In our case, a small cell contained the gas (hydrogen or deuterium) at low pressure (5 mbar), whose Lyman- $\alpha$  transition had to be found. Partial thermal dissociation of the gas molecules was achieved by a resistively heated tantalum wire. Through two windows lying opposite to each other, less than 50  $\mu$ J laser radiation at 243 nm entered the cell, to induce two-photon absorption in the atoms of the gas. Subsequent photo-ionisation, i.e. absorption of a third photon, produced free hydrogen respectively deuterium ions, which were measured at a pickup electrode (-9 V bias voltage) of the cell as a current signal. By tuning the laser radiation at 243 nm over the two-photon resonance for the  $1 \rightarrow 2$  transition, the ion current varied, representing therefore the two-photon absorption profile for the  $1S \rightarrow 2S$  transition of hydrogen or deuterium in the cell. This shows Figure 3.5.

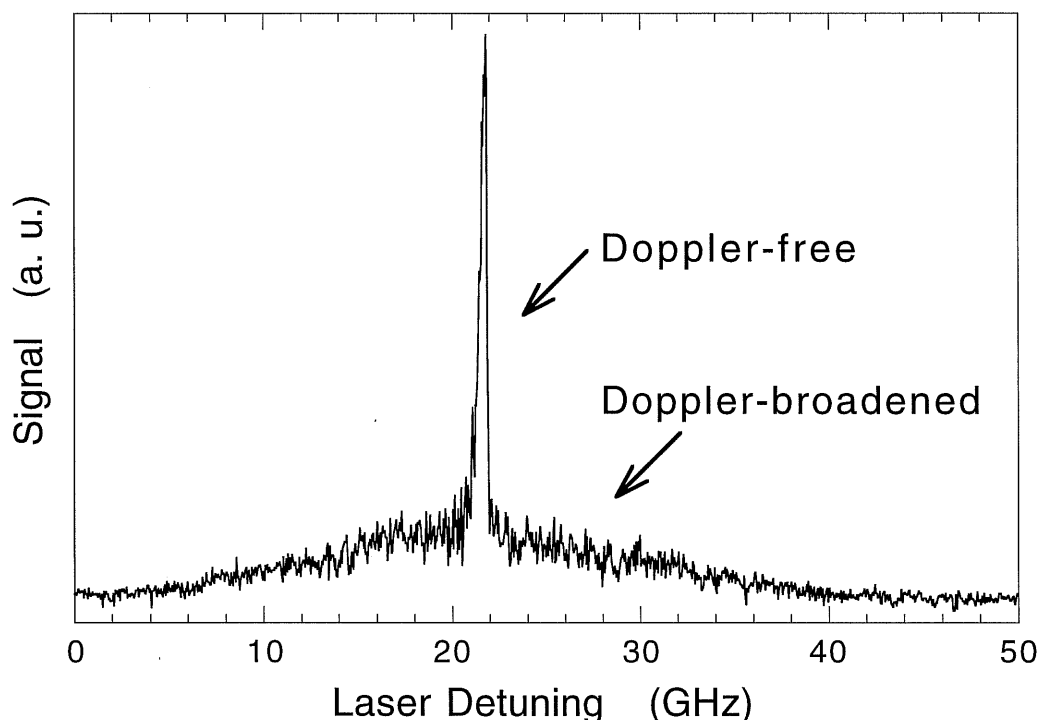


**Figure 3.5** Optogalvanic reference cell signal in deuterium. The signal varies with the detuning of the OPO-Ti:Sa-laser radiation.

Two-photon absorption in the reference cell was achieved by passing the laser radiation through a collimating lens and retro-reflecting it by a concave mirror back into the focus within the cell. Due to the linear polarization, the two photons for an absorption can come out of the same beam at 243 nm. However, only atoms belonging to the correct matching frequency classes can be excited and then ionized. This yields a Doppler-broadened signal. But if the laser radiation is tuned in resonance with the Lyman- $\alpha$  transition, *all atoms* in the cell are in resonance, if the two photons do not originate from the same beam. Thus, a well-pronounced *Doppler-free signal* arises on top of the Doppler-broadened contribution.

The laser frequency in a  $L_{\alpha}$ -TALIF measurement was locked to the Doppler-free signal peak of the reference cell with an accuracy of  $10^{-7}$  by the computer controlled, actively stabilized optical parametric oscillator of the OPO-Ti:Sa-system.

Using the optogalvanic effect is not only a simple and cheap method of controlling the frequency of a laser but also a very sensitive one. Figure 4.1 shows an optogalvanic signal where even the hyperfine structure of hydrogen was resolved.

### 3.3 Lyman- $\alpha$ Detector System

From the beginning of the conceptual phase of the hardware, suited for  $L_{\alpha}$ -TALIF measurements, clearly not only producing high-quality laser radiation at 243 nm was a demanding task. Constructing a versatile VUV- $L_{\alpha}$ -detection-system, meeting requirements like fast response, high sensitivity restricted to a spectral range at 121.6 nm as small as possible, was at least equally important and demanding. In 1994 PTB's  $L_{\alpha}$ -detection-system was ready for testing at the PSI-1. Already then, the prerequisites for options like stepwise signal attenuation by use of  $L_{\alpha}$ -interference filters, oxygen gaseous filtering and gating of the photomultiplier cathode were implemented at the detection system.

A first test of the detection-system at PSI-1 equipped with the interference filters only, led to a remarkable decrease of the photomultiplier tube's (PMT) sensitivity. Already mentioned in Chapter 2.3, the reason for this was a too high load on the PMT due to a broad VUV background emission of hydrogen and deuterium plasmas at PSI-1. This showed, that the anticipated options with the  $L_{\alpha}$ -detection

system had to be activated, to allow for a high detection sensitivity during measurements of absolute atomic number densities at PSI-1.

Tailoring these options of the detection-system precisely to the encountered PSI-1 background emission, its characteristic was analysed by passive VUV-spectroscopy (Ch. 3.1.2). Additionally, a *measurement system* based on a 0.3 m-VUV-spectrometer was developed and established at PTB. Characterization of the VUV-transmission of all optical components, adaptation of the oxygen filter and the gating electronic to the actual needs, as well as controlling the stability of the  $L_{\alpha}$ -lamps used in detector calibration, are the purpose of this measurement system.

In the following chapters the  $L_{\alpha}$ -detection system is described as it was used in the  $L_{\alpha}$ -TALIF measurement campaigns in 1996 and 1997 for absolute atomic number densities in PSI-1 hydrogen and deuterium plasmas.

### 3.3.1 The photomultiplier tube

The heart of the detector system is the *photomultiplier tube* (PMT). It is an electron multiplier (Model EM 143/1A; THORN EMI Electron Tubes Ltd., Middlesex UK), which is suited for the detection of single XUV photons in the spectral range of 30...140 nm. It is a fast PMT (rise time 2 ns, FWHM: 3 ns) with extremely low background counts (typ. 3 counts  $s^{-1}$  at 3 kV operating voltage). To protect the PMT from the relatively low magnetic fields at the PSI-1 it has been surrounded with a jacket of  $\mu$ -metal.

The used PMT model is originally a windowless one. However, the actual device was custom made for PTB in that by THORN EMI sealed it with a  $MgF_2$ -window. This window automatically served as the short wavelength cutoff of the PMT's spectral sensitivity, due to the vanishing transmission of  $MgF_2$  for radiation below 112 nm. The upper sensitivity cutoff is caused by the vanishing quantum efficiency of CuBe for radiation above 149 nm. CuBe was the material of the dynodes in the PMT, from which the first also served as the cathode. Beneficially, both wavelength dependant material parameters acted together as a spectral filter. This is depicted in Figure 3.6 where both curves are shown in their spectral dependence.

Herein we find the reason why measurements of PSI-1's background (Fig. 3.2) showed significant edges at 114 nm and 127 nm, respectively. Not the plasma background decreased at these wavelengths but the spectral sensitivity of the PMT with  $MgF_2$  optics.

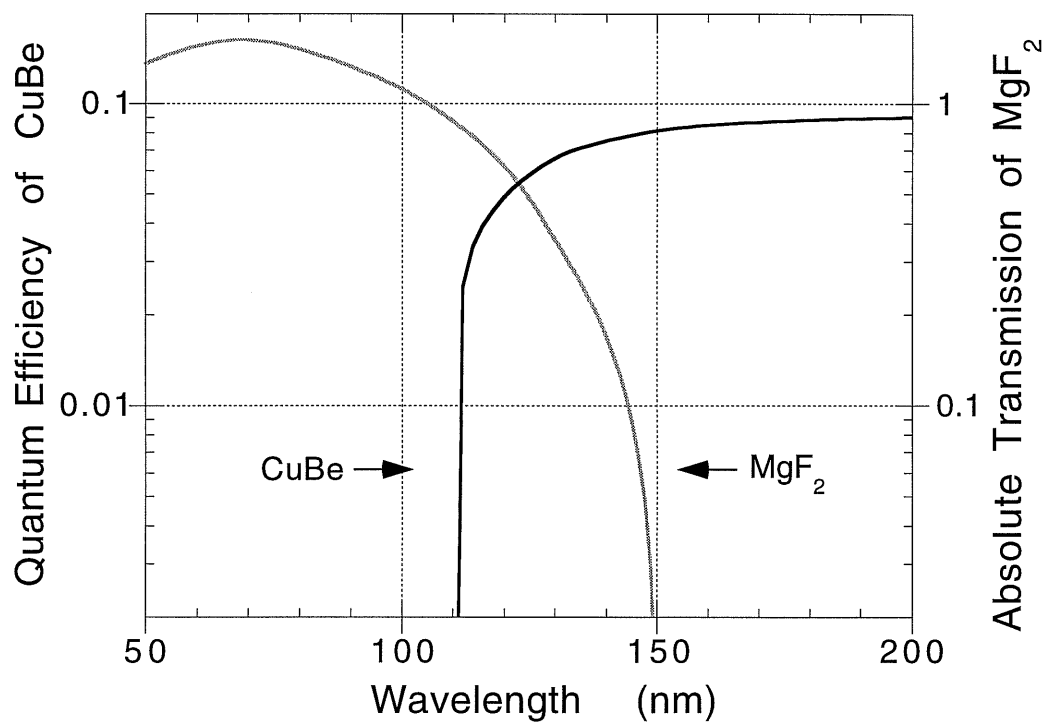


Figure 3.6 Spectral variation of the quantum efficiency of CuBe and transmission of MgF<sub>2</sub> in a wavelength range around Lyman- $\alpha$ .

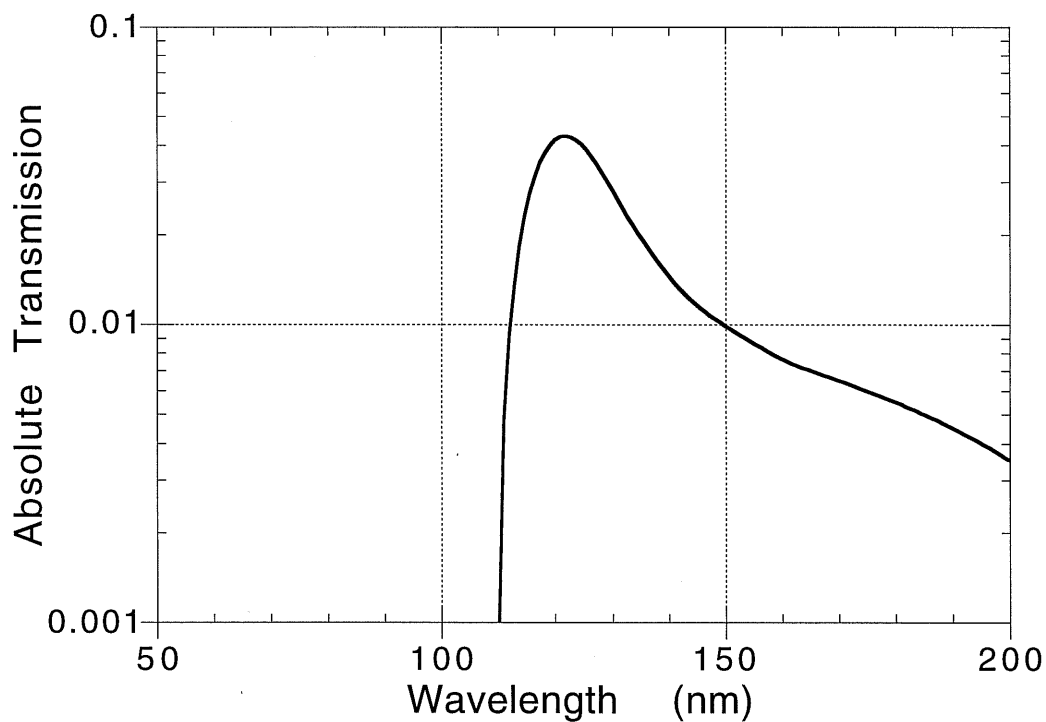


Figure 3.7 Measured spectral transmission of a Lyman- $\alpha$  interference filter (Acton Research) in a wavelength range around Lyman- $\alpha$  [50].



Furthermore, this configuration was not susceptible to normal straylight at 243 nm from the laser beams as it would have been the case with a solar blind photomultiplier tube. Although such PMT's possess an approximately seven-times higher quantum efficiency in the VUV spectral range it was shown at the beginning of 1994 that they can't be used at PSI-1 even in combination with  $L_\alpha$ -interference filters. Figure 3.7 shows a typical spectral curve of a  $L_\alpha$ -interference filter made by Acton Research yielding to a general decrease of the detection system's sensitivity in the VUV spectral range, i.e. on the expense of transmission right at Lyman- $\alpha$ , as well.

The PMT, the filters and the variable imaging system were inserted into a moveable UHV *detector chamber*. For measurements a shutter to the observation chamber at PSI-1 was opened and the detector chamber was driven downwards into the measurement position. Figure 3.8 shows a side view of the whole detection system, which sat on top of the observation chamber of the PSI-1 (port D in Fig. 3.1) looking downwards into the plasma. The UHV detector chamber was closed with a  $MgF_2$  window. In front of this window up to two  $L_\alpha$ -interference filters could be mounted in case a general reduction of the sensitivity was needed, e.g. when  $L_\alpha$ -TALIF measurements were done at high PSI-1 discharge currents of 300 A or higher.

The *imaging system* consisted of a  $MgF_2$  lens ( $\varnothing = 5.1$  cm;  $f = 125$  mm @ 122 nm), positioned at a distance  $s = 0.26$  m from a spatial filter in front of the PMT and allowed for a 1:1 projection of the measurement volume.

To optimize the signal-to-background ratio  $S_{LIF} / S_P$  (Eq. (2.15)) the *spatial filter* was mounted onto the PMT's  $MgF_2$ -window, having the advantage that the whole PMT cathode was illuminated by two-photon absorption induced  $L_\alpha$ -fluorescence.

Load on the PMT was further reduced by implementing an electronic *gating circuit* with the PMT. The laser system operated at a pulse repetition rate of 10 Hz, hence, every 100 ms a several nanoseconds lasting TALIF signal occurred. Hence, it was reasonable to activate the PMT only for some microseconds around the arrival of the two laser pulses and to deactivate it until the next pair of pulses. Although the PMT was not designed for gated operation we managed to develop a circuit for switching the voltage between the first two dynodes. As a result, the dc load at the PMT was 60 times smaller with gate closed compared to open gate operation.

The *measurement volume* was constituted by the volume of the laser beams over the length of the cathode (1.5 cm) and was therefore as small as  $V = 0.1$  cm<sup>3</sup>. This provided the *high spatial resolution* of the  $L_\alpha$ -TALIF measurements.

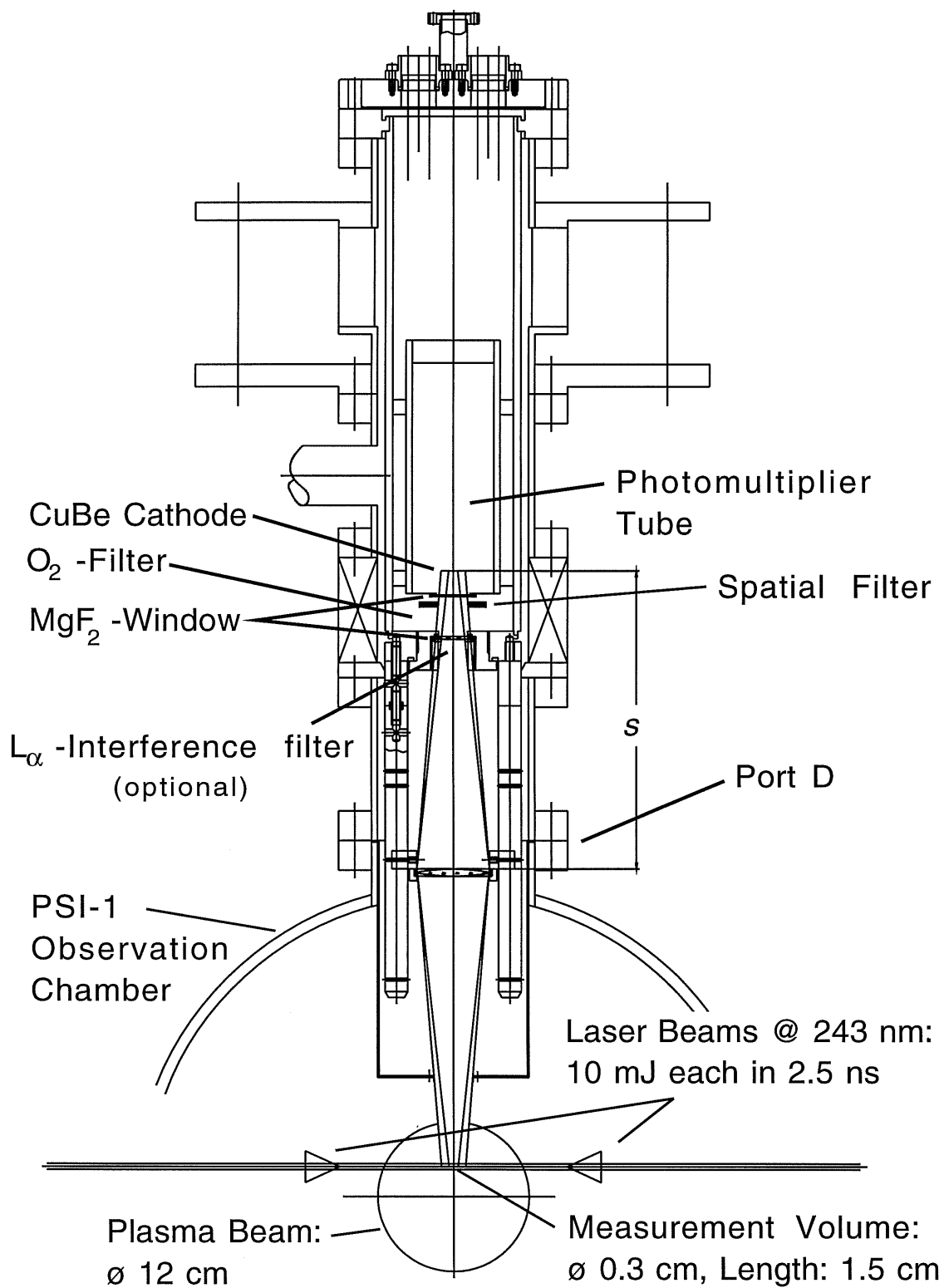
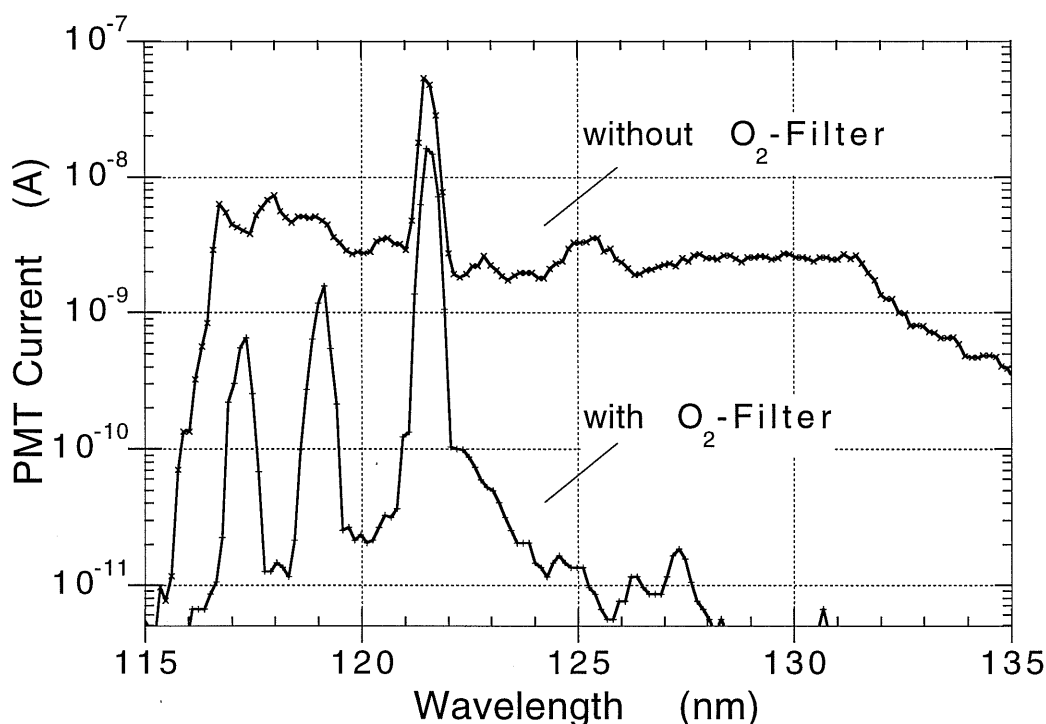


Figure 3.8 Cross section through the detection system sitting on top of PSI-1 (Port D).

### 3.3.2 The oxygen $L_{\alpha}$ -filter

The UHV detector chamber with the PMT inside could be readily filled with oxygen gas of high purity to serve as an additional but *variable spectral filter*. This was possible because oxygen absorbs VUV radiation around Lyman- $\alpha$ , while right at 122 nm it shows a transmission window [51]. The absorption length between the PMT window and the window of the detector chamber was 4 cm. Figure 3.9 shows the spectrum of the Lyman- $\alpha$  lamp (Chapter 3.3.3) in terms of PMT current signal over wavelength. It was recorded again with the Keihtley electrometer and PMT, however, this time on PTB's 0.3 m-VUV-spectrometer system already mentioned in the introduction to this chapter. The oxygen absorption corresponds to an  $O_2$  pressure of 0.5 bar and an absorption length of 4 cm.

Oxygen absorption provides a very selective  $L_{\alpha}$ -filter, which suppresses strongly the molecular background emission present at PSI-1. However, two moderate transmission windows at 119 nm and 117 nm remain. Nevertheless, another advantage of the oxygen filter was to vary its overall transmission in the spectral range of Lyman- $\alpha$  *steadily* simply by altering the oxygen pressure  $p$  in a range  $0.3 \text{ bar} < p \leq 1.0 \text{ bar}$ .



**Figure 3.9** Transmission curves for radiation of a  $L_{\alpha}$ -Lamp with and without an oxygen filter.  $O_2$  pressure and absorption length product equal to  $0.5 \text{ bar} \cdot 4 \text{ cm}$ .

### 3.3.3 Calibration of the $L_\alpha$ -detector system

In order to measure atomic number densities as absolute values, i.e. in number of atoms per volume unit, it is also necessary to calibrate the detection system. This means, that one has to know the relation between an irradiance entering the detection system and the resulting current signal at the PMT (Eq. (2.8)).

Calibration of the detection system was possible by use of  $L_\alpha$ -hydrogen lamps. Such lamps (Model LGV-1), which were designed by the All Russian Institute (Moscow, Russia) in order to emit radiation predominantly in the Lyman- $\alpha$  line of hydrogen (Figure 3.9), are simply operated at a direct-current of several milli amps. Two lamps had been calibrated with *synchrotron radiation* at the PTB laboratory at BESSY-1, Berlin. Such a calibrated lamp was then used as a transfer standard to calibrate another  $L_\alpha$ -lamp at our 0.3 m-VUV-spectrometer. This process provided the actual detector calibration  $L_\alpha$ -lamp (N° 806). Its radiant intensity was:

$$I_L = 91 (1 \pm 15\%) \mu\text{W}/\text{sr} . \quad (3.1)$$

Undoing the detection system from the plasma generator and lifting it about 0.4 m above its port, allowed to assemble it easily with a calibration unit, in which the calibration lamp had been inserted. This procedure made detector calibrations possible whenever needed. Decrease of the detectors sensitivity could be kept below 5% within the whole time of experiments at the PSI-1. This good stability is contributed to the optional  $L_\alpha$ -filter management allowing always to choose the load for the PMT to lie in the longtime stable operating range.

As we have seen in Chapter 2.3, the calibration lamp's radiant intensity  $I_L$  is needed in Eq. (2.8), which expresses the detector calibration procedure. In Eq. (2.9) it allows then to deliver the plasma background radiance  $L_P$  as an *absolute* reference value. This value is not only important to quantify the difficulties against which the  $L_\alpha$ -TALIF measurements succeeded, but enters also Eq. (2.15) - the equation for the sought number densities - via Eq. (2.10).

# 4

## Experimental Results

In June 1996 first  $L_{\alpha}$ -TALIF measurements were performed, focussing on all aspects which had to be optimized or adapted for the final measurement campaigns in November 1996 and June 1997. Density measurements were mainly done in the last two campaigns with different aspects we focused on. Numerous secondary examinations to provide the essential foundation for these main investigations had to be done in advance and synchronously. Chapter 4.1 gives the results of the most important such preparatory examinations like the measurement of the spectral widths of the absorption and laser profile. Furthermore, the calculation of the Lyman- $\alpha$  yield  $Y^*$  for actual laser beam profiles and its proof, assessment and error discussion are given.

The principle of the  $L_{\alpha}$ -TALIF measurement procedure shall be explained in Chapter 4.2. Looking at the comprehensively developed *electronic data processing* will lead to the discussion of single laser shot  $L_{\alpha}$ -TALIF signals. This gives rise to considerations about the measurement limit in respect to *photon statistics*.

Last but not least, we shall arrive at the final results for the atomic number densities in various PSI-1 plasmas and the kinetic temperature in Chapter 4.3 and Chapter 4.4 respectively. The *complete error discussion* and the important detection limit for density measurements at the PSI-1 is given, too.

## 4.1 Preparatory Examinations

In order to calculate the Lyman- $\alpha$  yield as accurate as explained in Chapter 2.4 one has to know the cross sections for two-photon absorption and photo ionization in hydrogen. They are available from scientific publications. However, necessary quantities, which depend on the very conditions of the experiment, have to be measured. Such a quantity is the *spectral bandwidth* of the laser radiation at 243 nm. Another such quantity, depending strongly on the conditions of the PSI-1 plasmas (i.e. magnetic and electric fields), is the *spectral width of the absorption line profile* in hydrogen. The determination of both is explained in Chapter 4.1.1 and 4.1.2, respectively. In Ch. 4.1.2 cross checks to results of the IPP are depicted, too.

Starting from such theoretical and experimental data for the yield calculations one arrives at a relation between a laser irradiance and the resulting  $L_\alpha$ -yield (Fig. 2.11). However, irradiances in real laser beam profiles show a spatial distribution and so one has to apply this relation to the *actual irradiance distribution* as discussed in Chapter 4.1.3. An error discussion for the final  $L_\alpha$ -yield values is given at the end of Chapter 4.1.4.

### 4.1.1 Spectral bandwidth of the laser

The optogalvanic reference cell served not only for finding the Lyman- $\alpha$  two-photon transition wavelength (243 nm) for the tunable laser system (Ch. 3.2.2), but allowed to find an upper boarder for the spectral width of the laser radiation at this wavelength. Figure 4.1 shows the optogalvanic signal if the reference cell is filled with hydrogen and the laser radiation is tuned across the two-photon absorption resonance. Each dot represents the optogalvanic signal for a laser pulse. The separation of the two peaks, which are emphasized by curves resulting from a Gauss fit, shows the hyperfine splitting of hydrogen. The corresponding frequency scale for Figure 4.1 is taken from the hyperfine splitting of 621 MHz [38] at the laser frequency. It allows the determination of the spectral width of the peaks to be  $(0.36 \pm 0.02)$  GHz. Deuterium is less suited for this purpose because its hyperfine structure splitting is too small (140 MHz) [38].

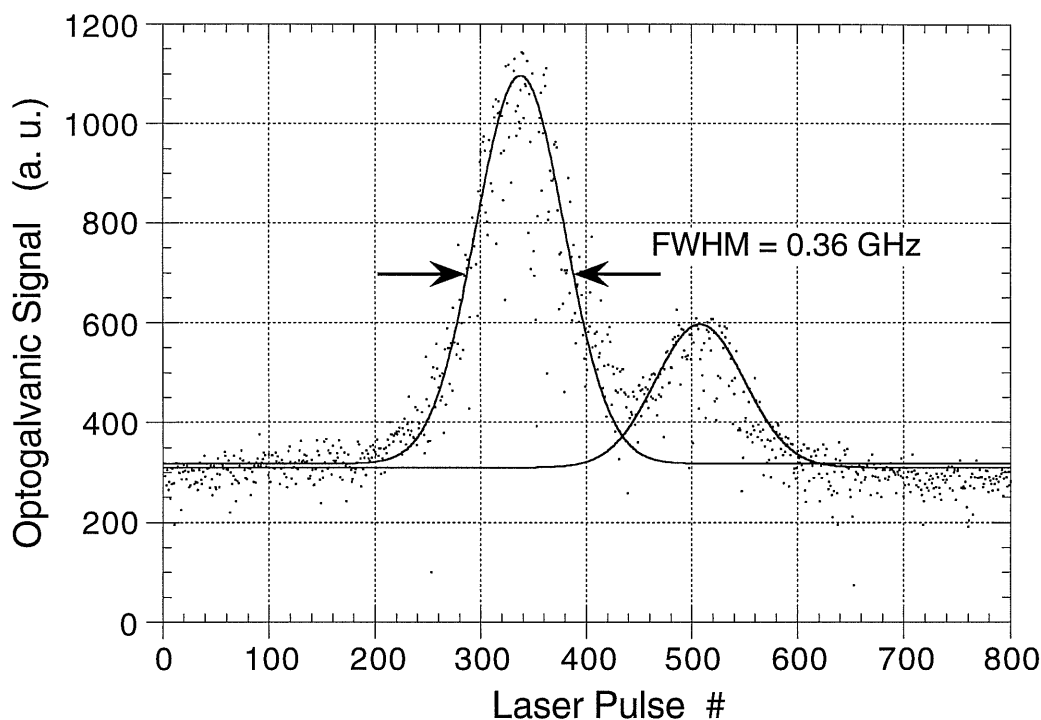


**Figure 4.1** Doppler-free signal for the Lyman- $\alpha$  transition in the optogalvanic reference cell filled with hydrogen. For each pulse of the tuned laser radiation the resulting current value is shown. Both peaks are fitted with Gauss curves.

Due to the conditions in the reference cell (pressure: 4 mbar and negligible electromagnetic field strength) the broadening of the two hyperfine structure components can be neglected. Thus, the laser's spectral bandwidth is 0.36 GHz. The ratio of the two peak maximum values in Fig. 4.1 is almost 3:1, as it is expected by looking at the quantum numbers  $F = 1$  and  $F = 0$ , which characterize the hyperfine splitting.

#### 4.1.2 Spectral bandwidth of the $L_{\alpha}$ -absorption profile

As explained in Chapter 2.2, we measured mostly at deuterium instead of hydrogen. Because the spectral width of deuterium under PSI-1 conditions enters the calculation of the  $L_{\alpha}$ -yield, it had to be measured. The procedure for that was as follows: A  $L_{\alpha}$ -TALIF measurement was done with the laser *tuned* across the two-photon resonance. Plotting the TALIF signals against the laser's detuning one gets a smooth Gauss-like curve. Simultaneously, the signal of the deuterium filled optogalvanic reference cell was recorded, as well. With the knowledge of the hyperfine structure of the unperturbed deuterium atom of about 0.14 GHz [38] convoluted with the measured spectral width of the laser, the underlying frequency scale of the deuterium TALIF spectrum could be determined. So one gets to a spectral width of

the deuterium absorption profile at standard PSI-1 plasma conditions of 0.58 GHz and with the spectral width of the laser (0.36 GHz) deconvoluted from it:

$$\Delta\nu = (0.45 \pm 0.04) \text{ GHz} . \quad (4.1)$$

Comparing this result with the ion density parameter in the theoretical curves of Fig. 2.6 could lead to the assumption the ion density during TALIF measurements at PSI-1 lay well above  $10^{13} \text{ cm}^{-3}$ . However, this *ion density* would be either eight or fourteen times larger compared to either theoretical calculations [52] or Langmuir probe measurements at PSI-1 [53]. The reason for this is the fact that the spectral width of the  $L_\alpha$ -TALIF profile at PSI-1 given in Eq. (4.1) is dominated by two broadening mechanisms:

- *the residual Doppler width:*

The moderate focusing of the lenses at the laser beam entry ports of PSI-1 lead to converging beams, i.e. spread in the wave vectors of both counter propagating laser beams and thus to a non-vanishing, so called residual Doppler width  $\Delta\nu_{rD}$ . It can be calculated from the measured kinetic temperature (Ch. 4.4) in a PSI-1 plasma and the laser beam crossing angle accounting for it. The calculated value for this contribution is:  $\Delta\nu_{rD} \approx 0.31 \text{ GHz}$ .

- *the ionisation and AC Stark broadening:*

Figures 2.9 and 2.11 show that already at irradiances of  $100 \text{ MW/cm}^2$  a considerable amount of atoms is ionized. For such irradiances are typical for the profile of the laser beams, ionisation broadening takes place within the 2.5 ns laser pulse width. It can be approximated by use of linear relation connecting the irradiance to the resulting ionisation broadening [54]. Another related effect of the same order of magnitude is the shift of the emission frequency towards higher values due to the AC Stark effect [54]. Also this process leads to a further broadening of the absorption line and hence the value in Eq. (4.1). The contribution of both mechanisms put together is approximated to be  $\Delta\nu_{i\&AC} \approx 0.32 \text{ GHz}$ .

Deconvoluting those broadening mechanisms from the measured profile width leads to a remaining Stark broadened width of less than 0.1 GHz. However, this profile width is in general accordance with calculated Stark broadening [31] for charged particle densities as they are quoted by the IPP [52, 53].

Furthermore, such a reduced spectral width also corresponds acceptably to the measured  $2S \rightarrow 2P \rightarrow 1S$  decay time in deuterium of about 8 ns.



### 4.1.3 Lyman- $\alpha$ yield for real laser irradiance distributions

The relation for the Lyman- $\alpha$  yield  $Y$  as given in Figure 2.11 connects a value for the laser irradiance  $E$  with the resulting yield  $Y(E)$ . This dependence allows therefore to account for the spatial irradiance distribution of the laser in the measurement volume.

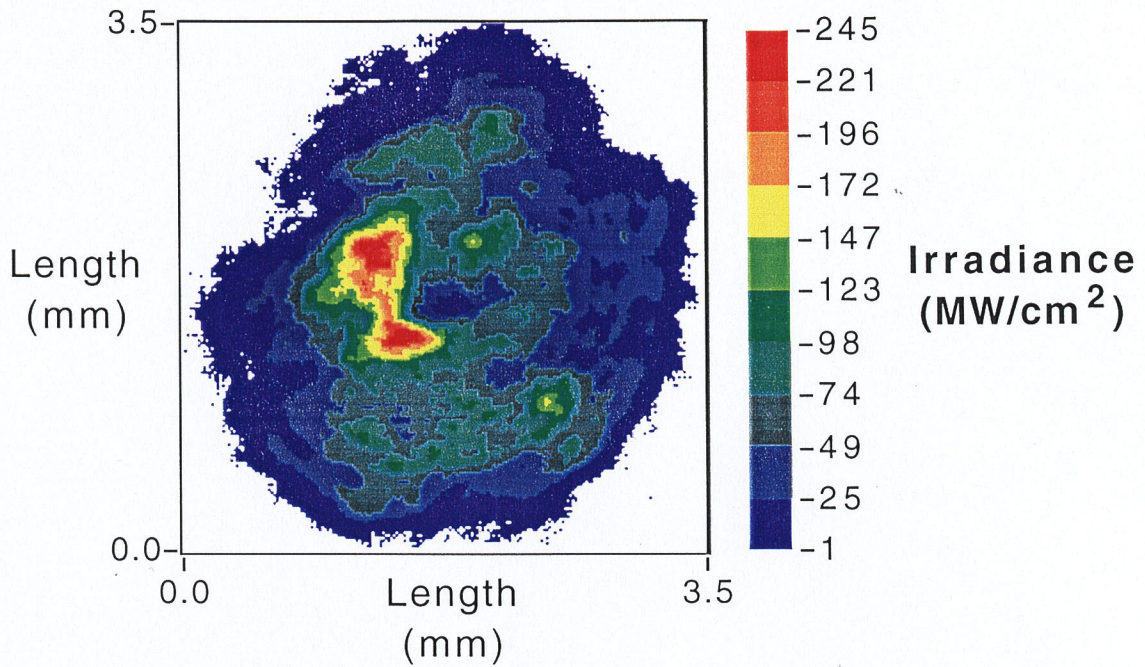
To determine the variation of  $E$  within the laser's beam profile, we recorded them during  $L_{\alpha}$ -TALIF measurements with a CCD camera (Model VC 44, PCO Computer Optics GmbH, Kelheim, Germany). Although the beam profiles were recorded outside the PSI-1, they represent the laser beam profile in the measurement volume within the plasma generator. This was simply achieved by positioning the camera in the very same distance away from the collecting lens, as the measurement volume in the plasma generator laid (Fig. 3.4). Attenuation of the laser radiation was achieved by multiple wedge-plate reflection. Together with the measured energy and temporal FWHM of the laser pulses, this CCD intensity picture can be transformed into the *spatial irradiance distribution* for the laser beam.

Figure 4.2 shows a two-dimensional plot of a typical laser irradiance distribution at a wavelength of 243 nm, like it was present in the measurement volume during  $L_{\alpha}$ -TALIF measurements. With a typical pulse energy of 9.5 mJ within 2.5 ns for partial beam, i.e. after the main laser beam had been split into two beams, the maximum local irradiance is 245 MW/cm<sup>2</sup>, whereas most of the pixels have an irradiance of about 100 MW/cm<sup>2</sup>.

Assigning to each pixel's irradiance value in Figure 4.2 the corresponding yield according to the relation shown in Figure 2.11, delivers a spatial distribution for the Lyman- $\alpha$  yield. This *Lyman- $\alpha$  yield distribution* is shown in Figure 4.3.

Interesting to note is the fact, that the maximum irradiance areas in the beam profile with its 245 MW/cm<sup>2</sup> lie already beyond the maximum yield in Figure 2.11. Therefore, the corresponding areas in the yield profile (Fig. 4.3) are not the ones with the maximum yield. However, they are surrounded by large areas with higher yield values, for these areas are belonging to smaller irradiances, which lie closer to the optimum irradiance of 125 MW/cm<sup>2</sup>.

In a final step, determination of the atomic number density requires integrating the Lyman- $\alpha$  yield over the whole measurement volume.



**Figure 4.2** Irradiance distribution of the laser beam profile (as present in the measurement volume). It was recorded perpendicularly to the direction of beam propagation with a CCD camera. The axis lengths are given; the pulse energy was 9.5 mJ and the temporal FWHM was 2.5 ns.

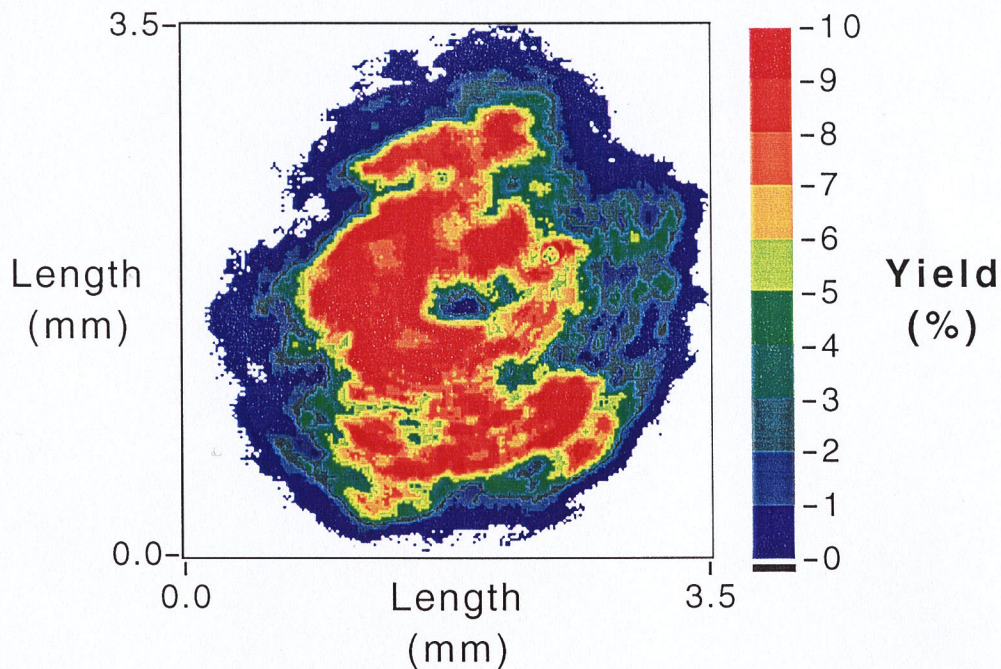


**Figure 4.3** Lyman- $\alpha$  yield distribution for the irradiance distribution of Fig. 4.2. The transformation from the irradiance distribution to the yield distribution was done by use of the relation given in Fig. 2.11.

It is important to notice, that the atomic number density can be regarded as constant within the tiny measurement volume of only  $0.1 \text{ cm}^3$ . Furthermore, the two-dimensional yield distribution is constant over the  $1.5 \text{ cm}$  length of the measurement volume. Therefore, the volume integration of the product  $N \cdot Y$  in Eq. (2.7) is restricted to an area integration of  $Y$  over the laser beam cross section, i.e. the cross section of the measurement volume. The law of mean in integral calculus allows now to calculate this integral as a product of the mean value for  $Y^*$  and the cross section area. The *averaged* Lyman- $\alpha$  yield  $Y^*$  belonging to the distribution in Figure 4.3 is:

$$Y^* = 3.9\%. \quad (4.2)$$

Checking the calculation of the yield and therefore its dependence on various experimental parameters basically, the following experiment was performed. During a  $L_\alpha$ -TALIF measurement in a hydrogen-deuterium plasma, the pulse energy of the laser beams at  $243 \text{ nm}$  was decreased from its maximum value by use of a variable attenuator, which was put into the beam paths solely for this experiment. The attenuator worked on the principle of dielectric surfaces, reflecting a certain amount of energy out of the beam. For the attenuator was located within the laser spectrometer, i.e. about  $20 \text{ m}$  away from the measurement volume, it did not affect the beam profile there significantly.

Figure 4.4 shows the variation of the  $L_\alpha$ -TALIF signal depending on the varied laser pulse energy. Because all the other experimental conditions remained unchanged, this variation with pulse energy must be represented solely by the according variation of the calculated Lyman- $\alpha$  yield - if the yield is calculated correctly. Therefore, Fig. 4.4 shows additionally the Lyman- $\alpha$  yield calculated for the pulse energies of that experiment. The yield values are also plotted on a logarithmic axis, however, in arbitrary units. As one can see, the measured signals and the calculated yields do fit well together. This proof is especially sensitive in respect to the position of the maximum in the curve of Fig. 2.11: Maximum yield at another irradiance and another shape of the yield curve in Fig. 2.11 would not lead to such good accordance in Fig. 4.4.

To allow for an assessment of the averaged  $L_\alpha$ -yield as given in Eq. (4.2) in respect of the laser beam quality that affects the yield, the yield for an *ideal irradiance profile*, i.e. a smooth Gauss profile of the same area, was computed, as well. Compared to the average Lyman- $\alpha$  yield for a Gauss profile, we did achieve *90% of this maximum value* with the profile shown in Figure 4.2.

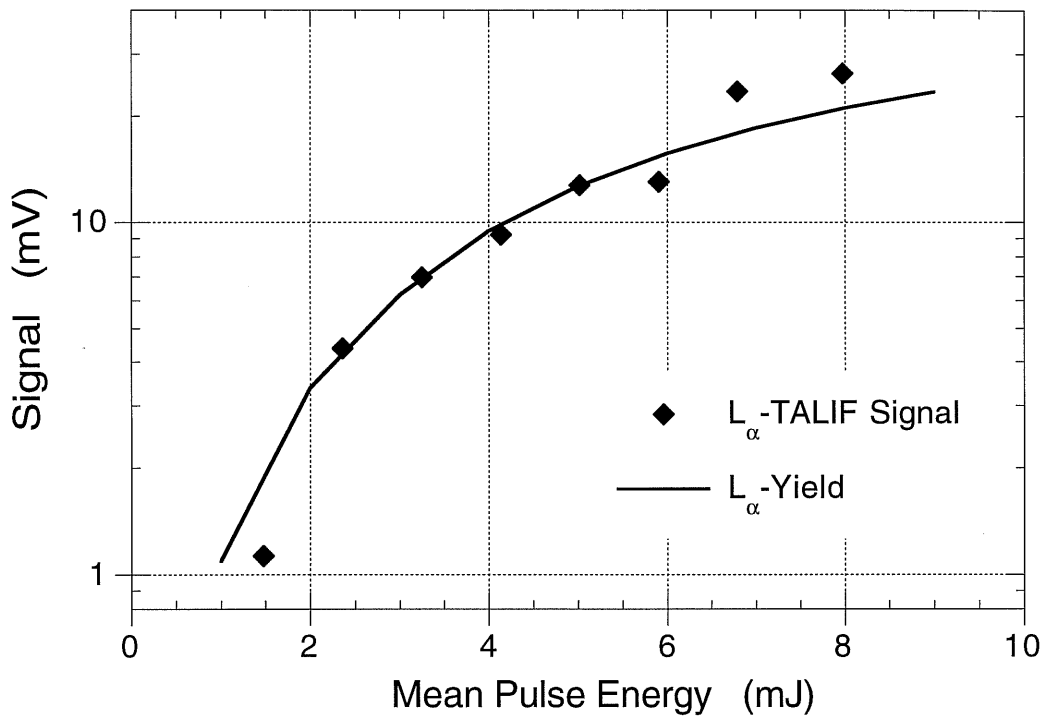


**Figure 4.4**  $L_{\alpha}$ -TALIF signal varying with the pulse energy for each laser beam as present in the measurement volume. The calculated  $L_{\alpha}$ -yields for those pulse energies are shown on the same logarithmic axis, however with arbitrary units.

This good result shows, that the procedure of measuring the laser's irradiance distribution, transforming it into a  $L_{\alpha}$ -yield distribution and finally concentrating the meaning of its impact into a single number - the spatially averaged  $L_{\alpha}$ -yield -, provided an effective means for assessing and thereby *improving the actual beam profile* with respect to its quality for  $L_{\alpha}$ -TALIF generation. As  $L_{\alpha}$ -TALIF measurements were usually performed with a pulse energy with about 10 mJ in each of the counterpropagating beams, i.e. in the flat part of the curve in Fig. 4.4. This means, that the single shot  $L_{\alpha}$ -TALIF signals were only weakly dependent on the pulse energy.

As far as the long-term stability of the beam profile is concerned, comparison of the yield values for all the irradiance profiles recorded within a typical  $L_{\alpha}$ -TALIF measurement campaign, i.e. over several days, lead to a remarkably small variation in the Lyman- $\alpha$  yield of solely 20%.

#### 4.1.4 Error discussion for the Lyman- $\alpha$ yield

Besides the theoretically well known cross-sections for two-photon absorption and photo-ionization from the  $n = 2$  level in hydrogen (Eqs. (2.18), (2.20)), the following

measured quantities (with their errors) enter the computation of the  $L_\alpha$ -yield:

- laser spectral width:  $\pm 10\%$ ,
- laser pulse energy and temporal pulse width:  $\pm 15\%$  each,
- width of the two-photon absorption profile:  $\pm 10\%$ ,
- $2S \rightarrow 2P \rightarrow 1S$  decay time:  $\pm 25\%$ .

Because these quantities are linked in a system of *coupled, nonlinear rate equations* the only adequate way to get the final error for  $Y^*$  is to calculate the variation of  $Y^*$  by use of Eqs. (2.23) and (2.24) caused by the uncertainties of the input quantities. These uncertainties are combined in such a way that the resulting variation of  $Y^*$  becomes as large as possible. The procedure lead to a maximum variation for the Lyman- $\alpha$  yield  $Y^*$  of

$$\Delta Y^* = 20\%.$$

This beneficial result is due to the system of coupled, nonlinear rate equations.

#### 4.1.5 Analysis of fluorescence reabsorption at PSI-1

$L_\alpha$ -TALIF only delivers the correct atomic number densities if the  $L_\alpha$ -TALIF radiation is not affected by reabsorption on its way to the detection system. An estimate of the underlying radiative transfer at PSI-1 for  $L_\alpha$ -radiation is difficult because it depends on density and temperature distribution of atoms and charged particles and the correlated  $L_\alpha$ -absorption profiles.

Therefore, the  $L_\alpha$ -absorption conditions at PSI-1 were investigated experimentally for a hydrogen plasma generated at discharge currents in between 30...400 A. For this, the  $L_\alpha$ -radiation of the  $L_\alpha$ -lamp was sent perpendicularly to the plasma beam of PSI-1 and focussed onto the entry slit of a 0.3 m Acton Research Spectrometer. The optical path for the  $L_\alpha$ -radiation in that arrangement was much longer - both, inside the plasma beam and outside it - as it is the case at  $L_\alpha$ -TALIF measurements.

Comparison of the measured spectrum of the lamp at  $L_\alpha$  when its radiation has penetrated through the plasma of PSI-1 with the case of propagating through an evacuated observation chamber, i.e. without any hydrogen plasma, showed no measurable absorption of  $L_\alpha$ -radiation. Therefore, it can be stated that the  $L_\alpha$ -TALIF measurements allow for *correct density determination*.

## 4.2 Principle of Measurements

### 4.2.1 Data recording and $L_\alpha$ -TALIF measurements

For  $L_\alpha$ -TALIF measurements of the atomic number density, the laser frequency was kept fixed - by optogalvanic control - at the centre of the  $1S \rightarrow 2S$  resonance frequency of the isotope under examination. Additionally, the laser frequency was tuned across the resonance to obtain the spectral dependence of  $L_\alpha$ -TALIF signals, e.g. for the measurement of kinetic temperatures.

For each laser pulse, the resulting fluorescence radiation led to a current pulse at the PMT, which was transformed into a voltage at a resistor of  $50 \Omega$  and recorded with a fast digital storage oscilloscope (Hewlett Packard, HP 54542 A). The dotted curve in Figure 4.5 shows such a voltage signal caused by the plasma background emission and the  $L_\alpha$ -TALIF signal for a single laser shot. The dots represent the actual points of measurement made by the oscilloscope at a sampling rate of 2 GHz. Typically, the recorded time interval per single signal had a length of about  $0.1 \mu s$ . This allowed for the recording of several hundreds of signals (Fig. 4.5) in a single run, before the oscilloscope's memory had to be read out.

The plasma for the shown  $L_\alpha$ -TALIF signal consisted of 100% deuterium at a discharge current of 300 A. On top of the plasma background, which produced a dc signal of about 10 mV, sat the well-pronounced  $L_\alpha$ -TALIF signal peak. It appeared immediately with the exciting laser pulse and had a temporal FWHM of about  $(8 \pm 1)$  ns. This time can also be regarded as the *time constant* for the  $2S \rightarrow 2P \rightarrow 1S$  decay channel.

The laser frequency was kept in resonance with the  $1S \rightarrow 2S$  transition in deuterium. Comparing the single signal with an average over five signals shows the *good shot-to-shot stability* of the signals: Clearly, the part of the signal due to the plasma background is smoother in the average signal, but the TALIF peak did not vary significantly.

To answer the question, if there are any contributions to the  $L_\alpha$ -TALIF signal, which are not caused by two-photon absorption, Figure 4.5 additionally shows the

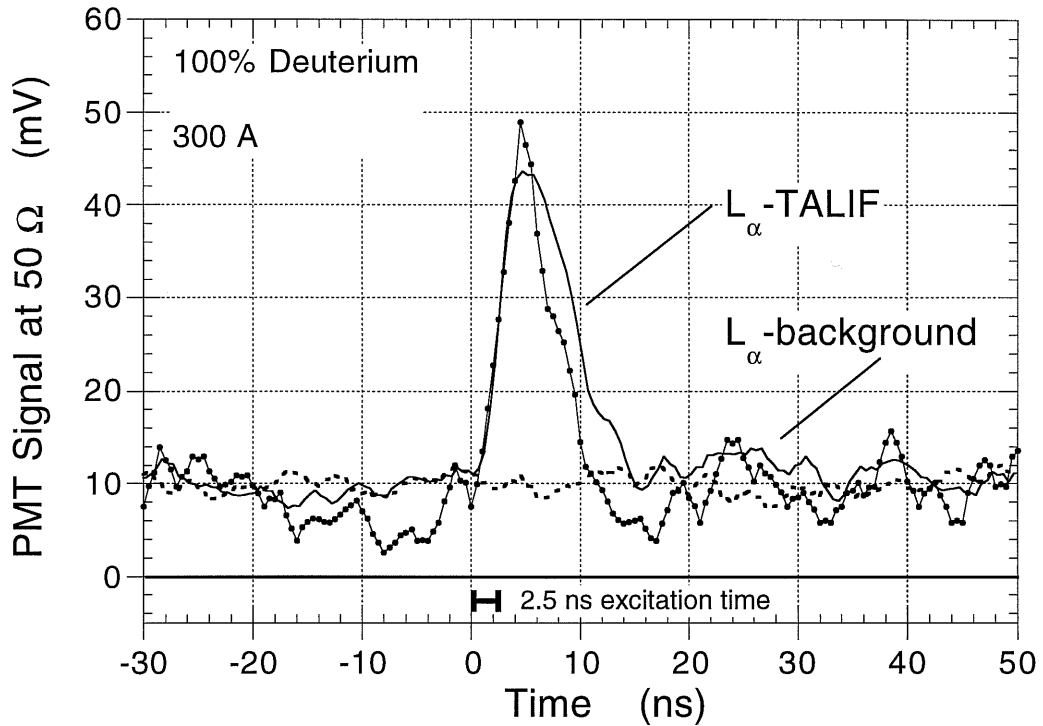


**Figure 4.5** PMT signals for a  $L_{\alpha}$ -TALIF measurement at PSI-1. The plasma consisted of 100% deuterium at a discharge current of 300 A. A single signal and averages over five signals are shown. The temporal FWHM of the laser radiation is indicated, as well.

$L_{\alpha}$ -detector signal without the TALIF peak in case that the laser is tuned out of resonance (striped curve). It is evident, that without two-photon absorption there is no other effect, e.g. straylight or Rayleigh scattered radiation at 243 nm, contributing to the  $L_{\alpha}$ -TALIF signal.

Seeking *atomic number densities* in the plasma (Eq. (2.15)), needs to analyse such measurement signals in the following way: The plasma background radiance  $L_P$  according Eq. (2.9) can be easily found by measuring the dc voltage (or equivalently the current, labeled  $C_P$  in Eq. (2.9)) in an averaged signal beside the  $L_{\alpha}$ -TALIF peak: about 10 mV in Figure 4.5. The  $L_{\alpha}$ -TALIF signal peak itself is integrated over its whole width  $\Delta t$  (10 ns in Fig. 4.5), which delivers the *mean*  $L_{\alpha}$ -TALIF signal voltage  $S_{LIF}$  (Eq. (2.11)).

#### 4.2.2 Statistical analysis of the $L_{\alpha}$ -TALIF signals

Statistical analysis of the signals was done to investigate the *single-shot detection noise* in the data. For doing this, it is necessary to relate the currents at the PMT to an average number of detected  $L_{\alpha}$ -fluorescence photons per time, e.g. 10 ns.

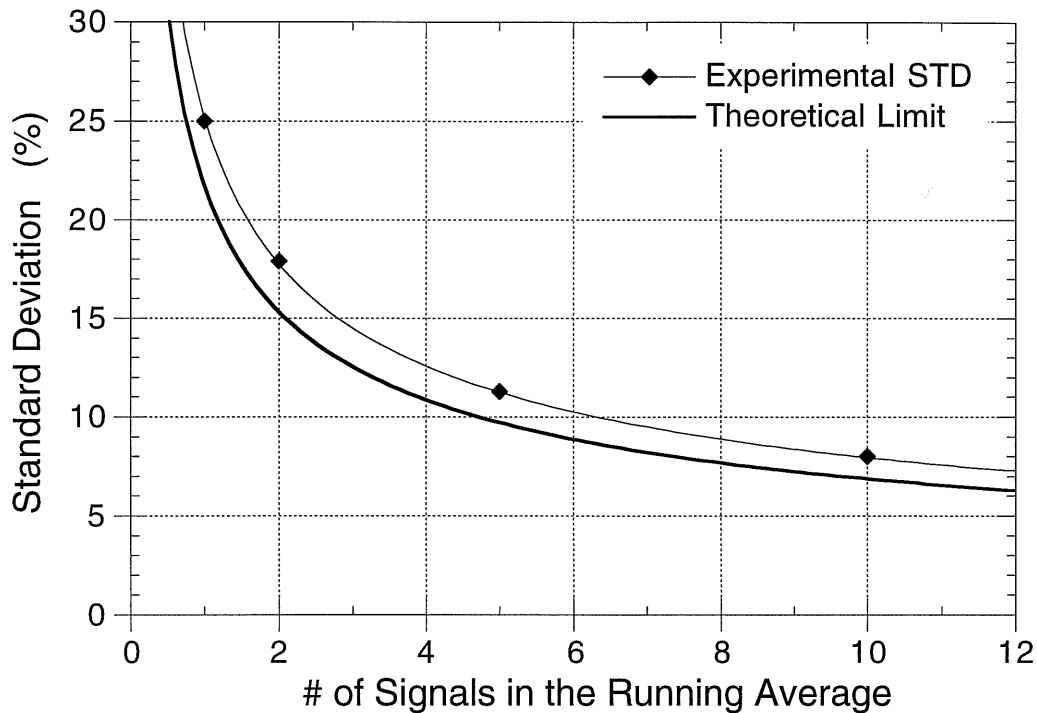


**Figure 4.6** Standard deviations for running averages over 2, 5 and 10 TALIF signals obtained from 600 recorded TALIF signals following one another at the laser's repetition rate of 10 Hz. Measurement was done in a pure deuterium plasma with a discharge current of 300 A. The theoretical limit according to Poisson statistics is given, too.

By use of the PMT gain of  $8.5 \cdot 10^5$  (at 2.75 keV PMT operation voltage) a photomultiplier signal average of 20 mV integrated over 10 ns corresponds to 29 photons. Based on this, the integral over any  $L_\alpha$ -TALIF signal leads to a number of detected  $L_\alpha$ -fluorescence photons  $N_\alpha$ , whereas the plasma background per time interval corresponds to another number of photons  $N_P$ .

According to Poisson<sup>#</sup> statistics, the expression

$$\frac{\Delta N_\alpha}{N_\alpha} = \frac{\sqrt{N_\alpha + N_P}}{N_\alpha} \quad (4.1)$$

gives the theoretical limit for the standard deviation  $\Delta N_\alpha / N_\alpha$  of the detected  $L_\alpha$ -fluorescence photons. Figure 4.6 shows the comparison of Poisson statistics with various standard deviations of running averages for the mean signal voltage in  $L_\alpha$ -TALIF signals of a pure deuterium plasma of 300 A.

---

# Siméon-Denis Poisson (1781-1840), French mathematician.



## 4.3 Atomic Densities and $L_\alpha$ -background

We like to mention, that recorded  $L_\alpha$ -TALIF signals (Fig. 4.5) combined with the actual calibration of the detection system allow the direct determination of the  $L_\alpha$ -background emission of PSI-1 plasmas, whereas the determination of atomic number densities requires furthermore the Lyman- $\alpha$  yield as present in the measurement volume.

For the  $L_\alpha$ -TALIF signal has to be measured against the present background emission of the plasma, both quantities have to be known for discussing the detection sensitivity achievable at PSI-1 and to assess the potential of  $L_\alpha$ -TALIF diagnostic in respect to its application at fusion plasmas.

The performed  $L_\alpha$ -TALIF examinations can be grouped into two main measurement campaigns. The first one in November 1996 focussed to the detection of *higher densities*. Therefore, it used mainly higher discharge currents (300...400 A) in pure deuterium plasmas of PSI-1. The second campaign took place in June 1997 and was mainly dedicated to the detection of *low densities* as present in plasmas generated at lower discharge currents (75...100 A). In the second campaign also the detectable density limit was examined. For this last purpose, hydrogen-deuterium mixtures (50% H + 50% D... 99% H + 1% D) at a discharge current of mainly 100 A were used.

The latter conditions were especially chosen because at 100 A the  $L_\alpha$ -background emission at PSI-1 is quite similar to the ones commonly stated for existing tokamak fusion machines.

Chapter 4.3.1 introduces into the results for the  $L_\alpha$ -background emission at PSI-1 which are also important for the assessment of the achievable detection limit at PSI-1 which shall be discussed in Chapter 4.3.4. Following PSI-1's background emission, Chapter 4.3.2 presents the results for *atomic number densities* of deuterium for different plasmas at PSI-1. Chapter 4.3.3 discusses the *general error* for the number densities and the closing is done in Chapter 4.3.4 by giving the detection limit of  $L_\alpha$ -TALIF diagnostic achieved at the plasma generator PSI-1.

### 4.3.1 $L_\alpha$ -background emission at PSI-1

First analysis of  $L_\alpha$ -TALIF measurements focussed on the *quantitative* determination of the plasma background emission, i.e. TALIF signals were also analysed in respect of the dc background contribution they always contain.

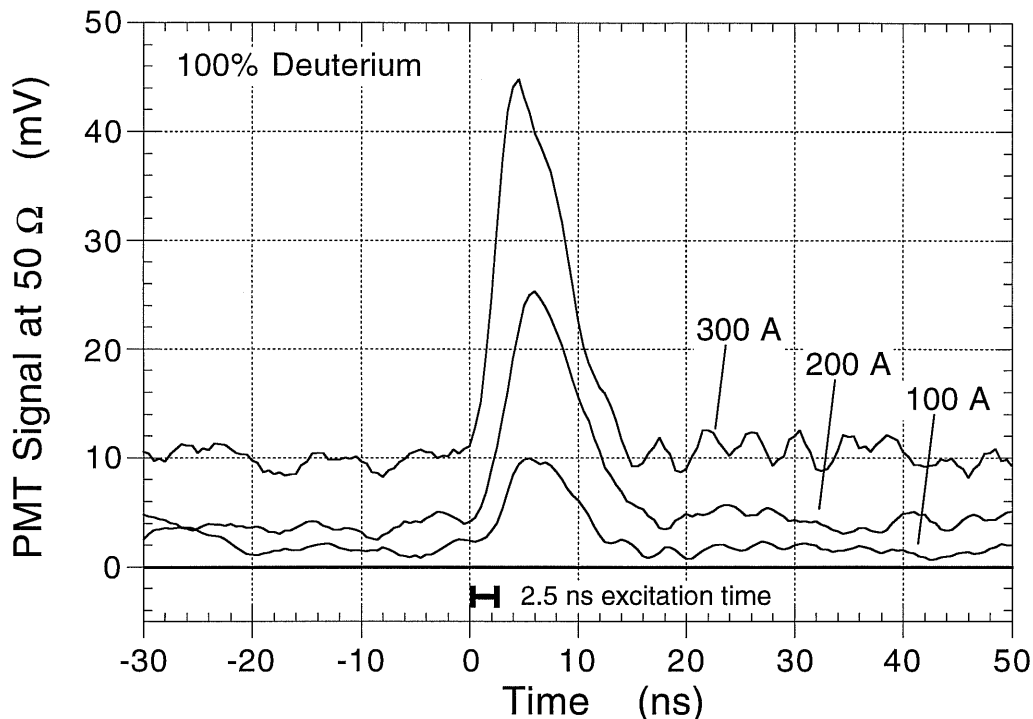


**Figure 4.7** Averaged (10#) PMT signals for  $L_{\alpha}$ -TALIF measurements at various discharge currents (100 A...300 A) in a 100% deuterium plasma. The temporal FWHM of the laser is indicated.

Figure 4.7 presents averages over ten  $L_{\alpha}$ -TALIF signals each for deuterium. The measurement was done in a pure deuterium plasma, for which the discharge current of PSI-1 was reduced from 300 A to 100 A in three steps. At such high discharge currents the PMT had to be protected against the especially strong plasma background emission by use of the  $O_2$  filter and one to two  $L_{\alpha}$ -interference filters. Although the latter ones also decreased the detector's sensitivity for the  $L_{\alpha}$ -TALIF signal itself, the signals at the PMT were quite strong and hence convenient to measure. Additionally, the laser's temporal FWHM is indicated in the figure. It represents the time of excitation of the atomic  $1S \rightarrow 2S$  transition.

Although maybe not obvious at first sight, Figure 4.7 shows that towards lower discharge currents at PSI-1 the signal-to-noise ratio  $S_{LIF}/S_P$  increases from about two at 300 A to almost four at 100 A.

Taking from such recorded  $L_{\alpha}$ -TALIF signals the dc background as already explained with Fig. 4.5, yields the results shown in Figure 4.8: the variation of the photon radiance  $L_P$  of the plasma background in a pure deuterium plasma at PSI-1 with the discharge current.

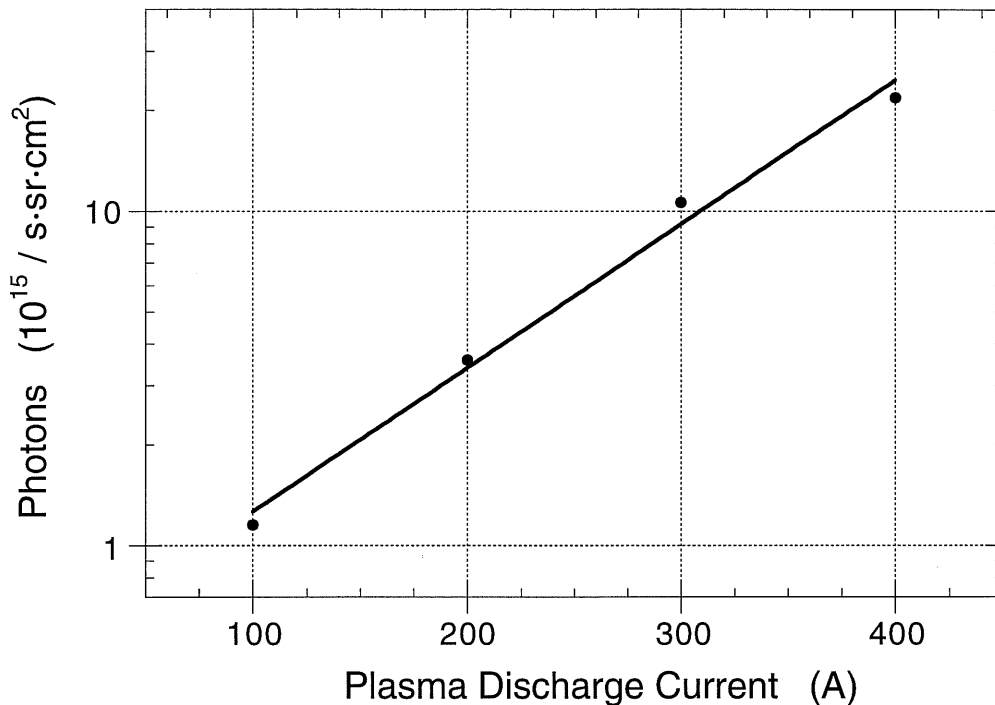


**Figure 4.8** Dependence of the photon radiance  $L_P$  for the background emission in a deuterium plasma at PSI-1 with the discharge current.

At a current of 400 A the photon radiance due to plasma background emission within the spectral sensitivity range of the detection system is as much as *twenty times higher* if compared with the number commonly stated for tokamak plasmas ( $10^{15}$  photons/s·sr·cm<sup>2</sup>).

#### 4.3.2 Measurement of atomic number densities

Measurements, which were done to find out the *lowest deuterium concentration* detectable in standard PSI-1 plasmas, benefitted from the above mentioned low background radiation at lower discharge currents. This allowed to remove the  $L_\alpha$ -interference filters from the detection system and what increased its sensitivity. This made lower deuterium densities better detectable.

Figure 4.9 presents  $L_\alpha$ -TALIF signals for measurements in hydrogen/deuterium mixed plasmas. The mixtures were varied from 50% H with 50% D to a mixture of 99% H with 1% D. The latter curve is shown only to given an idea of the alteration of the signals with decreasing deuterium density. Clearly, its signal-to-background ratio is quite small and therefore linked to a considerable uncertainty. Comparing the integrated areas of the  $L_\alpha$ -TALIF peaks with the corresponding deuterium concentrations in this figure does not fit together perfectly due to the pulse energy.

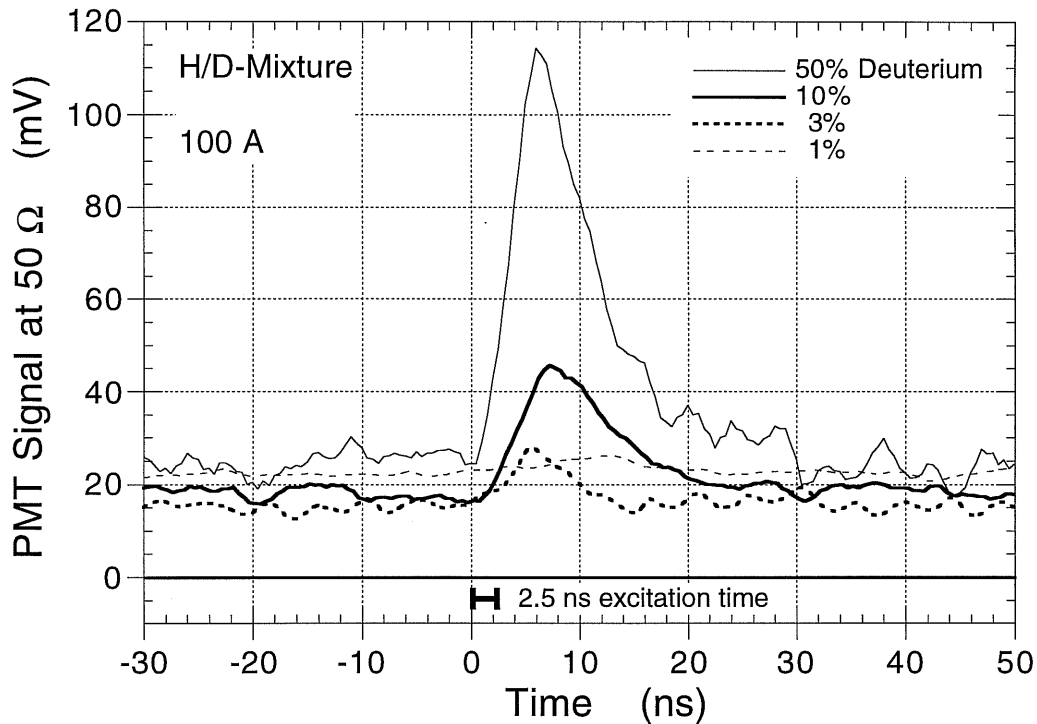


**Figure 4.9** Averaged  $L_{\alpha}$ -TALIF signals for deuterium in a hydrogen plasma with decreasing concentrations of deuterium. The discharge current was 100 A. The temporal FWHM of the laser is indicated.

*Absolute atomic number densities* gained from such  $L_{\alpha}$ -TALIF signals are presented in Figure 4.10. It comprises the most important *density results* for the two main measurement campaigns:

- *November 1996*: Dependence of  $L_{\alpha}$ -TALIF signals on the discharge current in a pure deuterium plasma;
- *June 1997*: Dependence of  $L_{\alpha}$ -TALIF signals on the deuterium concentration in a hydrogen plasma.

Now, that *all* the experimental parameters are considered via the  $L_{\alpha}$ -yield for the analysis, the final density results clearly show *the correct relations* as they are expected by looking at the corresponding concentrations. The error bars shall be discussed in the following chapter. All performed density measurements put together, they spanned densities of almost three orders of magnitude.

Our results can be connected to results made by the IPP with passive spectroscopy lately. Within accuracy, our atomic number density at 300 A in a pure deuterium plasma matches sufficiently to the result of  $2 \cdot 10^{12} \text{ cm}^{-3}$  as obtained by Meyer [55].

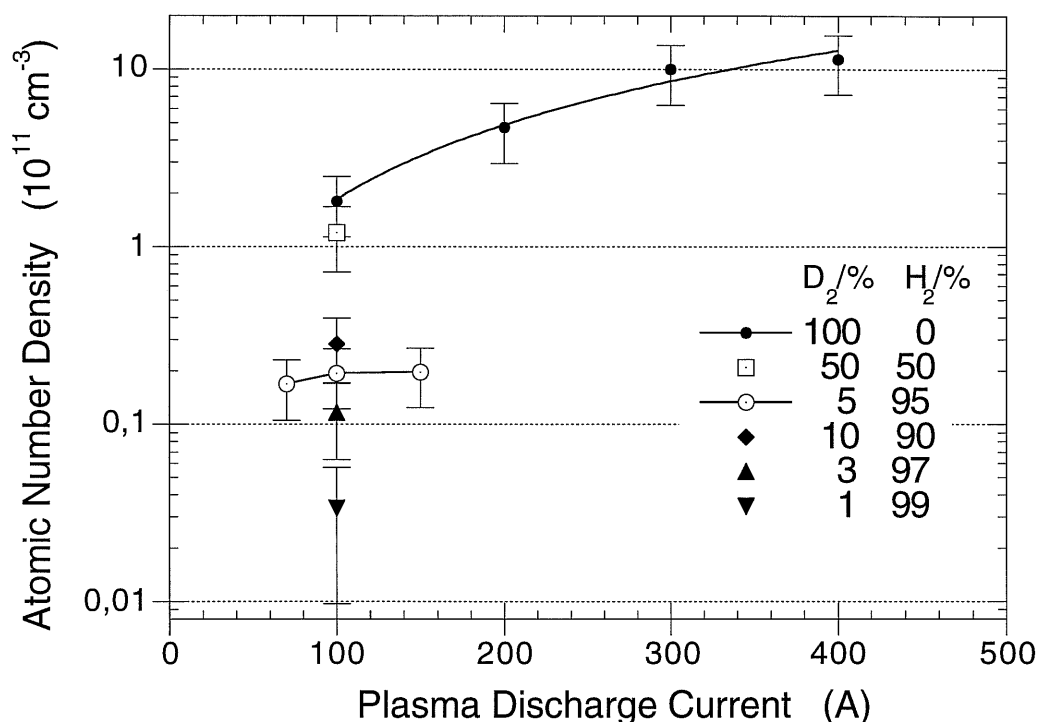


**Figure 4.10** Measured atomic number densities for deuterium at PSI-1. Densities here vary either with the discharge current at PSI-1 or with the input gas mixtures at a fixed current of 100 A.

Comparison of the atomic deuterium densities determined by use of  $L_\alpha$ -TALIF with the theoretical values Kastelewicz et al [52] calculated by use of the joint two-dimensional, hydrodynamic plasma code "B2" with the three-dimensional Monte-Carlo code "EIRENE" for the location of our measurement volume, also shows principal accordance of the results.

#### 4.3.3 Error discussion for atomic number densities

Absolute values for the atomic number density are calculated by Equation (2.15). The resulting relative error  $\Delta N/N$  for the density is given by summing up the quadratic relative errors of each factor in Equation (2.15). As explained in Ch. 4.1.4, the  $L_\alpha$ -yield error is 20%. The second largest contribution comes from the solid angles, because they comprise the measurement of numerous lengths, respectively their exact reproduction during measurement runs at the PSI-1 plasma generator. Set to an absolute error of 5 mm in the worst case, they add up to 18%. Next come errors of 15% each, given by the behaviour of the  $L_\alpha$ -calibration lamp (Eq. (3.1)) and the laser beam irradiance distribution recorded with the CCD camera.

Errors discussed so far are effecting all  $L_\alpha$ -TALIF measurements in the same way. However, the uncertainty for the signal-to-noise ratio  $S_{LIF}/S_P$  depends on the efficiency, with which the TALIF signal peak can be produced and measured against the plasma background radiation at PSI-1. And it depends on the atomic number density itself, which also has a fundamental influence on the strength of TALIF signal peak. For example, in plasmas, where the concentration of the isotope to measure is small, the relation of the photons in the TALIF peak to the number of background in an equal time is small and leads therefore to a large error for the signal-to-noise ratio  $S_{LIF}/S_P$ .

Finally, the resulting *global error* comes up to be  $\pm 37\%$  in cases where the ratio  $S_{LIF}/S_P$  is at least one.

#### 4.3.4 $L_\alpha$ -TALIF detection limit at PSI-1

As shown in Fig. 4.6, the plasma generator PSI-1 is characterized by an unexpected high plasma background radiation in the spectral region of Lyman- $\alpha$ . Consequently, the sensitive  $L_\alpha$ -detector had to be protected against a resulting destructive load on its PMT. Although an oxygen filter could be used, the TALIF signal itself was always affected, i.e. decreased, as well.

Under somehow reasonable plasma background conditions at low discharge currents, a deuterium atomic number density in the order of  $10^9$  atoms per cubic-centimetre was still detectable, however, with an unacceptably high error of  $\pm 80\%$ . However, a density as small as  $10^{10} \text{ cm}^{-3}$  can be regarded as the *detection limit* for  $L_\alpha$ -TALIF at the plasma generator PSI-1.

## 4.4 Kinetic plasma temperatures at PSI-1

Measuring the kinetic temperature was done by using a deliberately introduced *residual Doppler width* (Ch. 2.1). Choosing a small crossing angle between the two counterpropagating laser beams (Fig. 3.4) of 52 mrad causes the absorption profiles to have a residual Doppler width of 2.6% of the full Doppler width. Such a width is measured in our case by tuning the laser wavelength over the resonance for the  $1S \rightarrow 2S$  transition.

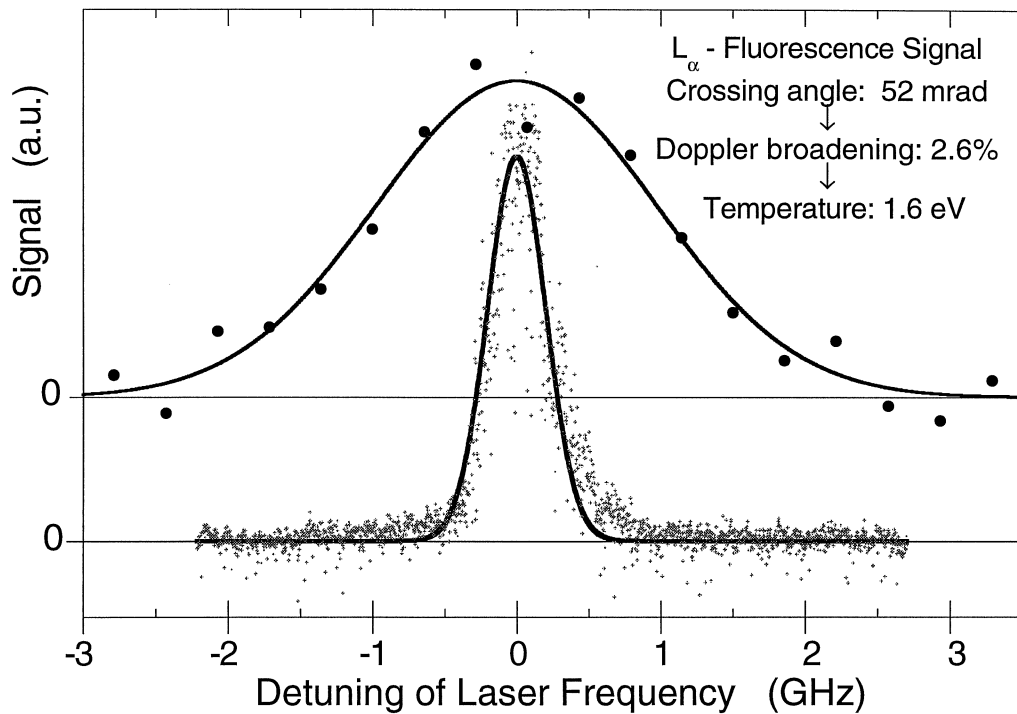


**Figure 4.11** Residual Doppler profile of  $L_{\alpha}$ -TALIF signals in a deuterium plasma at a discharge current of 300 A yielding a kinetic temperature of 1.6 eV (upper curve). The corresponding signal of the optogalvanic reference cell shows the laser wavelength being tuned over the  $1S \rightarrow 2S$  resonance (lower curve).

Figure 4.11 shows the spectral dependence of the mean voltage in the  $L_{\alpha}$ -TALIF signal peak on the laser's frequency detuning (upper curve), i.e. the residual Doppler width of the  $L_{\alpha}$ -TALIF signal. The measurement was performed in a pure deuterium plasma at 300 A. Additionally, the signal of the optogalvanic reference cell is shown with arbitrary units (lower curve). Its signal rises strongly, when the laser wavelength becomes resonant to the  $1S \rightarrow 2S$  transition.

Fitting a Gauss curve to the  $L_{\alpha}$ -TALIF signals yields a residual Doppler width. This width is then transformed into a full Doppler width  $\Gamma$  and inserted into Eq. (2.7). The resulting kinetic temperature of deuterium atoms at a discharge current at 300 A at PSI-1 is:

$$T = 1.6 \text{ eV} \cdot (1 \pm 37\%).$$

The error is mainly due to the error of the  $L_{\alpha}$ -TALIF signals (Ch. 4.3.3).

# 5

## Conclusion

The potential of *two-photon absorption laser-induced Lyman- $\alpha$  fluorescence* ( $L_{\alpha}$ -TALIF), as a novel technique for the absolute measurement of hydrogen isotope densities in magnetically confined plasmas was successfully demonstrated. We performed measurements at the *plasma generator PSI-1*, which was operated by the Max-Planck-Institut für Plasmaphysik, Berlin Branch. At this machine, the plasma of a high-current stationary arc discharge expanded magnetically guided into an observation chamber, where then  $L_{\alpha}$ -TALIF measurements took place.

The key to *isotope selectivity* is that two-photon absorption gives sub-Doppler resolution, if the atoms can absorb two photons from two laser beams propagating in opposite direction. Pulsed tunable laser radiation at a wavelength of 243 nm was produced by a *laser spectrometer*, using only solid-state lasers. It is characterized by a *high shot-to-shot stability* in respect to pointing stability, small spectral bandwidth ( $< 0.4$  GHz), pulse duration (2.5 ns), pulse energy (30 mJ) and beam profile. It allowed for the efficient two-photon absorption laser-induced excitation of a  $n = 1 \rightarrow n = 2$  transition in hydrogen isotopes. The measurement volume was as small as  $0.1 \text{ cm}^{-3}$  in a plasma beam of 10 cm diameter, delivering *spatially highly resolved* densities. For the lasers were operated with a pulse repetition rate of 10 Hz, the high shot-to-shot stability allowed to gain atomic densities with *good temporal resolution* as well.



---

For measuring the induced fluorescence radiation at Lyman- $\alpha$  ( $\lambda = 121.6$  nm) a gated *VUV-detection system* was developed. Its flexible filter system allowed to modify the detector's sensitivity over three decades. This was elementary, otherwise the photomultiplier would have been damaged by UV background irradiances at the PSI-1, which were up to twenty times stronger than the one being reported for current tokamak fusion machines ( $10^{15}$  photons / (s·sr·cm<sup>2</sup>)).

In order to obtain *absolute values* for the atomic number densities, not only the detection system was *calibrated* by use of a special Lyman- $\alpha$  lamp serving as a transfer standard for synchrotron radiation from BESSY I, but the *Lyman- $\alpha$  yield*  $Y$  was calculated as well.  $Y$  gives the percentage of atoms related to the total number of atoms in the groundstate, which will emit a Lyman- $\alpha$  photon after excitation by two-photon absorption. Calculations involved the numeric solution of coupled time resolved nonlinear rate-equations. To represent the conditions relevant for the emission of Lyman- $\alpha$  photons as accurate as possible, the actual laser beam profiles were considered in the calculations, too.

Measurements at hydrogen, deuterium and H/D-mixed plasmas confirmed theoretical predictions made by Seidel for PSI-1 plasmas. The lowest measured atomic number densities with an acceptable error of  $\pm 50\%$  were  $1 \cdot 10^{10}$  cm<sup>-3</sup>. The detection limit for a laser pulse energy of 10 mJ per beam lay close to the theoretical detection limit according to Poisson statistic for typical PSI-1 plasmas.

Introducing a small crossing angle between the normally anti-parallel laser beams caused a residual Doppler-width in the absorption profiles. Therefore, measuring the fluorescence while tuning the laser radiation around 243 nm yielded kinetic temperatures. The measured result for a standard PSI-1 deuterium plasma was 1.6 eV· ( $1 \pm 35\%$ ).

Drawing the *conclusion* for this feasibility study shows, that L $_{\alpha}$ -TALIF is a powerful direct access to atomic number densities of hydrogen isotopes. We have demonstrated its capabilities even with disturbing background irradiances such as twenty times as high compared to the corresponding value commonly stated for tokamaks.

Predictions for the application of L $_{\alpha}$ -TALIF diagnostic at true fusion plasma devices are now possible because of:

- fusion plasma relevant two-photon absorption profiles have been calculated by Seidel and Voslamber;

- experimental results for  $L_\alpha$ -TALIF measurements are in general agreement with this theory;
- experimental knowledge and experience allow to define the layout for the laser spectrometer and the detection system suited for fusion plasmas;
- versatile formalism for the calculation of the  $L_\alpha$ -yield under various plasma conditions

We are therefore convinced, that with pulse energies of 100 mJ per beam for high-quality laser radiation at 243 nm  $L_\alpha$ -TALIF measurements for hydrogen isotopes shall be possible down to densities of  $10^8$  atoms per cubic-centimetre.

Indeed, the detection limit for hydrogen isotopes with  $L_\alpha$ -TALIF at magnetically confined fusion plasmas suffers from the fact, that the underlying two-photon excitation probability unfortunately decreases with increasing ion-temperature. However, the probability remains almost constant for  $H_\alpha$ -TALIF excited out of the ground-state. This is under theoretical investigation by Seidel and Voslamber. It is a two-photon excited Lyman- $\beta$  transition, which would allow for the subsequent detection of Balmer<sup>#</sup>- $\alpha$  ( $3 \rightarrow 2$ ) fluorescence. For the wavelength of this fluorescence lies in the convenient visible light spectrum ( $\lambda_H = 656$  nm), detection would also be significantly more effective and easier in respect of durable materials for transmission optics even under tough tokamak conditions.

---

# J.J. Balmer (1825-1898), Swiss teacher.

# 6

## List of Symbols

Constants	Name	Value
$c$	vacuum speed of light	$3.00 \cdot 10^8$ m/s
$h$	Planck's constant	$6.63 \cdot 10^{-34}$ J·s
$k_B$	Boltzmann's constant	$1.38 \cdot 10^{-23}$ J/K

Variables	Quantity	SI-Unit
$\varnothing$	diameter	m
$\lambda$	wavelength	m
$\Omega$	solid angle	sr
$\sigma_{12}^{(2)}$	two-photon absorption cross section	$\text{m}^4$
$\nu$	frequency	$\text{s}^{-1}$
$\Delta\nu$	spectral bandwidth (FWHM)	$\text{s}^{-1}$
$\Delta\nu_{i\&AC}$	spectral broadening due to ionisation and frequency shift (FWHM)	$\text{s}^{-1}$
$\Delta\nu_{rD}$	residual Doppler width (FWHM)	$\text{s}^{-1}$
$\Gamma$	full Doppler width (FWHM)	$\text{s}^{-1}$

$A$	Area	$\text{m}^2$
$C$	Current	A
$E$	irradiance	$\text{J} / \text{m}^2\text{s}$
$f$	focal length	m
$F$	orbital quantum number (atom)	-
$l$	orbital quantum number (electron)	-
$I$	radiant intensity	$\text{J} / \text{sr s}$
$L$	radiance	$\text{J} / \text{m}^2 \text{sr s}$
$L^{\cdot}$	photon radiance	$1 / \text{m}^2 \text{sr s}$
$L(\nu)$	line shape function	$\text{Hz}^{-1}$
$l$	orbital quantum number	-
$N$	number density	$\text{m}^{-3}$
$N_{\alpha}$	number of photons at 121.6 nm	-
$N_{\text{BG}}$	plasma background photons	-
$n$	principal quantum number	-
$p$	pressure	bar (1 bar = $10^5$ Pa)
$Q$	pulsed radiant energy	J
$Q_{\gamma}$	energy per laser photon	J
$S$	current signal integrated over time	C
$s$	distance	m
$t$	time	s
$V$	volume	$\text{cm}^3$
$V(\nu)$	normalized laser radiation spectral distribution	$\text{Hz}^{-1}$
$Y$	time integrated Lyman- $\alpha$ yield	-
$Y^*$	spatial average of the Lyman- $\alpha$ yield $Y$	-
$Z(t)$	normalized laser radiation temporal distribution	$\text{s}^{-1}$

---

Indices	Full Name
$\alpha$	Lyman- $\alpha$
D	deuterium
H	hydrogen
I	Ion
i	ionised/ionisation
P	plasma
L	lamp
T	tritium

Abbreviations	Full Name
@	at the given wavelength
a. u.	arbitrary units
BBO	$\beta$ -Barium Borate
BESSY-1	source of high-quality synchrotron radiation at Berlin, Germany
CCD	charge-coupled device
D.L.	diffraction-limited laser beam-quality
FWHM	full width at half maximum
IPP	Institut für Plasmaphysik, Max-Planck-Institut, Berlin and Greifswald
ITER	International Thermonuclear Experimental Reactor
KTP	potassium titanyl phosphate crystal for frequency conversion processes
$L_\alpha$	Lyman- $\alpha$ : 1 $\rightarrow$ 2 transition (121.6 nm) - or v.v. - in hydrogen isotopes
LIF	laser-induced fluorescence
OPA	optical parametric amplifier
OPO	optical parametric oscillator
PC	personal computer
PD	photo diode
pixel	picture element

PMT	photomultiplier tube
PSI-1	Name of the plasma generator operated by the IPP
PTB	Physikalisch-Technische Bundesanstalt, Berlin
SH	second harmonic (of a laser's fundamental wavelength)
SLM	single-longitudinal mode
TALIF	two-photon absorption laser-induced fluorescence
TH	third harmonic (of a laser's fundamental wavelength)
Ti:Sa	Titanium:Sapphire
UHV	ultra high vacuum
VUV	vacuum ultraviolet
XUV	extreme ultraviolet

# 7

## Literature

- [1] Velikhov EP.  
World power energetics - fusion reactors - ITER project.  
J Nuc Mat. 1996; 237 (Part A): 1-3.
  
- [2] Atkins R, Houtermans FG.  
Zur Frage der Aufbaumöglichkeit der Elemente in Sternen.  
Z Phys. 54; 1929: 656-65.
  
- [3] Gamow G, Teller E.  
The rate of selective thermonuclear reactions. Phys Rev. 53; 1938: 608-9.
  
- [4] Weizsäcker CFv.  
Phys Z. 39; 1938: 633.
  
- [5] Bethe HA.  
Energy production in stars. Phys Rev. 55; 1939: 176.
  
- [6] Aymar R.  
ITER Overview.  
Fusion Eng. 1997; 36: 9-21.

- 
- [7] Mukhovatov V et al.  
ITER physics program and implications for plasma measurements.  
Rev Sci Instr. 1997; 68: 1250-5.
- [8] Green BJ, Huguet M.  
The ITER project - status and prospects.  
IEEE Transactions on Magnetics. 1996: 32: 2224-9.
- [9] Gasparotto M.  
Present status of fusion research - the next-step tokamak (ITER) and  
the demonstration reactor (DEMO). Appl Rad & Isotopes. 1995; 46: 531-6.
- [10] Young KM, Costley AE et al.  
An overview of ITER diagnostics (invited).  
Rev Sci Instrum. 1997; 68: 862-7.
- [11] Costley AE et al.  
Requirements for ITER diagnostics.  
In: Stott PE, Gorini G, Sindoni E, eds. Diagnostics for Experimental  
Thermonuclear Fusion Reactors I. New York: Olenum Press; 1996: 12-22.
- [12] Herrmann W.  
Messungen und Überlegungen zum Isotopenverhältniss in ASDEX Upgrade.  
In: 128. PTB Seminar zur Bestimmung der Wasserstoff-Isotopen-  
Konzentration in magnetisch eingeschlossenen Fusionsplasmen.  
1995. PTB Berlin, Germany.
- [13] Mertens Ph, Silz M.  
Radial profiles of atomic deuterium measured in the boundary  
of TEXTOR 94 with laser-induced fluorescence.  
J Nuc Materials. 1997; 241-243: 842-7.
- [14] Demtröder W.  
Laser Spectroscopy. 2nd ed. Berlin: Springer-Verlag; 1996.



- 
- [15] Dux R, Grützmacher K, de la Rosa MI, Wende B.  
Absolute determination of local ground-state densities of atomic hydrogen in nonlocal-thermodynamic-equilibrium environments by two-photon polarization spectroscopy. *Phys Rev E*. 1995; 51: 1416-27.
- [16] Thomson M, Czarnetzki U, Döbele HF.  
A novel scheme for detection of atomic hydrogen by four-wave mixing: first experimental results.  
In: *Proceedings of the 8<sup>th</sup> International Symposium on Laser-Aided Plasma Diagnostics*. Doorwerth, The Netherlands; 1997: 127-31.
- [17] ITER Progress Meeting on Diagnostic Systems.  
Max-Planck Institut für Plasmaphysik; Garching, Germany: January 1997.
- [18] Voslamber D, Mandl W.  
Determination of the D/T fuel mixture using two-photon laser induced fluorescence in combination with neutral beam injection.  
Rep. EUR-CEA-FC-1607. 1997. CEN Cadarache; St. Paul-lez-Durance, France.
- [19] Hemsworth RS et al.  
Neutral beams for ITER.  
*Rev Sci Instrum*. 1996; 67: 1120-5.
- [20] Sasao M, Taniike A, Nomura I, Wada M, Yamaoka H, Sato M.  
Development of diagnostic beams for alpha particle measurement on ITER.  
*Nuc Fusion*. 1995; 35: 1619-24.
- [21] Stern RA, Johnson JA.  
Plasma ion diagnostics using resonant fluorescence.  
*Phys Rev Lett*. 1975; 34: 1548-50.
- [22] Fujimoto T, Sawada K, Takahata K.  
Ratio of Balmer line intensities resulting from dissociative excitation of molecular hydrogen in an ionizing plasma. *J Appl Phys*. 1989; 66: 2315-9.
- [23] Goepfert-Meyer M.  
Über Elementaraktē mit zwei Quantensprüngen. *Ann Phys*. 1931; 9: 273-94.

- [24] Kaiser W, Garrett CGB.  
Two-photon excitation in  $\text{CaF}_2:\text{Eu}^{2+}$ . *Phys Rev Lett.* 1961; 7: 229.
- [25] Hänsch TW, Lee SA, Wallenstein R, Wiemann C.  
Doppler-free two-photon spectroscopy of hydrogen 1S-2S.  
*Phys Rev Lett.* 1975; 37: 307-9.
- [26] Bloembergen N, Levenson MD.  
Doppler-free two-photon absorption spectroscopy.  
In: Shimoda K, ed. *High-resolution laser spectroscopy*.  
Berlin: Springer-Verlag; 1976: 315-69. (Topics in Applied Physics; vol 13).
- [27] Voslamber D.  
Determination of magnetic field direction in tokamaks from laser-induced Lyman- $\alpha$  fluorescence I: one-photon excitation.  
Rep. EUR-CEA-FC-1342. 1988. CEN Cadarache; St. Paul-lez-Durance, France.
- [28] Voslamber D.  
Determination of neutral particle density and magnetic field direction from laser-induced Lyman- $\alpha$  fluorescence II: two-photon excitation.  
Rep. EUR-CEA-FC-1387. 1990. CEN Cadarache; St. Paul-lez-Durance, France.
- [29] Danzmann K, Grützmacher K, Wende B.  
Doppler-free two-photon polarization spectroscopy measurement of the Stark-broadened profile of the hydrogen  $L_\alpha$ -line in a dense plasma.  
*Phys Rev Lett.* 1986; 57: 2151-3.
- [30] Grützmacher K, de la Rosa I, Seidel J, Steiger A, Voslamber D.  
Two-photon induced  $L_\alpha$ -fluorescence as a means for isotope-selective hydrogen density determination in tokamak plasmas.  
In: *Contributed papers of the 21<sup>st</sup> EPS Conference on Controlled Fusion and Plasma Physics*. Montpellier: European Physical Society. 1994: 18 B III: 1288-91.
- [31] Seidel J.  
Private communication. PTB, Berlin; 1995.

- 
- [32] Voslamber D.  
Some novel concepts for spectroscopic diagnostics in Tokamaks.  
In: May AD, Drummond JR, Oks E, eds. AIP Conference Proceedings 328.  
Woodbury: American Institute of Physics; 1995: 3-27.
- [33] Goeckner MG, Goree J.  
Laser-induced fluorescence measurement of plasma ion temperatures:  
Corrections for power saturation.  
J Vac Sci Technol. 1989; A7: 977-89.
- [34] Seiser Ch, Grützmacher K, Steiger A.  
Lyman- $\alpha$  Ausbeute bei Zwei-Photonen-LIF für die Tokamak-Diagnostik.  
In: DPG Verhandlungen 61. Bayreuth: Deutsche Physikalische Gesellschaft.  
1997: P 7.1.
- [35] Bassani F, Forney JJ, Quattropani A.  
Choice of gauge in two-photon transition: 1S-2S transition  
in atomic hydrogen. Phys Rev Lett. 1977; 39: 1070.
- [36] Seidel J.  
Plasma broadening of hydrogen two-photon absorption lines.  
In: Burnett K, ed. Spectral Line Shapes 2. Berlin: de Gruyter; 1983: 381-93.
- [37] Loudon R.  
The Quantum Theory of Ligth.  
2nd ed. Oxford: Oxford University Press; 1983: 338 ff.
- [38] Radzig AA, Smirnov BM.  
Reference Data on Atoms, Molecules and Ions. 1st ed. Berlin: Springer-  
Verlag; 1985. (Goldanskii VI, Gomer R, Schäfer FP, Toennies JP, eds; Springer  
series in chemical physics; vol 31).
- [39] Czarnetzki U, Miyazaki K, Kajiwara T, Muraoka K, Maeda M, Döbele HF.  
Comparison of various two-photon excitation schemes for laser-induced  
fluorescence spectroscopy in atomic hydrogen.  
J Opt Soc Am. 1994; B 11: 2155-62.

- [40] Bohmeyer W.  
Diagnostikverfahren für die Plasmaparameter der Plasmaquelle PSI-1.  
In: 128. PTB Seminar zur Bestimmung der Wasserstoff-Isotopen-  
Konzentration in magnetisch eingeschlossenen Fusionsplasmen.  
1995. PTB Berlin, Germany.
- [41] Drawing according freely to a template of  
Max-Planck Institut für Plasmaphysik, Garching (Germany): Berlin Division.
- [42] Koechner W.  
Solid-State Laser Engineering. 4th ed. Berlin: Springer-Verlag; 1996.  
(Schawlow A, Shimoda K, Siegman AE, Tamir T, eds;  
Springer series in optical sciences; vol 1).
- [43] Grützmacher K, Steiger A.  
Gepulstes Single-Longitudinal-Mode Festkörper-Laserspektrometer für Zwei-  
Photonen-Spektroskopie an Wasserstoff in Tokamakplasmen.  
In: DPG Verhandlungen 56. Hannover: Deutsche Physikalische Gesellschaft.  
1992: P 19.48.
- [44] Grützmacher K, Dux R, Steiger A.  
Gepulstes Single-Longitudinal-Mode Festkörper-Laserspektrometer für Zwei-  
Photonen-Spektroskopie an Wasserstoff in Tokamakplasmen - Ergebnisse.  
In: DPG Verhandlungen 57. Greifswald: Deutsche Physikalische Gesellschaft.  
1993: P 15.67.
- [45] Grützmacher K, Dux R, de la Rosa I, Steiger A.  
Gepulstes Einmoden-Festkörper-Laserspektrometer zur Erzeugung sehr  
großer Pulsenergie im UV.  
In: DPG Verhandlungen 58. Hamburg: Deutsche Physikalische Gesellschaft.  
1994: Q 3D.1.
- [46] Steiger A, Grützmacher K, de la Rosa I.  
Pulsed single mode UV-laser source for nonlinear plasma spectroscopy.  
In: Proceedings of the 7<sup>th</sup> International Symposium on Laser-Aided Plasma  
Diagnostics. Fukuoka, Japan; 1995: 156-61.

- 
- [47] Eds: Bosenberg WR, Eckhardt RC.  
Feature on Optical Parametric Devices.  
in: J Opt Soc Am. 1995; 11: 2084-320.
- [48] Bosenberg WR, Guyer DR.  
Broadly tunable, single-frequency optical parametric frequency-conversion system. J Opt Soc Am. 1993; B 10: 1716-22.
- [49] Barbieri B, Beverini N.  
Optogalvanic Spectroscopy. Rev Mod Phys. 1990; 62: 603-44.
- [50] Steiger A.  
Private communication. PTB, Berlin; 1995.
- [51] Samson JAR.  
Techniques of Vacuum Ultraviolet Spectroscopy. 1967. Pied Publications, Lincoln, Nebraska, USA. 2<sup>nd</sup> ed: 204 ff.
- [52] Kastelewicz H, Reiter D, Schneider D, Coster D, Meyer H.  
Plasmamodellierung für den PSI-1. Frühjahrstagung der Deutschen Physikalischen Gesellschaft. 1997; Mainz, Germany: P. 13.10.
- [53] Grote H.  
Private communication. IPP, Berlin; 1996.
- [54] Beausoleil RG.  
Continuos-wave measurement of the 1S-2S transition frequency in atomic hydrogen: The 1S lamb shift. PhD Thesis. 1986. Stanford University, USA.
- [55] Meyer H.  
Private communication. IPP, Berlin; 1997.



---

# Acknowledgements

Since April 1995 I have been engaged with performing this feasibility study at the Physikalisch-Technische Bundesanstalt, Berlin-Charlottenburg to which many people contributed. I want to use this occasion to express my thanks to all of them. First I'd like to acknowledge *Professor Wende's* sustaining commitment all over the time and his open-mindedness in any respect.

I am deeply indebted to *Dr. Grützmacher*, who is the head of the laboratory of "Hochtemperaturmetrologie", for his immense support as well physically as in any other respect. Therefore, working together with him during the last three years has meant not only to learn how to do smart physics but a lot more beyond that.

Special thanks are due to my colleague *Dr. Steiger* for his seemingly unlimited openness, joy for discussing and his strong support at any time.

I also want to thank *Mr. Breuer* and *Mr. Johannsen* who managed to care for many details in and around a project of that complexity and size.

A lot of members of the IPP were committed to this project, as well. I am especially grateful to *Mr. Reiner*, *Dr. Grote*, *Dr. Bohmeyer* and *Professor Fußmann*.

*Dr. Voslamber* and *Dr. Seidel* contributed the strong theoretical foundation for this work, which makes me equally strong indebted to them.

*Dr. Hollandt* and *Mr. Paustian* from from PTB's laboratory at BESSY I have made calibration of the  $L_{\alpha}$ -lamps with synchrotron radiation possible, which I acknowledge thankfully.

*Professor Sahm* and *Professor Weber* I do thank for their willingness of assessing this PhD thesis. I am specially thankful to *Professor Weber* who allowed me to gain a deeper insight into optics.

Finally, I want to give a faint idea of the deep gratitude towards my aunt *Inge* and uncle *Edwin*, who put me on the path of learning and which has lead me to this happy moment in my life over the last two decades.

# Curriculum Vitae

## *PERSONAL DETAILS*

Name: CHRISTIAN SEISER  
Date of Birth: 19<sup>th</sup> July 1967  
Place: Lörrach, Germany

## *FIRST EDUCATION*

8/74 - 3/78 J. P. Hebel-Grundschule, Lörrach  
3/78 - 7/79 Grund- & Hauptschule, Rheinfelden, Germany  
9/79 - 5/88 Gymnasium, Rheinfelden

## *PRACTICALS*

Laboratory practicals at  
1983 Hoffmann-La Roche, Grenzach, Germany  
1984 Ciba Geigy, Basel, Switzerland

## *CIVIL SERVICE*

6/88 - 12/88 Caretaker employee, Studienhaus Rüspe,  
Rüspe, Germany  
1/89 - 2/90 Individual care for seriously handicapped persons,  
Freiburg, Germany

## *UNIVERSITY EDUCATION*

10/89 - 9/92 Studies in physics, Albert-Ludwigs-Universität, Freiburg  
10/92 - 3/95 Continuation of physics, Technische Universität, Berlin, Germany  
Focus on applied physics and quantum optics  
2/94 - 2/95 Diploma thesis: Frequency Conversion of Titanium Sapphire  
Laser Radiation; Prof. H. Weber, Optical Department, TU Berlin

## *CAREER EXPERIENCE*

4/95 - 6/98 Scientific employee, Physikalisch-Technische Bundesanstalt, Berlin



Theory of lighth and colours - though not occupying much of my time - seemed more important to me than anything else I ever did or will ever do.

*Thomas Young* (1773 - 1829)